



NTNU – Trondheim
Norwegian University of
Science and Technology

Degradation mechanisms due to wear and corrosion interaction of cutter tools used in Tunnel Boring Machines.

Erlend Krogstad

Materials Technology

Submission date: June 2013

Supervisor: Ragnhild Aune, IMTE

Co-supervisor: Nuria Espallargas, IPM
Pål Jakobsen, BAT

Norwegian University of Science and Technology
Department of Materials Science and Engineering

Preface and Acknowledgements

This is a master thesis carried out for the Department of Engineering Design and Materials (IPM).

The master thesis was carried out to acquire understanding on how the wear and corrosion mechanisms affect the steel disc cutters used in tunnel boring applications during excavation. The steel was tested in different environments and different lubricants were added to investigate its effect on the wear and corrosion performance of the steel. All the laboratory experiments were done at the Tribology Lab and Metallurgy Lab at IPM NTNU.

I would like to thank my supervisors, Nuria Espallargas and Pål Drevland Jakobsen for their help during this project. I would especially like to thank Nuria who has been very helpful and has answered a lot of questions during this time, and for her help and guidance performing the laboratory experiments. I would also like to thank Aidan von Bonin and Cristian Torres for their help in teaching me how to use the laboratory equipment, and answering questions when help was needed.

29/06/2013, Trondheim

Erlend Krogstad

Summary

A better understanding of the wear and corrosion mechanisms at work on the steel cutters during tunnel boring is needed to further improve the use of tunnel boring machines in tunnel excavation.

In this master thesis several experiments were conducted to determine the wear and corrosion properties of a steel designed for tunnel boring machines. In tunnel boring it is common to use lubrication to decrease the wear of the steel. Therefore, to test the corrosiveness of the lubricants, several polarization curves were measured for the steel at different conditions. The tests were performed for the three lubricants that was used in this master thesis: ABR5, SLF41, and SLF47B. And the electrolyte used during the polarization tests were: 3% lubricant, 3% lubricant with 1.4% NaCl and 3% lubricant with 3.4% NaCl. To test the wear and how wear and corrosion affected the steel, reciprocal ball-on-plate tests were performed during several different conditions. The steel was rubbed against a rock surface of Iddefjords Granite in dry conditions, distilled water, and in 3% of three different types of foam additives (polymer lubricant). The lubricants were supplied and produced by BASF and were ABR5, SLF41 and SLF47B. All of the tests were also conducted in 1.4% and 3.4% NaCl-solution. For repeatability purposes all the tests were performed twice.

The dry test showed severe wear on both the steel and the rock surface. The adding of water caused little difference in friction but it did reduce the wear. By adding foam the friction and wear significantly decreased, however, it caused some corrosion on the steel. SLF41 was the least effective foam with regards of wear, suggesting that it did not achieve elastohydrodynamic lubrication and it also generated relatively large amounts of corrosion on the steel. ABR5 and SLF47B were the most efficient reducing wear. In 1.4% NaCl solution SLF41 and SLF47B performed poorer than it did without NaCl and at 3.4% NaCl. However, the poor result of SLF47B with 1.4% NaCl is believed to be caused by failure during testing. At 3.4% NaCl the tribocorrosional behavior of all the foams was poorer than without the presence of NaCl. However, using SLF47B led to less corrosion than the other foams, maybe suggesting some type of corrosion inhibitors might be present. The tests showed that the foams clearly have a positive effect with regards to wear, but some had corrosive effects on the steel. It will be important to consider the environment were the tunnel excavation is done to ensure that the correct foam that yields the lowest wears and corrosion possible is chosen.

Sammendrag

Det trengs bedre forståelse av slitasje- og korrosjonsmekanismene som virker på kutterring stålet i tunneboringsmaskiner for og ytterligere kunne forbedre bruken av de under tunnelboring.

I dette prosjektet ble flere eksperimenter utført for å undersøke slitasje- og korrosjonsegenskapene til ett stål designet for bruk i tunnelboring. Under tunnelboring brukes det som regel ett smøremiddel for å redusere slitasje på stålet. Derfor ble flere polariseringskurver laget ved å teste stålet i elektrolytter av 3% smøremiddel. For å undersøke hvordan saltvann påvirker dette ble testene også utført med smøremiddel i 1.4% NaCl og i 3.4% NaCl. Dette ble gjort ved å utføre ball-on-plate tester under flere forskjellige testforhold. I denne testen ble stålet gnidd mot en steinflate under tørre forhold, i vann og i vann med tilsatts av forskjellige skum (polymer smøremiddel). Smøremiddelet, i form av skum, ble produsert og levert av BASF og var ABR5, SLF41 og SLF47B. Alle testene ble også gjennomført hvor det destillerte vannet ble byttet ut med en 3.4% NaCl-løsning. For repeterbare målinger ble alle testene utført to ganger.

Den tørre testen resulterte i alvorlig slitasje på både stålet og steinen. Tilsetning av vann forårsaket liten forskjell i friksjon, men viste noe reduksjon av slitasje. Ved å tilsette skum sank både friksjon og slitasje betydelig, noe som antyder at elastohydrodynamisk lubrikasjon ble oppnådd. Men skummet forårsaket også noe korrosjon på stålet. SLF41 var det minst effektive skummet da det ikke klarte å oppnå elastohydrodynamisk lubrikasjon, og det var også det skummet som forårsaket mest korrosjon på stålet. ABR5 og SLF41B gav begge god smurning og redusert slitasjen på stålet veldig mye. Når det destillerte vannet ble byttet ut med saltvannsløsning økte både friksjon og slitasjen noe. Ved 1.4% NaCl presterte både SLF41 og SLF47B dårligst. Korrosjonen økte betraktelig under alle de testede forholdene men ikke for SLF47B noe som kan tyde på at korrosjonshemmende stoffer var tilstede. Testene viste at tilsatts av skum har en betydelig positiv effekt på slitasjen av stålet, men kan ha noe korroderende virkninger på stålet. Det er viktig og utføre undersøkelser av miljøet hvor tunnelboringen foregår slik at det skummet som gir minst slitasje og korrosjon velges.

Table of Contents

Preface and Acknowledgements.....	I
Summary	II
Sammendrag	III
Table of Contents	IV
List of Figures.....	VI
List of Tables.....	XI
Abbreviations	XII
1. Introduction.....	1
2. Theory.....	2
2.1 Tunnel boring machines	2
2.1.1 Hard Rock TBMs	4
2.1.2 Soft ground TBMs.....	8
2.1.3 Cutter discs in hard rock TBM operations.....	9
2.1.4 Foam additive lubricant for hard rock tunneling	10
2.2 Metallurgy	11
2.2.1 Steel.....	12
2.3 Corrosion mechanisms	14
2.3.1 Pitting	17
2.3.2 Pourbaix diagram	19
2.3.3 Polarization.....	20
3.3.3 Passivation.....	23
2.4 Tribology.....	28
2.4.1 Wear mechanisms.....	28
2.4.2 Lubrication.....	37
2.4.3 Aqueous Lubrication.....	40
3. Experimental setup	43
3.1 Test materials.....	43
3.2 Test procedures.....	44
3.2.1 Corrosion performance	44
3.2.2 pH measurements	45
3.2.3 Viscosity.....	45
3.2.4 Reciprocal ball-on-plate.....	45

4.	Results	47
4.1	Rock characterization	47
4.2	Steel Characterization	47
4.3	Polarization curves	48
4.4	pH Measurements	55
4.5	Viscosity.....	56
4.6	Reciprocal Ball-on-Plate	58
4.6.1	Topography of the steel balls	66
4.6.2	Wear on the rocks	77
5.	Discussion	82
5.1	Rock and steel characterization	82
5.2	Polarization curves	83
5.3	Tribocorrosion	88
6.	Conclusion	93
7.	Reference list.....	94

List of Figures

Figure 1 - Schematic diagram of breaking out process of rock by a cutter disc [2].	2
Figure 2 - Overview of various TBM systems with full-face excavation [2].	5
Figure 3 - A gripper TBM [5].	6
Figure 4 - An enlargement TBM [5].	6
Figure 5 - A single shielded TBM [6].	7
Figure 6 - A double shielded TBM [6].	7
Figure 7 - Schematic illustrating how a slurry shield TBM works [10].	8
Figure 8 - Schematic illustrating how an earth pressure balanced TBM works [10].	9
Figure 9 - A typical cutter disc design [4].	10
Figure 10 - Cutter disc placement on a TBM [4].	10
Figure 11 - Common metallic crystalline systems.	11
Figure 12 - Effect of NaCl on corrosion rate for steel [17].	15
Figure 13 - Corrosion of a divalent metal M in an oxygen containing electrolyte [17].	16
Figure 14 - Anodic over potential curve for an active-passive metal in a pitting environment. E_p = pitting potential, E_{pass} = passivation potential, i_{kr} = critical current density and i_p = passive current density [17].	17
Figure 15 - Different shapes of corrosion pits [17].	17
Figure 16 - Pourbaix diagram for iron in water at 25 °C [17].	19
Figure 17 - Wiring diagram for potentiostatic experiments [17].	20
Figure 18 - Over potential curves and corresponding polarization curves [17].	21
Figure 19 - Six possible types of behavior for an active-passive alloy in a corrosive environment [20].	22
Figure 20 - Anodic polarization and over voltage curve for iron in sulfuric acid [17].	23
Figure 21 - Anodic polarization curve of Fe-66Ni-16Mo in 50% H ₂ SO ₄ in absence (a) and in presence (b) of the oxidizing agent (Fe ₂ (SO ₄) ₃) [21].	24
Figure 22 - Evans diagram showing a situation of unstable passivity. The corrosion potential can be located in either the active or passive region [21].	25
Figure 23 - Evans diagram showing the significance of the value of the passivation potential. The corrosion potential can be located in the passive (a) or active (b) region [21].	26
Figure 24 - Evans diagram showing the effect of passivation current density on corrosion behavior: (a) corrosion potential in the active region; (b) corrosion potential in the passive region [21].	26
Figure 25 - Anodic partial current density for the dissolution of iron measured in 0.15 M phosphate solutions of different pH [21].	27
Figure 26 - Characterization of wear [22].	29
Figure 27 - Appearances of worn surfaces [22].	30
Figure 28 - Subsurface deformation during passage of a grit [23].	32
Figure 29 - Influence of the hardness of the abrasive on the wear of metals [22].	33
Figure 30 - Types of adhesion bonding mechanisms [22].	34
Figure 31 - Origin of surface fracture and formation of wear particles [22].	35
Figure 32 - SEM image of boron disc adhesive wear scar [24].	35
Figure 33 - Stribeck Curve and lubrication regimes [22].	38
Figure 34 - Film-forming properties of different types of aqueous surfactant solutions [27].	41
Figure 35 - The potentiostat	44

Figure 36 - The cell setup	44
Figure 37 - PHM210 pH meter.....	45
Figure 38 - ResMat Tribocorr test machine.....	46
Figure 39 - Simplified model of the test method.	46
Figure 40 - Polarization curves for ABR5.	48
Figure 41 - Polarization curves for 3% ABR5	49
Figure 42 - Polarization curves for 3% ABR5 + 1.4% NaCl	49
Figure 43 - Polarization curves for 3% ABR5 + 3.4% NaCl	50
Figure 44 - Polarization curves for SLF41.	50
Figure 45 - Polarization curves for 3% SLF41.....	51
Figure 46 - Polarization curves for 3% SLF41 + 1.4% NaCl	51
Figure 47 - Polarization curves for 3% SLF41 + 3.4% NaCl	52
Figure 48 - Polarization curves for SLF47B.	52
Figure 49 - Polarization curves for 3% SLF47B	53
Figure 50 - Polarization curves for 3% SLF47B + 1.4% NaCl	53
Figure 51 - Polarization Curves for 3% SLF47B + 3.4% NaCl.....	54
Figure 52 - pH-values of the lubricants.	55
Figure 53 - pH values of the lubricants in the different electrolytes.	56
Figure 54 - Viscosity of lubricants.....	57
Figure 55 - Viscosity of lubricants.....	57
Figure 56 - Average COF for the different test scenarios.....	59
Figure 57 - Coefficient of friction for dry rubbing.	59
Figure 58 – Coefficient of friction for wet rubbing.....	60
Figure 59 - Coefficient of friction for wet rubbing with 1.4% NaCl.....	60
Figure 60 - Coefficient of friction for wet rubbing with 3.4% NaCl.....	61
Figure 61 - Coefficient of friction for wet rubbing with 3% ABR5 foam.....	61
Figure 62 - Coefficient of friction for wet rubbing with 3% ABR5 foam and 1.4% NaCl.....	62
Figure 63 - Coefficient of friction for wet rubbing with 3% ABR5 Foam and 3.4% NaCl.....	62
Figure 64 - Coefficient of friction for wet rubbing with 3% SLF41 Foam.....	63
Figure 65 - Coefficient of friction for wet rubbing with 3% SLF41 and 1.4% NaCl.....	63
Figure 66 - Coefficient of friction for wet rubbing with 3% SLF41 foam and 3.4% NaCl.....	64
Figure 67 - Coefficient of friction for wet rubbing with 3% SLF47B foam.....	64
Figure 68 - Coefficient of friction for wet rubbing with 3% SLF47B and 1.4% NaCl.....	65
Figure 69 - Coefficient of friction for wet rubbing with 3% SLF47B foam and 3.4% NaCl.....	65
Figure 70 - Wear track on the steel ball from dry wear at 100x magnification.....	66
Figure 71 - Wear track on the steel ball from dry wear at 400x magnification.....	66
Figure 72 - Wear track on the steel ball from dry wear at 100x magnification.....	66
Figure 73 - Wear track on the steel ball from dry wear at 400x magnification.....	66
Figure 74 - Wear track on the steel ball from wet wear at 100x magnificatio.....	66
Figure 75 - Wear track on the steel ball from wet wear at 400x magnification.....	66
Figure 76 - Wear track on the steel ball from wet wear at 100x magnification.....	66
Figure 77 - Wear track on the steel ball from wet wear at 400x magnification.....	66
Figure 78 - Wear track on the steel ball from 1.4% NaCl at 100x magnification.....	67
Figure 79 - Wear track on the steel ball from 1.4% NaCl at 400x magnification.....	67
Figure 80 - Wear track on the steel ball from 1.4% NaCl at 100x magnification.....	67

Figure 81 - Wear track on the steel ball from 1.4% NaCl at 400x magnification.	67
Figure 82 - Wear track on the steel ball for wet wear with 3.4% NaCl at 100x magnification.	67
Figure 83 - Wear track on the steel ball for wet wear with 3.4% NaCl at 400x magnification.	67
Figure 84 - Wear track on the steel ball for wet wear with 3% ABR5 at 100x magnification.	67
Figure 85 - Wear track on the steel ball for wet wear with 3% ABR5 at 400x magnification.	67
Figure 86 - Wear track on the steel ball for wet wear with 3% ABR5 at 100x magnification.	68
Figure 87 - Wear track on the steel ball for wet wear with 3% ABR5 at 400x magnification.	68
Figure 88 - Wear track on the steel ball for wet wear with 3% ABR5 and 1.4% NaCl at 100x magnification.....	68
Figure 89 - Wear track on the steel ball for wet wear with 3% ABR5 and 1.4% NaCl at 400x magnification.....	68
Figure 90 - Wear track on the steel ball for wet wear with 3% ABR5 and 1.4% NaCl at 100x magnification.....	68
Figure 91 - Wear track on the steel ball for wet wear with 3% ABR5 and 1.4% NaCl at 400x magnification.....	68
Figure 92 - Wear track on the steel ball for wet wear with 3% ABR5 and 3.4% NaCl at 100x magnification.....	68
Figure 93 - Wear track on the steel ball for wet wear with 3% ABR5 and 3.4% NaCl at 400x magnification.....	68
Figure 94 - Wear track on the steel ball for wet wear with 3% ABR5 and 3.4% NaCl at 100x magnification.....	69
Figure 95 - Wear track on the steel ball for wet wear with 3% ABR5 and 3.4% NaCl at 400x magnification.....	69
Figure 96 - Wear track on the steel ball for wet wear with 3% SLF41 at 100x magnification.	69
Figure 97 - Wear track on the steel ball for wet wear with 3% SLF41 at 400x magnification.	69
Figure 98 - Wear track on the steel ball for wet wear with 3% SLF41 at 100x magnification.	69
Figure 99 - Wear track on the steel ball for wet wear with 3% SLF41 at 400x magnification.	69
Figure 100 - Wear track on the steel ball for wet wear with 3% SLF41 and 1.4% NaCl at 100x magnification.....	69
Figure 101 - Wear track on the steel ball for wet wear with 3% SLF41 and 1.4% NaCl at 400x magnification.....	69
Figure 102 - Wear track on the steel ball for wet wear with 3% SLF41 and 1.4% NaCl at 100x magnification.....	70
Figure 103 - Wear track on the steel ball for wet wear with 3% SLF41 and 1.4% NaCl at 400x magnification.....	70
Figure 104 - Wear track on the steel ball for wet wear with 3% SLF41 and 3.4% NaCl at 100x magnification.....	70
Figure 105 - Wear track on the steel ball for wet wear with 3% SLF41 and 3.4% NaCl at 400x magnification.....	70
Figure 106 - Wear track on the steel ball for wet wear with 3% SLF41 and 3.4% NaCl at 100x magnification.....	70
Figure 107 - Wear track on the steel ball for wet wear with 3% SLF41 and 3.4% NaCl at 400x magnification.....	70
Figure 108 - Wear track on the steel ball for wet wear with 3% SLF47B at 100x magnification.	70
Figure 109 - Wear track on the steel ball for wet wear with 3% SLF47B at 400x magnification.	70

Figure 110 - Wear track on the steel ball for wet wear with 3% SLF47B at 100x magnification.	71
Figure 111 - Wear track on the steel ball for wet wear with 3% SLF47B at 400x magnification.	71
Figure 112 - Wear track on the steel ball for wet wear with 3% SLF47B and 1.4% NaCl at 100x magnification.....	71
Figure 113 - Wear track on the steel ball for wet wear with 3% SLF47B and 1.4% NaCl at 400x magnification.....	71
Figure 114 - Wear track on the steel ball for wet wear with 3% SLF47B and 1.4% NaCl at 100x magnification.....	71
Figure 115 - Wear track on the steel ball for wet wear with 3% SLF47B and 1.4% NaCl at 400x magnification.....	71
Figure 116 - Wear track on the steel ball for wet wear with 3% SLF47B and 3.4% NaCl at 100x magnification.....	71
Figure 117 - Wear track on the steel ball for wet wear with 3% SLF47B and 3.4% NaCl at 400x magnification.....	71
Figure 118 - Wear track on the steel ball for wet wear with 3% SLF47B and 3.4% NaCl at 100x magnification.....	72
Figure 119 - Wear track on the steel ball for wet wear with 3% SLF47B and 3.4% NaCl at 400x magnification.....	72
Figure 120 - Wear track on the steel ball from dry wear.	73
Figure 121 - Wear track on the steel ball from dry wear.	73
Figure 122 - Wear track on the steel ball from wet wear.	73
Figure 123 - Wear track on the steel ball from wet wear.	73
Figure 124 - Wear track on the steel ball from wet wear with 1.4% NaCl.....	73
Figure 125 - Wear track on the steel ball from wet wear with 1.4% NaCl.....	73
Figure 126 - Wear track on the steel ball from wet wear with 3.4% NaCl.....	73
Figure 127 - Wear track on the steel ball for wet wear with 3.4% NaCl.	73
Figure 128 - Wear track on the steel ball from lubricated wear with 3% ABR5.....	74
Figure 129 - Wear track on the steel ball from lubricated wear with 3% ABR5.....	74
Figure 130 - Wear track on the steel ball from lubricated wear with 3% ABR5 and 1.4% NaCl	74
Figure 131 - Wear track on the steel ball from lubricated wear with 3% ABR5 and 1.4% NaCl	74
Figure 132- Wear track on the steel ball from lubricated wear with 3% ABR5 and 3.4% NaCl (2).....	74
Figure 133 - Wear track on the steel ball from lubricated wear with 3% ABR5 and 3.4% NaCl (3).	74
Figure 134 - Wear track on the steel ball from lubricated wear with 3% SLF41.....	74
Figure 135 - Wear track on the steel ball from lubricated wear with 3% SLF41.....	74
Figure 136 - Wear track on the steel ball from lubricated wear with 3% SLF41 and 1.4% NaCl (1).	75
Figure 137 - Wear track on the steel ball from lubricated wear with 3% SLF41 and 1.4% NaCl (3).	75
Figure 138 - Wear track on the steel ball from lubricated wear with 3% SLF41 and 3.4% NaCl.....	75
Figure 139 - Wear track on the steel ball from lubricated wear with 3% SLF41 and 3.4% NaCl.....	75
Figure 140 - Wear track on the steel ball from lubricated wear with 3% SLF47B.....	75
Figure 141 - Wear track on the steel ball from lubricated wear with 3% SLF47B.....	75
Figure 142 - Wear track on the steel ball from lubricated wear with 3% SLF47B and 1.4% NaCl (3). ..	75
Figure 143 - Wear track on the steel ball from lubricated wear with 3% SLF47B and 1.4% NaCl (4). ..	75
Figure 144 - Wear track on the steel ball from lubricated wear with 3% SLF47B and 3.4% NaCl (2). ..	76
Figure 145 - Wear track on the steel ball from lubricated wear with 3% SLF47B and 3.4% NaCl (4). ..	76
Figure 146 - Average area of wear track after ball-on-plate testing.....	76

Figure 147 - Wear track on the rock from dry wear 50x magnification.....	77
Figure 148 - Wear track on the rock from dry wear 200x magnification.....	77
Figure 149 - Wear track on the rock from dry wear 450x magnification.....	77
Figure 150 - Wear track on the rock from wet wear 50x magnification.....	77
Figure 151 - Wear track on the rock from wet wear 200x magnification.....	77
Figure 152 - Wear track on the rock from wet wear 450x magnification.....	77
Figure 153 - Wear track on rock from dry wear.....	78
Figure 154 - Wear track on rock from dry wear.....	78
Figure 155 - Wear track on rock from wet wear.....	78
Figure 156 - Wear track on rock from wet wear.....	78
Figure 157 - Wear track on rock from wet wear with 1.4% NaCl.....	78
Figure 158 - Wear track on rock from wet wear with 1.4% NaCl.....	78
Figure 159 - Wear track on rock from wet wear with 3.4% NaCl.....	78
Figure 160 - Wear track on rock from lubricated wear with 3% ABR5.....	79
Figure 161 - Wear track on rock from lubricated wear with 3% ABR5.....	79
Figure 162 - Wear track on rock from lubricated wear with 3% ABR5 and 1.4% NaCl.....	79
Figure 163 - Wear track on rock from lubricated wear with 3% ABR5 and 1.4% NaCl.....	79
Figure 164 - Wear track on rock from lubricated wear with 3% ABR5 and 3.4% NaCl.....	79
Figure 165 - Wear track on rock from lubricated wear with 3% ABR5 and 3.4% NaCl.....	79
Figure 166 - Wear track on rock from lubricated wear with 3% SLF41.....	79
Figure 167 - Wear track on rock from lubricated wear with 3% SLF41.....	80
Figure 168 - Wear track on rock from lubricated wear with 3% SLF41 and 1.4% NaCl.....	80
Figure 169 - Wear track on rock from lubricated wear with 3% SLF41 and 1.4% NaCl.....	80
Figure 170 - Wear track on rock from lubricated wear with 3% SLF41 and 3.4% NaCl.....	80
Figure 171 - Wear track on rock from lubricated wear with 3% SLF41 and 3.4% NaCl.....	80
Figure 172 - Wear track on rock from lubricated wear with 3% SLF47B.....	80
Figure 173 - Wear track on rock from lubricated wear with 3% SLF47B.....	80
Figure 174 - Wear track on rock from lubricated wear with 3% SLF47B and 1.4% NaCl.....	81
Figure 175 - Wear track on rock from lubricated wear with 3% SLF47B and 1.4% NaCl.....	81
Figure 176 - Wear track on rock from lubricated wear with 3% SLF47B and 3.4% NaCl.....	81
Figure 177 - Wear track on rock from lubricated wear with 3% SLF47B and 3.4% NaCl.....	81
Figure 178 - Mohs-Vickers Hardness Conversion Chart [31].....	82
Figure 179 - Polarization curves of all the foams with 100% concentration.....	83
Figure 180 - Polarization curves for all the foams with 3% concentration.....	84
Figure 181 - Pourbaix diagram for iron in water with the results of 3% lubrication.....	85
Figure 182 - Polarization curves for all the foams at 3% concentration + 1.4% NaCl.....	85
Figure 183 - Purbaix diagram for iron in 3.5% NaCl with the results for foam at 3% concentration with 1.4% NaCl.....	86
Figure 184 - Polarization curves for all the foams at 3% concentration + 3.4% NaCl.....	86
Figure 185 - Pourbaix diagram for iron in 3.5% NaCl with results for foam at 3% concentration with 3.4% NaCl.....	87
Figure 186 - Polarization curves for SLF41.....	90
Figure 187 - COF of friction as a function of time for all performed tests of SLF47b + 1.4% NaCl.....	91

List of Tables

Table 1 – Important characteristics of soil and rock to be identified [4].	3
Table 2 – Moh’s hardness for different mineral types [7-9].	7
Table 3 - Physical properties of the foams.	43
Table 4 - Test matrix for polarization tests.	44
Table 5 - Test matrix for the reciprocal ball-on-plate test.	46
Table 6 - Composition of Iddefjord granite (including Moh’s hardness values as stated in the theory section of this thesis)	47
Table 7 - Composition of the H13 steel.	47
Table 8 - pH-values of the lubricants.	55
Table 9 - Viscosity of lubricants.	56
Table 10 - Average COF for the ball-on-plate tests.	58
Table 11 - SEM pictures of the steel surface after reciprocal ball-on-plate test.	66
Table 12 - Optical microscope pictures of steel surface after reciprocal ball-on-plate test.	73
Table 13 - Optical microscope pictures of steel surface after reciprocal ball-on-plate test continued.	74
Table 14 - SEM pictures of the rock surface after reciprocal ball-on-plate test.	77
Table 15 - Optical microscope pictures of steel surface after reciprocal ball-on-plate test.	78

Abbreviations

TBM	-	Tunnel Boring Machine
EPB TBM	-	Earth Pressure Balanced Tunnel Boring Machine
EHL	-	Elastohydrodynamic Lubrication
BCC	-	Body-Centered Cubic
FCC	-	Face-Centered Cubic
HCP	-	Hexagonal Close-Packed
SEM	-	Scanning Electron Microscope
XRD	-	X-Ray Diffraction
COF	-	Coefficient of Friction
E_{corr}	-	Corrosion Potential
I_{corr}	-	Corrosion Current

1. Introduction

Tunnel Boring Machines (TBM) are used to bore tunnels and can encounter different types of geology, mineralogy and chemistry, from sand and soft clay to soft and hard rock.

During tunnel boring the cutter discs in the TBMs will encounter a tribological environment leading to degradation of the quality of the steel and eventually cause it to fail. The cutter discs will be exposed to rocks and minerals which will wear the steel out. They will also encounter chemical compounds which can cause corrosion on the steel. Tunnel boring is performed all over the world. As a consequence, several different environments are encountered. Some tunnels are bored in areas where salt water is present, which is very important to consider with regards to corrosion. The salinity of the water will directly affect the tribological degradation of the cutter disc steel in the TBMs. When metallic alloys are subjected to both wear and corrosion simultaneously it will act very differently than it would if it was subjected to corrosion and wear separately. This phenomenon is called *Tribocorrosion* and it can be difficult to predict the outcome of such a situation. It is not possible to look at wear and corrosion separately when studying Tribocorrosion because they greatly affect one another.

The TBMs are equipped with metallic cutter ring discs on its excavation face. As mentioned these cutter discs are exposed to wear and corrosion during tunnel boring. Because of this, the tunnel boring needs to be stopped in order for the cutter ring discs to be changed. This is a costly and time consuming process, which by reduction of wear and corrosion on the cutter discs, could be shortened. It is these cutter ring discs and their steel composition which are of interest in this master thesis and their wear and corrosion properties will be explored. To reduce wear, it is common to use lubricants when using TBMs and therefore the effects of adding foam additives (polymer lubricants) will be analyzed.

Three different foams will be studied in this master thesis. They will be tested for the use in hard rock tunnel boring, where their main purposes are to reduce friction and wear, cool the cutter discs and to reduce the amount of dust in the air. This master thesis will mainly study their ability to reduce friction and wear and to determine their corrosive capabilities.

A steel alloy commonly used in TBMs was tested in a reciprocal ball-on-plate test against an Iddefjord Granite sample. The foams tested were MEYCO ABR5, MEYCO SLF41 and MEYCO SLF47B. The tests were performed with 3% foam in distilled water as well as in foam and water containing 1.4 wt.% and 3.4 wt.% NaCl. Dry and wet tests without foam were also performed for comparison. To test the corrosiveness of the steel polarization curves were measured for the steel in electrolytes containing 3% foam, 3% foam with 1.4% NaCl and 3% foam with 3.4% NaCl.

2. Theory

2.1 Tunnel boring machines

The first tunnel boring machine (TBM) was built by Charles Wilson in 1851. However, problems with the cutter technology and mechanical difficulties rendered it inefficient and unable to compete with the already existing drill & blast tunneling technique. It took over a century before this technology was rediscovered and reinstated. In 1952 James S. Robbins designed a TBM to use in the creation of four tunnels in South Dakota. The machine had a diameter of 7.85 m and weighed 114 tons. It had a cutter head consisting of two counter rotating heads, an inner and an outer section. The cutter head was fitted with fixed carbide drag bits radially arranged and parallel rows of freely rolling disc cutters, which were protruding slightly less than the carbide drag bits. However, this TBM was not created for use in hard rock. The first successful hard rock TBM was created by Robbins in 1956. This machine was smaller at a diameter of 3.28 m but it successfully bored through sandstone, shale and crystalline limestone. During the initial time of boring, it was decided to try removing the high wearing carbide drag bits, leaving only disc cutters on the single rotational head. The experiment turned out to be a success, and it became the accepted concept to use disc cutters exclusively in hard rock conditions [1].

A TBM is a machine for constructing tunnels with a circular full-cut cutter head equipped with disc cutters. The rock is cut by simultaneous rotation of the cutter head and the pressure of the blade on the face of the rock [2]. In general, TBMs are fitted with rolling cutter discs at the front of the machine. These discs are thrust against the rock surface with a high force while rotating. The rock material is then crushed and concentric grooves are formed [3]. This process is illustrated in Figure 1.

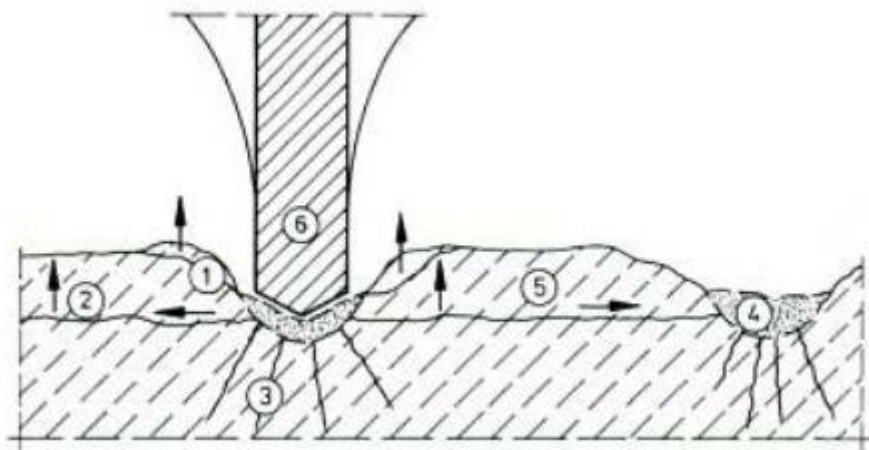


Figure 1 - Schematic diagram of breaking out process of rock by a cutter disc [2].

Where [2]:

- 1) Spalling caused by tension cracks
- 2) Shear failure or tension crack failure
- 3) Formation of radial cracks under the disc
- 4) Flowing of material out of the furrow of the disc
- 5) Typical shape of a larger chip
- 6) Disc cutter with almost constant thickness in cutting area

Depending on the geology of the excavation sites different types of TBMs are employed. In most cases, the ground condition is separated into two parts: Soft ground and Hard rock. There are several different parameters within these two ground conditions which must be evaluated before it can be determined if TBM technology is suitable. There are various types of TBM technology, each of which will be most efficient for specific criteria. Some of these important parameters are listed in Table 1 below [4].

Table 1 – Important characteristics of soil and rock to be identified [4].

Soil characterization	Rock characterization
<ul style="list-style-type: none"> - Soil density, wet and dry - Water content - Grain size distribution - Pore volume - Abrasiveness (grain shape and hardness) - Atterberg limits (when clay is present) - Mineralogical analysis – where relevant - Elastic modulus and Poisson ratio - Cohesion - Permeability - Angle of friction - Undrained shear strength 	<ul style="list-style-type: none"> - Rock density - Petrography - Abrasiveness, content of quartz - Mineralogical analysis – where relevant - Elastic modulus and Poisson ratio - Cohesion - Permeability - Angle of friction - Unconfined compression strength - Tensile splitting strength - Triaxial strength - Swelling capacity - Schists/bedding - Fissuring - Stability - RQD-value

2.1.1 Hard Rock TBMs

The definition of "hard rock" can easily lead to controversy, however, according to Odd G. Askilsrud a common definition of the term includes [1]:

- Unconfined compressive strength of the rock exceeding approximately 50-100 MPa
- A mineral matter that cannot economically be excavated by a road header.
- Something hard, consolidated and/or load bearing, which, where necessary, has to be removed by blasting.
- A rock sample that requires more than one blow by a geology hammer to split.
- Metamorphic and igneous rocks (i.e. not sedimentary rock)

In hard rock tunnel boring the disc cutters thrust into the rock surface with brute force. The cutters will penetrate the rock face with a certain depth. When the cutter tip is in contact with the rock face, the rock is crushed to powder. From this, cracks will propagate towards adjacent grooves which will cause pieces of rock to detach from the rock surface. A minimum thrust force is usually required depending on the type of rock and its properties. Among the most important parameters for TBMs is the quality of the cutter ring steel, which will be elaborated in the upcoming chapters [1].

There are several different TBM systems which can be used in tunnel boring [5]:

- Gripper
- Enlargement
- Shielded (Single shielded)
- Telescopic/double cylinder/gripping jacket

In Figure 2, a schematic of the different types of TBMs are presented.

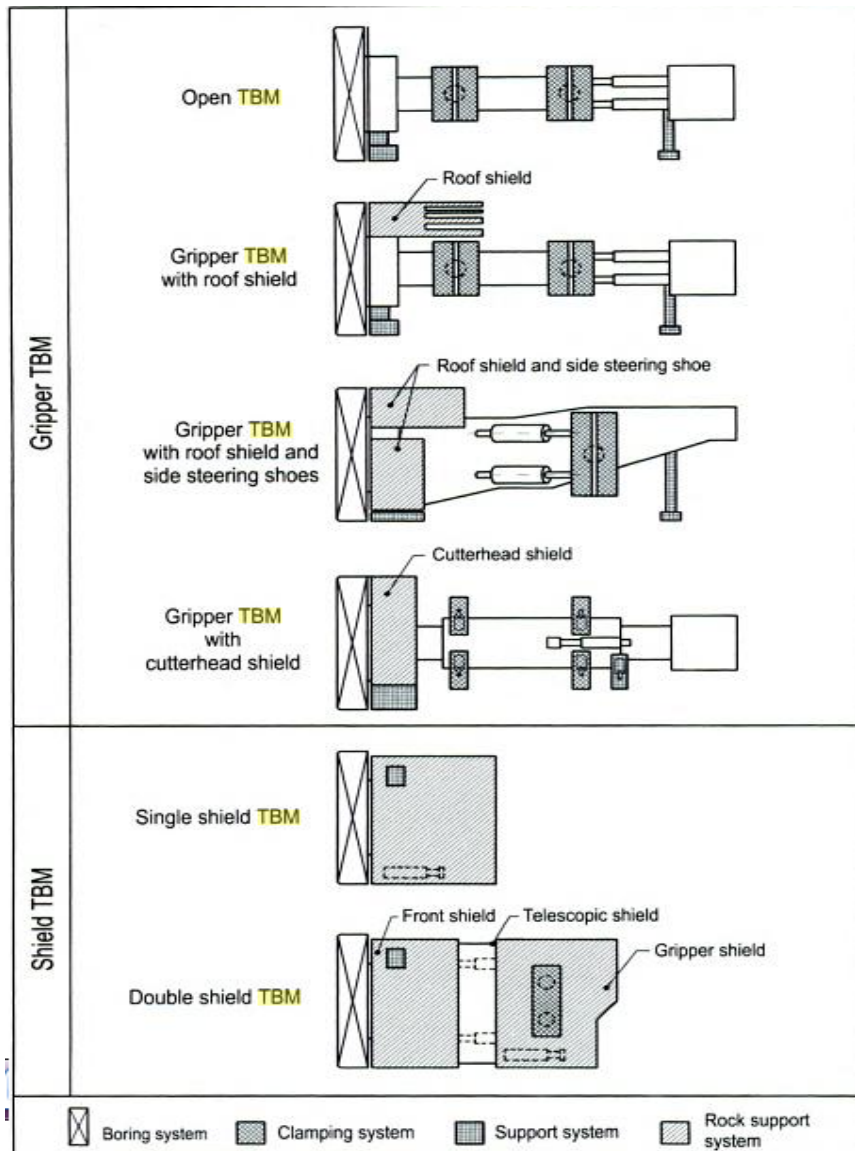


Figure 2 - Overview of various TBM systems with full-face excavation [2].

Gripper TBM

The gripper TBM, also often described as open TBM, is the classic form of tunnel boring machines [2]. Both the gripper TBM and the enlargement TBM belong to the category of open full-face gripping machines. These machines are suitable for all ground classes with medium to high “stand-up” time. The gripper TBMs are most economically used when the rock does not need constant support from rock anchors, steel arches or even shotcrete. The gripper TBMs produce thrust behind the cutter head by bracing radially against the tunnel wall using hydraulically moved clamping shoes, the so-called grippers. As time has passed, two different gripper types have been developed, single clamping and double clamping [2]. As illustrated in Figure 2 the gripper TBMs are further categorized into open TBMs, TBMs with roof, with partial shield, and with cutter head shield. A picture of a gripper TBM is shown in Figure 3 [5].

Enlargement TBM

The enlargement TBM system consist of two separate machines [5]:

- A pilot tunnel gripper TBM and
- An enlargement TBM

First, a pilot heading is driven along the entire length of the tunnel by the pilot gripper TBM. Afterward the enlargement TBM is used. The enlargement machine is equipped with an advanced gripper system that stabilizes itself on gripper plates in the previously created pilot heading. The back-up system is attached to the enlargement TBM, as in the case of other TBMs [5]. A picture of an enlargement TBM is shown in Figure 4.

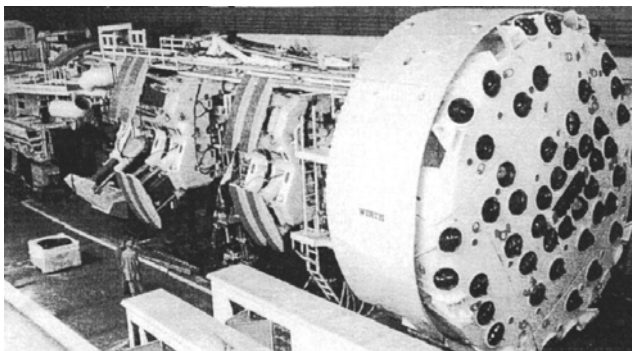


Figure 3 - A gripper TBM [5].

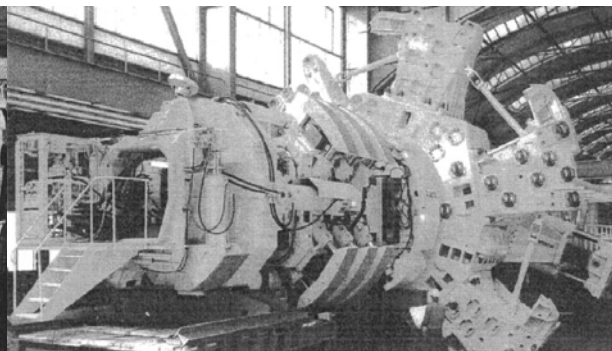


Figure 4 - An enlargement TBM [5].

Single shielded TBM

One of the main things that separate the Single shielded TBMs from the gripper TBMs is that single shielded TBM thrust forward with thrust jackets directly against the existing tunnel support. The single shielded TBMs are primarily used in hard rock with short stand-up time and in fractured rock. The cutter head is essentially not different from that of a gripper TBM in relation to excavation tools and muck transport. This TBM is equipped with a shield to protect the machine and the crew working with it. The shield extends from the cutter head over the entire machine and the tunnel lining is installed under the protection of the shield tail, where concrete segments are the most commonly used support system. According to geology and the application of the tunnel, the segments are either installed directly, or a temporary lining is set in with the later addition of in-situ concrete skin [2]. A picture of a single shield TBM is presented in Figure 5.

Double shield or telescopic TBM

The double shield or telescopic TBM is a variant of the shield TBM. It enables driving in fractured rock with low stand-up time, but has some differences from the single shield TBM. The double shield TBM consists of two main components, the front shield and the gripper or main shield. Both shield parts are connected with each other with telescopic jacks. The shield can move by two different methods. It can either clamp itself radially in the tunnel using the clamping units of the gripper shield; or where the geology is bad, it can push off the existing lining in the direction of the drive [2]. A picture of a double shield TBM is presented in Figure 6.

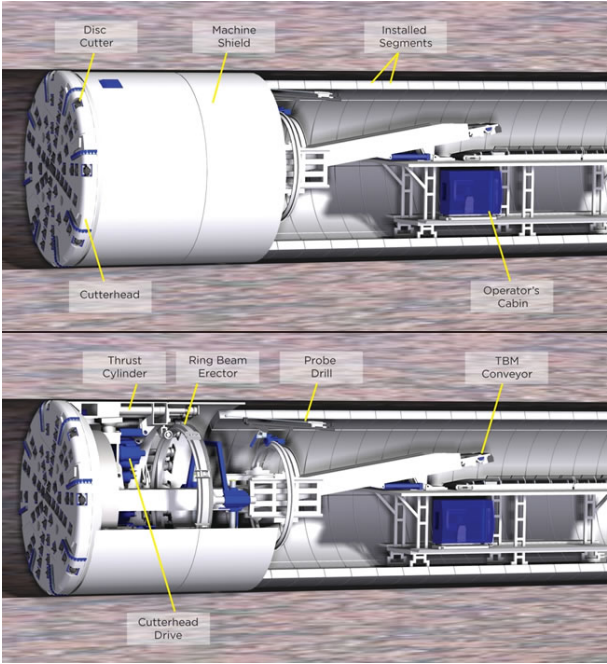


Figure 5 - A single shielded TBM [6].

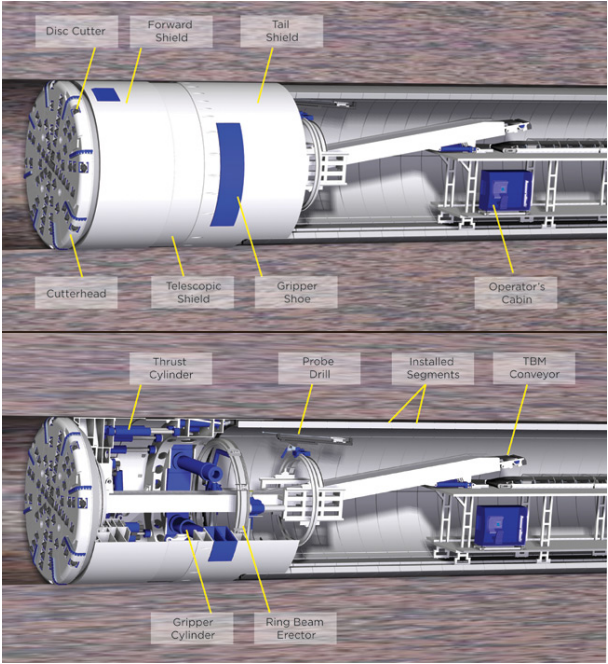


Figure 6 - A double shielded TBM [6].

Rock Characterization

The rocks which are encountered during excavation can have a very varied composition and therefore very different properties. Moh’s hardness is a relative indicator of a minerals resistance to scratching against other minerals. The higher the Moh’s hardness value, the more abrasive the rock is. Quartz is a mineral with one of the highest Moh’s hardness and therefore rocks with a high quartz content normally have high abrasiveness. In Table 2, some hardness values for different minerals are presented. These values could prove useful in evaluating the abrasiveness of different rock types by considering the hardness and composition of its mineral types [4].

Table 2 – Moh’s hardness for different mineral types [7-9].

Mineral type	Mineral	Moh’s Hardness
Feldspar	Plagioclase	6-6.5 [7]
	K-Feldspar	6 [7]
Quartz	Quartz	7 [7]
Mica	Mica	2-4 [8]
Chlorite	Chlorite	2-2.5 [9]

2.1.2 Soft ground TBMs

As with hard rock tunnel boring, the soft ground TBMs uses rotation and thrusting to excavate tunnels. Soft ground is often encountered when building tunnels in urban areas [4]. The mixed ground conditions in soft ground can cause problems for even the most advanced TBMs. Instead of costly changes and adaptations of the machine, it is usually simpler to treat the ground instead, to ensure properties that the TBM can handle. This can be achieved by either pumping water/bentonite slurry into the tunnel front, or by injecting soil conditioning products in front of the cutter head. When boring in soft soil there is generally two different types of TBM to be used: The slurry shield machine and the Earth pressure balanced machine [4].

Slurry shield TBM

The slurry shield TBM is used for tunnel boring in highly permeable unstable terrain, or under structures sensitive to ground disturbances. When digging in highly unstable or liquid terrain, the pressure exerted by the terrain is directly governed by the depth at which the digging is performed. Because of this it is very important to balance the pressure exerted by the terrain. To do this, the front shield of the TBM is filled with excavated material, a slurry, with the exception of one part which is filled with air. The pressure within this air bubble is subject to fine control [10]. The slurry is a vital link between the slurry shield TBM and the ground, and its success will depend on the performance of the slurry. It is therefore important to ensure that the slurry has the correct properties. This includes pH, density, water loss, yield value, plastic viscosity or solids content. To control these properties the slurry needs to be treated. This often consist of dilution, addition of fresh bentonite or additives such as polymers, dispersants or pH stabilizers [4]. The workings of the slurry shield TMB is illustrated in Figure 7.

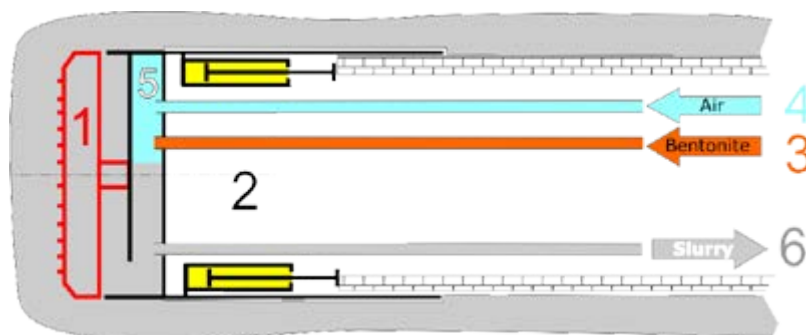


Figure 7 - Schematic illustrating how a slurry shield TBM works [10].

Earth Pressure Balanced TBM

The earth pressure balanced machine is suited for digging tunnels in unstable ground such as clay, silt, sand or gravel [10]. The working principle of the EPB TBM consist of ensuring the stability of the face by pressurizing the excavated spoil contained in the excavating chamber in order to balance the pressure of the ground [11]. The front shield of the EPB TBM is filled with debris extracted by the means of a screw conveyor. This screw compensates the pressure difference between the working face and atmospheric pressure. Additives might also be injected from nozzles at the excavating head to ensure that the spoils of the boring is transformed into a homogeneous paste [10, 11]. To do this foams are often used. They maintain the pressure, fluidize the soil, and reduce the permeability, soil stickiness and abrasion. Different types of additives are used to improve different complications during the tunnel boring. There are special anti-clogging agents used to avoid clogging problems, anti-abrasion additives for the cutter head and its tools as well as for the extraction screw [4]. Figure 8 illustrates how the EPB TBM works.

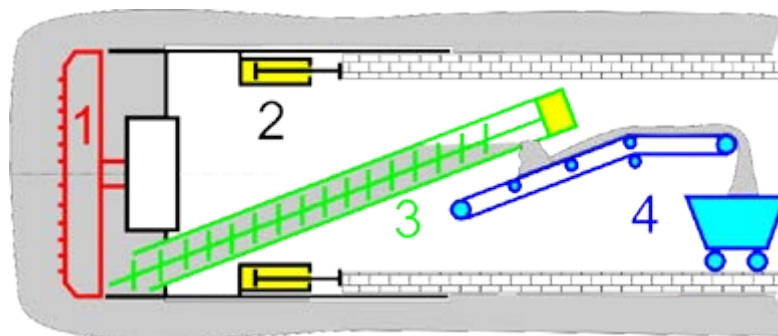


Figure 8 - Schematic illustrating how an earth pressure balanced TBM works [10].

2.1.3 Cutter discs in hard rock TBM operations

Despite considerable advances in cutter technology, cutters remain as one of the limiting factors related to tunnel boring due to the maximum thrust load that the cutters are able to take and the high abrasive wear of the cutter discs. In tunnel boring, one of the most important economic factors is related to cutter wear. This is in part due to incorrect interpretation of geological data, hence the difficulties in accurately predicting the frequency of cutter replacement needs. When cutters wear out, not only is there an increase in cost due to needing new cutters, but also due to long TBM downtime which causes reduction in the advance rates. Replacing the cutters is a time consuming process which brings the entire operation to a standstill [4]. A typical cutter disc design for hard rock tunnel boring is presented in Figure 9 and in Figure 10 the placement of the cutter discs on the TBM face is shown.

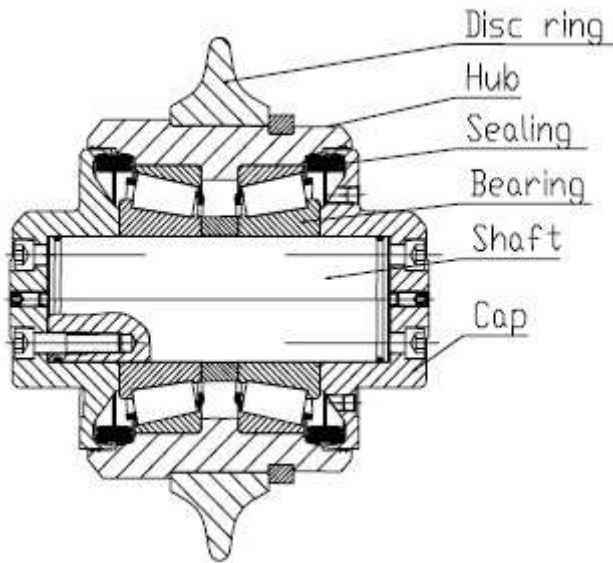
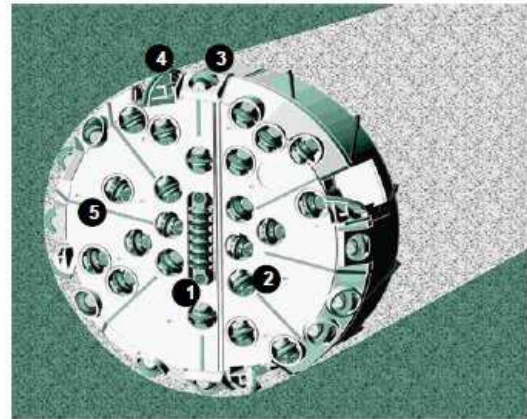


Figure 9 - A typical cutter disc design [4].



1 Centre Cutter
2 Face Cutter
3 Gauge Cutter
4 Scraper
5 Wear Plates

Figure 10 - Cutter disc placement on a TBM [4].

The main factors affecting the cutter wear are [4]:

- Cutter characteristics
- Properties of the rock/soil (strength, hardness, abrasiveness, quartz content)
- Effect of water
- Temperature

Optimization of the cutter steel is largely dependent on the rock type, and involves balancing the steel composition as well as heat treatment in order to obtain the right balance of hardness and toughness. An increase in hardness will come at the expense of toughness. The material may be hard enough to significantly reduce abrasive wear, but then it might not be tough enough to withstand chipping [4]. The corrosion and wear mechanisms will be explored in further detail in the upcoming chapters.

2.1.4 Foam additive lubricant for hard rock tunneling

As mentioned hard rock is normally a problem for the cutters. The cutters become damaged and/or heavily worn and the penetration rate is therefore reduced. The heat that is generated in the cutters by working on hard rock increases cutter wear and may lead to more cutter clogging followed by an increased wear on the cutter heads. This results in increased downtime for the TBM making the tunnel boring a more costly process. An additional problem in hard rock excavation is the formation of dust due to fine particles of the excavated material, which causes a health concern for the workers at the excavation site. To counteract these problems, chemical products have been developed to reduce, clogging, abrasion and wear on the cutter head. The technology is based on special anti-wear foam additives that are injected in front of the cutter head. The foam ensures an optimum distribution of the lubrication across the excavation face. It reduces abrasive wear, cools the cutter head and reduces the formation of dust [4].

In general the foam consists of polymers containing a hydrophilic head and a hydrophobic tail. The hydrophilic head will attach with water while the hydrophobic tail will “trap” air bubbles. This is what makes the foam expand when air is introduced into the solution [12]. Due to little information from the production company of the foam there is little information on how the foam actually works. But it is believed that the polymers create a film on the metal surface and thereby decrease the coefficient of friction. However, this will be discussed later in section 2.4.3.

2.2 Metallurgy

Steel is a term which includes a wide variety of iron alloys with very different properties. It is important to know some of the basic structures and processes which allow for these different properties.

The atomic and ionic arrangements of crystalline materials such as metals can be described by seven general crystal systems. Among these systems are: BCC (body-centered cubic), FCC (face-centered cubic) and HCP (hexagonal close-packed), all shown in Figure 11. Most structural metals crystallize into one of these three crystalline patterns. The BCC pattern is the most common in metal structures. These patterns affect the properties of the metal. In FCC metals, the critical resolved shear stress is low and an optimum number of slip planes are available, consequently, FCC metals tend to be ductile. In BCC metals, no close-packed planes are available and the critically resolved shear stress is high; thus, the BCC metals tend to be strong. The number of slip systems in HCP metals is limited, causing these metals to behave in a brittle manner [13].

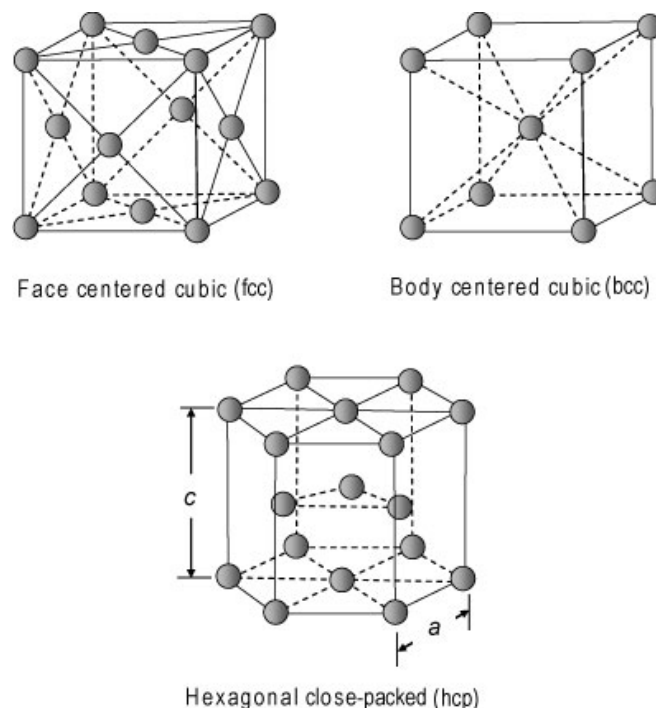


Figure 11 - Common metallic crystalline systems.

In addition to the crystalline structure, the mechanical properties of materials depend on their composition and microstructure. The composition, nature of bonding, crystal structure, defects, impurities, and grain size will all have a profound influence on the strength and ductility of the material. All of these are easily affected by material processing. The production method will therefore influence the final properties of the metal. The microstructure of the metal can be altered by hot- and cold working, annealing and quenching [13].

Products which are die forged are exposed to forces that plastically deform the metal. This is a form of cold working that introduces dislocations into the metallic structure, causing hardening of the metal. This method allows for a very high increase in strength of the metal, however, the ductility is also reduced. When a metal is cold worked, the grains rotate as well as elongate in the direction of the applied stress. Therefore a die forged product will achieve higher/lower strength at different areas depending on its shape and direction of applied stress. The plastic deformation allows forming of the product to its final shape, but it also strengthens the metal at the cost of ductility. In some cases one does not want to sacrifice all or any of the ductility for strength, therefore, it is common to heat treat the steel after cold working. This is called annealing, and it consists of three stages. First, there is a recovery stage. After cold working the microstructure of the metal is composed of mostly deformed grains containing large numbers of tangled dislocations. When the metal is heated, the additional thermal energy permits the dislocations to move and form the boundaries of polygonized subgrain structures. This low-temperature treatment removes residual stresses due to cold working without changing the dislocation density. The mechanical properties remain relatively unchanged, but the residual stresses are reduced if not completely removed. The corrosion resistance is often improved. The next stage is called recrystallization. Above a certain temperature new small grains nucleate at the cell boundaries of the polygonized structure, eliminating most of the dislocations. Because of this the recrystallized metal has low strength but high ductility. The last stage is grain growth. At an even higher temperature than the recrystallization temperature the grains begin to grow, with favored grains consuming the smaller grains [13].

2.2.1 Steel

The steel cutters used in TBMs are exposed to high forces and abrasive surfaces. Because of this the steel has to be able to withstand tough working conditions, which makes high strength a requirement. However, it is important to consider that strengthening of steel usually comes at the cost of higher brittleness, which is not ideal when used for tunnel boring [13].

Steel is a hard, strong, durable, and malleable alloy of iron and carbon. Iron is generally classified as steel if it has a carbon content of between 0.2 and 1.5 percent. Adding alloying elements to steel is often done in order to obtain the desired mechanical properties. They are added to steel to [13]:

- a) Provide solid-solution strengthening of ferrite
- b) Cause the precipitation of alloy carbides rather than that of Fe_3C
- c) Improve corrosion resistance and other special characteristics of steel
- d) To improve Hardenability

Hardness is an important factor related to wear. Hardenability is a term to describe the ease with which a steel can form martensite, which relates to how easily we can form martensite on a thick section of steel that is quenched [13]. One of the most common routes to strengthen steel is by quenching in order to form martensite and then reheat or temper at an intermediate temperature which will increase the toughness of the steel without too great a loss in strength. The cooling needs to be sufficiently rapid to avoid decomposition of austenite into products such as ferrite, pearlite and bainite. The effectiveness of the quenching will depend primarily on two factors: the geometry of the specimen and the composition of the steel [13].

Different alloying elements will have different effects on the steels properties. Some common alloying elements and their effect on the steel properties are listed below [14, 15]:

- Carbon:
 - Primary hardening element in steel
 - Hardness and tensile strength increases as carbon content increases up to about 0.85% C
 - Ductility and weldability decreases with increasing carbon
- Manganese:
 - Beneficial to surface quality, especially in resulfurized steels
 - Contributes to strength and hardness, but less than carbon
 - Ductility and weldability decreases with increasing manganese, but less than carbon
 - Significant effect on hardenability
- Phosphorus:
 - Increase strength and hardness
 - Decrease ductility and notch impact toughness
- Silicon:
 - Improves strength, elasticity and acid resistance
 - Detrimental to surface quality in low carbon steels
- Nickel:
 - Austenite stabilizer
 - Remains in solution in ferrite, strengthening and toughening the ferrite phase
 - Does not form carbides in steel
 - Increases hardenability and impact strength
- Chromium:
 - Ferrite stabilizer
 - Increase corrosion and oxidation resistance
 - Increase hardenability and wear resistance
 - Improve high temperature strength
 - Used as hardening element with a toughening element such as nickel to produce superior mechanical properties
- Molybdenum:
 - Increases hardenability
 - Enhances creep strength of low-alloy steels at elevated temperatures
 - Increases resistance to chloride penetration

- Vanadium:
 - Increase strength
 - Increase hardness
 - Increase creep and impact resistance
 - Ferrite stabilizer
 - Forms hard carbides

The mechanical properties of steel are not only determined by the alloying elements, but also the subsequent heat treatment. Heat treating is vital for achieving optimal physical properties. If a hard martensitic steel is tempered structural changes will occur in the steel which effectively changes its properties. The tempering temperature is vital for strength and toughness. Higher temperature increases the toughness, but will decrease the strength, and vice versa. It is important to consider these aspects when choosing a steel for a certain purpose. To obtain optimal properties of the steel both alloying elements and the subsequent treatment, either mechanical or tempering, should be carefully considered [16].

The steel used in this master thesis is described as H13 Modified steel which is currently also the reference steel in tunnel boring processes. The cutter discs are closed die forged, rough machined, heat treated, and then finish machined. The alloying elements in the H13 steel are:

- Carbon	0.43 – 0.46
- Manganese	0.20 – 0.50
- Silicon	0.80 – 1.20
- Chromium	5.00 – 5.50
- Vanadium	0.08 – 1.20
- Molybdenum	1.20 – 1.75
- Sulphur	0.015 max
- Phosphorus	0.015 max
- Iron	89.36 – 92.29

2.3 Corrosion mechanisms

Steel is an active-passive metal alloy, meaning that corrosion may occur depending on the pH-value of the water it is in contact with and the electrical potential. In tunnel boring there will always be water present and in some cases it is sea water or water containing salts and minerals from the ground, which will affect the corrosion rate of the steel [17].

One of the main conditions for corrosion in natural water is the presence of oxygen. The oxygen content in water and its diffusivity into the metal is often the rate controlling step. This especially applies to unalloyed and low alloy steels. Stainless steels however, are under anodic control. Unlike with atmospheric corrosion, the quality and composition of the steel has little effect on the corrosion in natural water because the composition and treatment of the steel has little effect on the barrier properties of the steel's outer layer. However, in the pH region <4 and >10 the composition of the

steel will impact the corrosion. In these areas hydrogen formation and passivation will occur respectively. At low pH levels the corrosion rate will increase with increasing C-, N-, P- and S-content and cold working. This is caused by reduced polarization for hydrogen reduction and partially for anodic dissolution reaction [17].

The pH-value of sea water is normally around 8-8.3, but with cathodic production of OH⁻ the pH will increase to the level of precipitation of CaCO₃ and some Mg(OH) and iron oxide. The precipitants will create a layer which will greatly prevent oxygen diffusion. In fact, the corrosion rate may be lower for steel in sea water than in regular soft water. Figure 12 shows the relative corrosion rate for iron with different concentrations of sodium chloride [17].

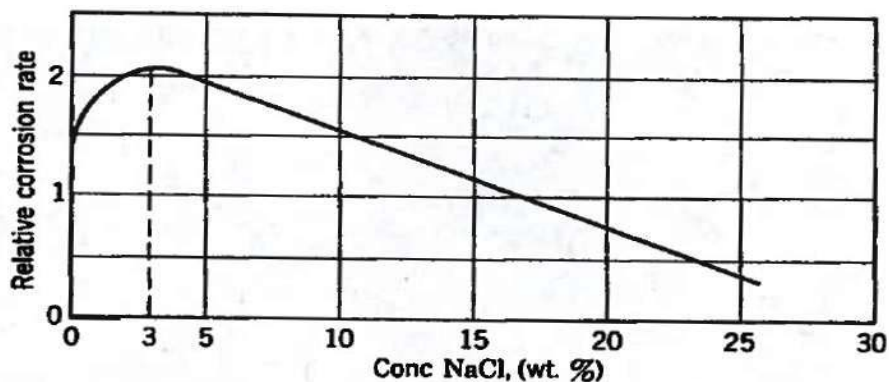


Figure 12 - Effect of NaCl on corrosion rate for steel [17].

One of the main corrosion types that will occur during tunnel boring is uniform corrosion. This type of corrosion occurs uniformly over the metal surface but is not considered especially dangerous due to the fact that the material loss is easily predicted. The corrosion rate can also be decreased by coating, inhibitors, etc. However, in the tunnel boring industry, it is not common to use corrosion protection methods. Because of this, material choices needs to be made by carefully considering the material loss and effects on the wear rate of the disc cutters [17].

Corrosion occurs when a metal is exposed to an electrolytic conducting liquid, known as an electrolyte, and the circuit becomes closed by ionic conduction through the electrolyte. In the corrosion process at least two reactions will always occur, a cathodic and an anodic reaction [17]. In the case of corroding iron the following anodic reaction takes place:



In water there are two possible cathodic reactions [17]:

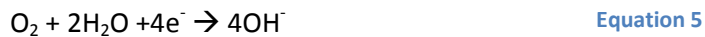


Which of these two reactions dominate the most will depend on the pH-level. In diluted strong acids saturated with air, the two will be fairly similar. However, the hydrogen reaction will dominate at low pH-levels while the oxygen will dominate at higher pH-levels [17].

By studying the reaction from Equation 3 one can see that in addition to having available oxygen the reaction also requires H^+ -ions (protons), which we usually only find in acidic solutions where the H^+ concentration is large. However, the oxygen reduction can take place in neutral and alkaline solutions as well because of the dissolution of oxygen in a process called depolarization [17]:

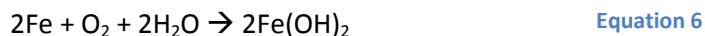


Combining Equation 3 and Equation 4 gives the following reaction [17]:



In acidic solutions the reaction from Equation 3 will describe the oxygen reduction, while the reaction in Equation 5 will describe the oxygen reduction for neutral and alkaline solutions [14].

In neutral/alkaline environments such as natural or salt water, the reaction of the overall corrosion process will be the combination of Equation 1 and Equation 5 [17]:



$Fe(OH)_2$ however, is not very stable and with access to water and oxygen, it will oxidize to hydrated iron oxide $Fe_2O_3 \cdot nH_2O$, iron oxide $Fe(OH)_3$ or $FeOOH + H_2O$ where $FeOOH$ is the typical red/brown rust. With little access to oxygen Fe_3O_4 is formed which is black (without water) or green (with water). The hydroxide film will cause a decrease in the corrosion rate. This is because the oxygen will have to diffuse through this precipitated layer and into the metal to cause further corrosion. The corrosion process of a hypothetical divalent metal, which is the same for iron, is shown in Figure 13 [17].

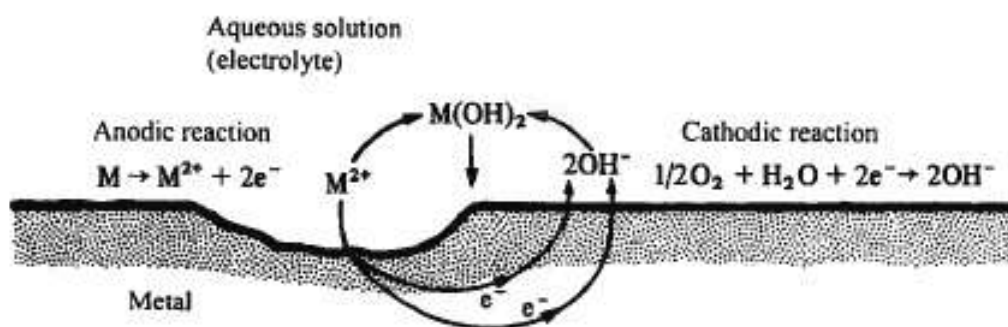


Figure 13 - Corrosion of a divalent metal M in an oxygen containing electrolyte [17].

2.3.1 Pitting

Pitting is a severe form of corrosion that can occur during tunnel boring. In contrast to uniform corrosion, whose rate is normally predictable, pitting corrosion tends to proceed at an unexpected and high rate of localized metal dissolution [18]. Pitting usually occurs on passivated metals and alloys in corrosive mediums containing chlorine-, bromine-, iodine or perchlorate ions when a certain critical value has been reached, called the pitting potential, see Figure 14. The pitting potential is not a thermodynamically defined potential and it is dependent on the rate of potential increase during recording of the polarization curve [17].

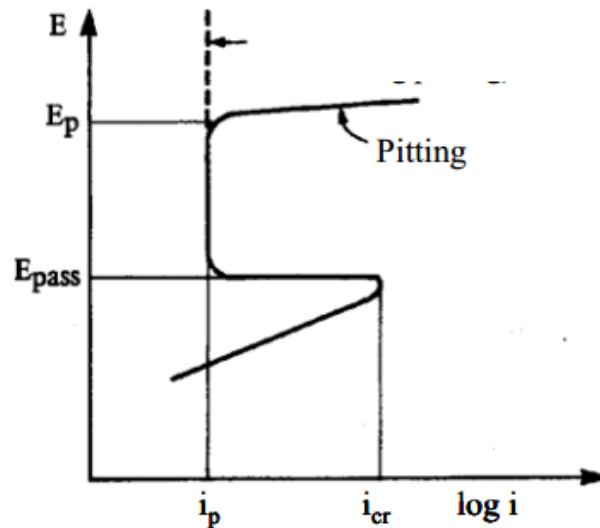


Figure 14 - Anodic over potential curve for an active-passive metal in a pitting environment. E_p = pitting potential, E_{pass} = passivation potential, i_{cr} = critical current density and i_p = passive current density [17].

This form of corrosion is characterized by narrow pits with a radius of the same order of magnitude as, or less than, the depth. The pits can have different shapes, but a common feature is the sharp boundaries. Some different pit shapes are illustrated in Figure 15 [17].

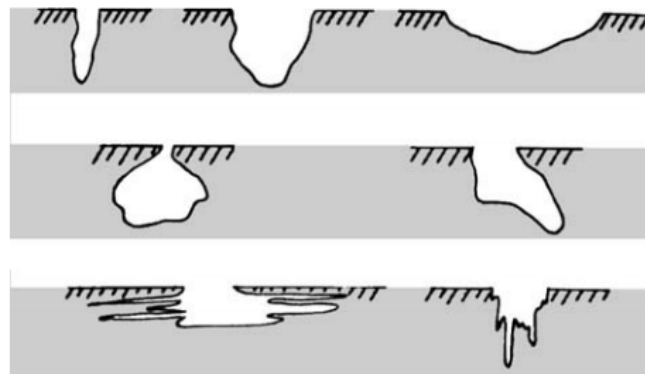


Figure 15 - Different shapes of corrosion pits [17].

Because of its shape, pitting can be difficult to observe. It is a dangerous form of corrosion because the metal in many cases can be penetrated without warning, and the corrosion is difficult to predict. This is a result of the extent and intensity of pitting corrosion, since it is very difficult to measure because the size and number of pits vary from region to region. Short-term testing in the laboratory for determination of pit growth is also problematic because, under realistic conditions, it may take longer time, before the pits become visible [17].

Pitting occurs in two stages: initiation and growth. Depending on how passivating the metal is, the pitting will initiate with pores in the top layer of the corrosion product, or it can initiate by halogen ions adsorbing and diffusing through the passive layer in certain places [17].

After initiation, the pits will start to grow. An anodic reaction will occur in the bottom of the pit, while a cathodic reaction occurs on the outside of the pit. This causes a charge difference, which causes negatively charged ions, e.g. chlorine ions, to migrate into the pit. This will cause iron chloride to hydrolyze, which will then cause the formation of hydrochloric acid. The hydrochloric acid causes the pH to decrease. The iron ions which are created inside the pit, will migrate and diffuse out of the pit. At the surface, dissolved iron chloride will react with the products from the cathode reaction and create iron hydroxide which will increase further corrosion by preventing replacement of the electrolyte in the pit, which becomes very acidic and aggressive [17].

There are several factors which influence pitting corrosion [17]:

- pH and chloride concentration. The pitting potential increases and pitting corrosion decreases with increasing pH and decreasing chloride concentration.
- Flow rate. Increased flow rate causes smaller but more pits and renders the pitting corrosion less severe.
- Gravitational force. Horizontal surfaces facing up are more susceptible to corrosion than surfaces facing down. Vertical surfaces are in between.
- Fe^{2+} ions accelerate the corrosion by increasing the potential.
- Metallurgical properties.
- The insulating abilities of the oxide layer. If the oxide layer insulates well, the surface will be ineffective as a cathode and pitting corrosion will seize or slow down.
- Surface roughness. Smooth surfaces get few, large pits, while rough surfaces get many, small pits.
- Temperature. Increasing temperature normally results in decreasing pitting potential causing an increase in pitting.
- Galvanic coupling with nobler metals causes an increasing tendency and rate for pitting to occur.

2.3.2 Pourbaix diagram

The pH is an important parameter for fluids and it greatly affects the equilibrium potential for a many of the electrode reactions. With this in mind, Marcel Pourbaix created a pH-potential diagram, also known as a Pourbaix diagram. These diagrams have become a very important tool for corrosion research. The Pourbaix diagram is basically a graphic representation of Nernst's equation for the relevant reactions occurring in a specific corrosion scenario. A Pourbaix diagram for iron in water at 25 °C is shown in Figure 16. It is based on the following reactions which may occur during the corrosion of iron [17]:

- | | |
|--|-------------|
| a) $\text{Fe}^{2+} + 2\text{e}^- = 2\text{Fe}$ | Equation 10 |
| b) $\text{Fe}_3\text{O}_4 + 8\text{H}^+ + 8\text{e}^- = 3\text{Fe} + 4\text{H}_2\text{O}$ | Equation 11 |
| c) $\text{Fe}_3\text{O}_4 + 8\text{H}^+ + 2\text{e}^- = 3\text{Fe}^{2+} + 3\text{H}_2\text{O}$ | Equation 12 |
| d) $\text{Fe}_2\text{O}_3 + 6\text{H}^+ + 2\text{e}^- = 2\text{Fe}^{2+} + 3\text{H}_2\text{O}$ | Equation 13 |
| e) $\text{O}_2 + 4\text{H}^+ + 4\text{e}^- = 2\text{H}_2\text{O}$ | Equation 14 |
| f) $2\text{H}^+ + 2\text{e}^- = \text{H}_2$ | Equation 15 |

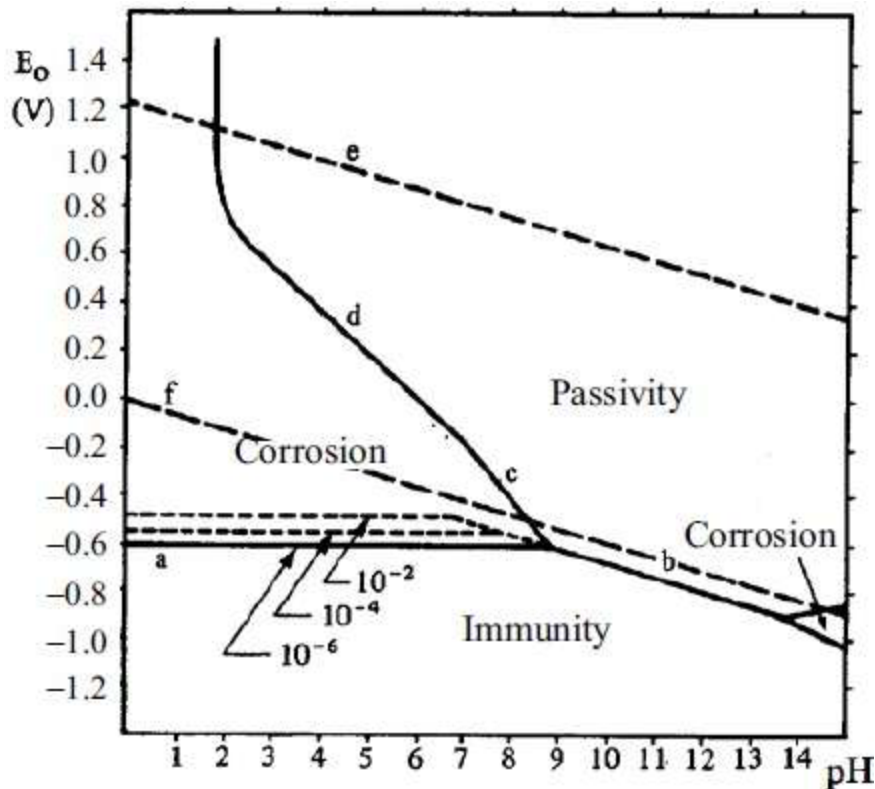


Figure 16 - Pourbaix diagram for iron in water at 25 °C [17].

It is assumed that the activity of the ferrous ions is $a_{\text{Fe}^{2+}} = 10^{-6}$ which is considered to be a bottom value for corrosion of significant importance [17].

As seen from reaction a) the equilibrium potential increases with increasing iron ion activity. If the potential is then increased to a value above the ion activity, the system will try to restore equilibrium- This can only happen by an increase in Fe^{2+} -activity, in other words corrosion [17].

Above the lines of reaction b), c) and d) the metal is in an oxidized state. A layer of oxides creates a diffusion barrier, causing the metal surface to passivate [17].

Below the lines of reaction a) and b) the metal is stable and is therefore immune to corrosion [17].

While Pourbaix diagrams can be extremely useful in establishing regions of immunity as well as corrosion and passivation for a metal/solution system, they do not provide any direct kinetic information. The real rate of corrosion and extent of passivation are not evident from a simple examination of the diagrams. Some oxides dissolve very slowly in certain solutions, driven by kinetics rather than thermodynamic mechanisms. The information given in the Pourbaix diagram are for thick, bulk oxides, which may be different from the very thin surface oxides films found on passivated metal surfaces [19].

2.3.3 Polarization

During polarization, the potential for the electrode reactions are shifted from equilibrium due to a net electrode reaction; a net current flows through the metal-liquid interface. The polarization can be measured by studying the over potential, which is the difference between the real potential and equilibrium potential. When corrosion occurs on a surface, the real potential on the surface must have a value in between the equilibrium potential for the anodic and the cathodic reactions [17].

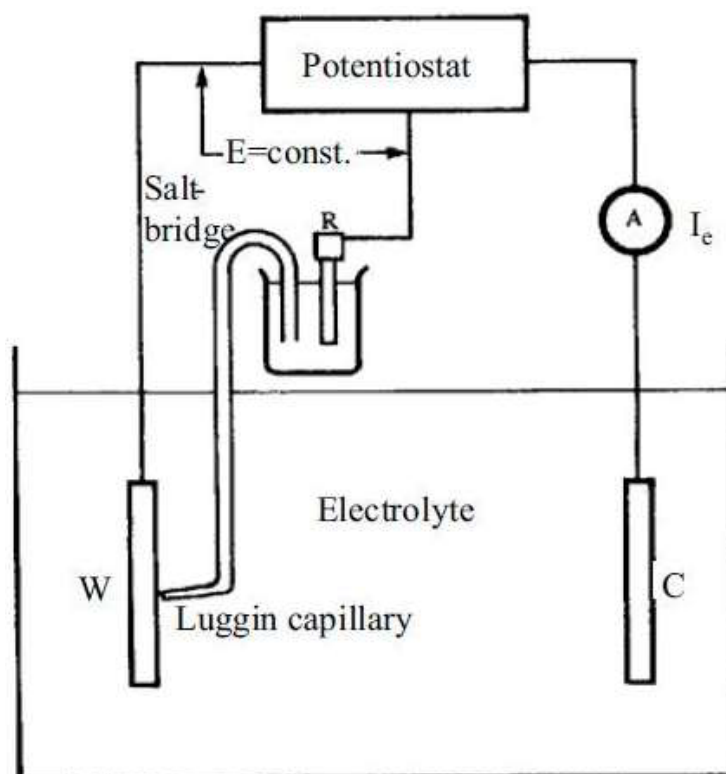


Figure 17 - Wiring diagram for potentiostatic experiments [17].

A potentiostat is an apparatus that holds a set electrode potential (on the material which is being tested) and delivers the required current to keep the potential constant. As shown in Figure 17, a potentiostat has three electrodes [17]:

1. Working electrode (material which is being tested), W
2. Counter electrode, C
3. Reference electrode, R

It is assumed that two reactions can occur at the working electrode with over potential curves and corrosion potential as shown in Figure 18.

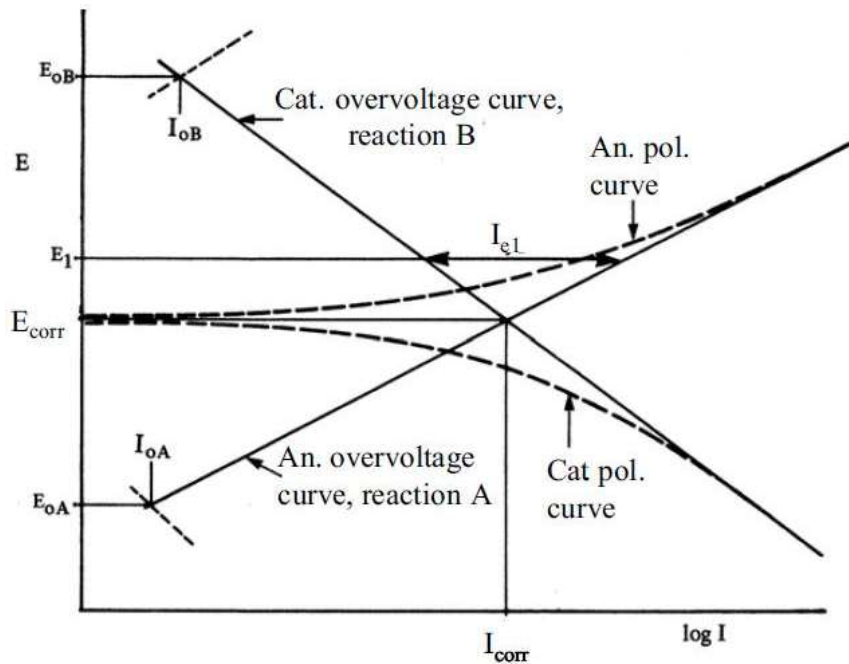


Figure 18 - Over potential curves and corresponding polarization curves [17].

When $E = E_{\text{corr}}$ no outer current is fed to the working electrode. By using the potentiostat to set an arbitrary potential E_1 , an outer current will be delivered, I_{e1} , which is the difference between anodic and cathodic reaction current at this potential. By plotting the outer current as a function of the potential, one gets polarization curves as shown in Figure 18 (the dotted lines) [17].

The rate in which the potentiostat scans during a polarization test, will affect the outcome of the test. A high scan rate will give results indicating where intense anodic activity is likely. The high speed scan has the object of minimizing film formation, so that the currents observed relate to a relatively film-free or thin film conditions. At slow scan rates of the potential range, the scan will indicate regions where relative inactivity is likely. A zero-scan rate provides the opportunity for maximum stability of the metal surface, but at high electropositive potentials, the environment could be affected or changed. In general corrosion tests should be conducted using several different parameters to ensure a broad aspect of information, which allows for better understanding of the processes involved [20].

The magnitude of the applied potential can be regarded as a measure of the oxidizing power of the corrodent, while $\log I$ reflects the rate of each reaction. From the shape of the produced curve several important facts can be collected from a polarization curve such as: kinetics of the corrosion reactions, protectiveness of a passive film, ability of a compound to act a corrosion inhibitor, relative corrosiveness of process streams, and corrosion rate of the metal. However, this information can be hard to obtain. In a case with an alloyed metal and a corrodent containing several possible corrosive elements the curves will be more difficult to analyze due to effects on the electrode reactions [17]. In Figure 19 the theoretical and measured behavior of an active-passive alloy is shown [20]. The polarization curve for iron is presented in Figure 20 where the different areas of immunity, activity, passivity and trans passivity of corrosion are displayed [17].

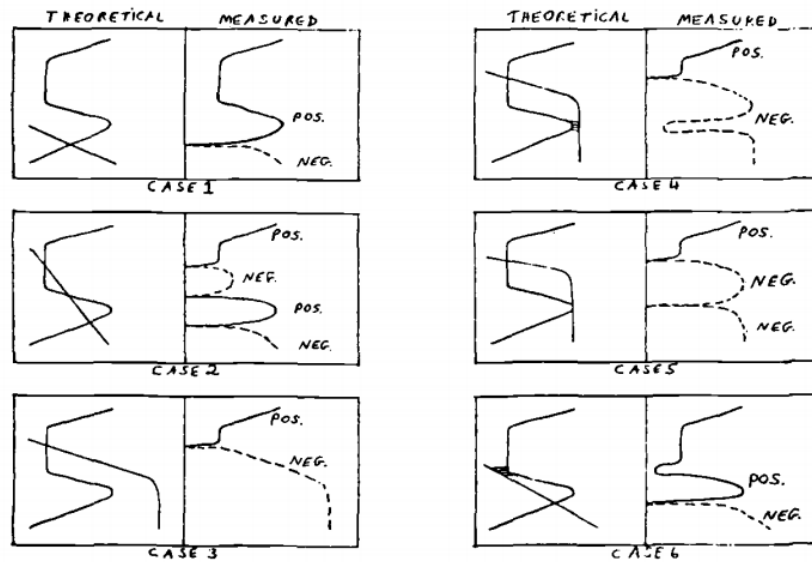


Figure 19 - Six possible types of behavior for an active-passive alloy in a corrosive environment [20].

Case number 1 in Figure 19 illustrates the polarization curves of normal corrosion of an active passive metal. In case number two, the cathodic line intersects with the anodic line at several different places, including the passive area. This is called unstable passivation and will be discussed later in this thesis. Case number 3 passivation of the metal is achieved because the corrosion potential is in the passive region. In case 4 the cathodic curves almost intersects at the critical current density and in the passive region. This leads to a large drop in the current density at this point, and a corrosion potential in the passive region. In case 5, unlike case 4, the cathodic curve intersects with the anodic curve at the critical current density. This causes unstable passivation. In case 6 the corrosion potential is in the active region, however, cathodic curve also grazes the anodic curve in the passive region, causing a drop in the current density.

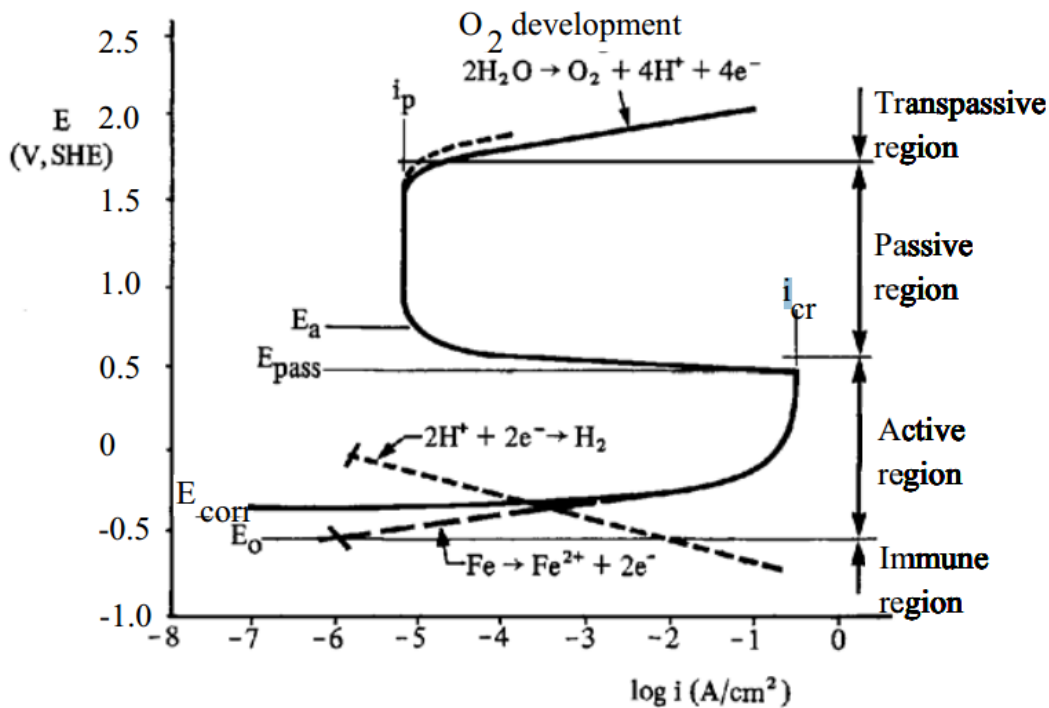


Figure 20 - Anodic polarization and over voltage curve for iron in sulfuric acid [17]

Both quantity and quality of a corrodent will affect the generation of polarization curves. But quantitatively they are also highly dependent on other factors such as surface conditions, temperature, flow rate, and geometry. These various factors can have different impacts depending on the conditions and environment. The surface condition can influence the current density. Coatings and fluid films on the surface, temperature, and the flow rate greatly influences the diffusion controlled corrosion, and the geometry will play a major role considering galvanic corrosion and cathodic protection [17].

3.3.3 Passivation

As previously mentioned, some metals like iron can passivate and thereby prevent further corrosion. Passivation is generally ascribed to the presence of a thin oxide film 1-4 nm thick that isolates the metal surface from the corrosive aqueous environment [19]. The reason for this passivation can be described by two competing theories: 1. the passivation can be a result of an oxide film on the surface or 2. it can be a result of a process which can be perceived as adsorption of oxygen on the metal surface [17].

A typical passivating oxygen film can be characterized by low ionic conductivity and low solubility which causes the film to efficiently prevent the transfer of metal ions from the metal to the liquid thereby preventing the anodic dissolution. The low ionic conductivity is due to the density of the film, which is assumed to be formed at the metal surface allowing for a more structural connection to the metal. Because of this and because of the low thickness of the film, many oxide films can conduct

electrons so that electrochemical reactions can occur on the outside of the film. The passivating films can be separated into three different groups [17]:

- a) Films which efficiently prevent anodic dissolution but not cathodic reaction. (The film is electron conducting but not ion conducting.) Examples of these films are typical passivating films on Fe, Ni, Cr and their alloys. In these instances the oxygen reduction can easily occur on the outside of the film.
- b) Films which greatly prevents both the anodic and the cathodic reaction. A typical example of these types of films is the passivating film occurring on aluminum, which in contrast to the films on Fe, Ni and Cr highly resists electron diffusion. However, the oxide films contain imperfections allowing for some electron conduction and cathodic activity.
- c) A covering layer which prevents anodic and cathodic reaction to some extent but usually not good enough to allow proper passivation. This is a porous layer, like rust or salt deposits, which precipitates from the liquid as a result of saturation. It is assumed that the oxygen reaction in this instance will occur on the metal at the bottom of pores, and that it slowed as a result of the covering layer which decreases the diffusion of oxygen close to the metal. The pores allow for anodic reaction to occur but this is also more or less slowed by the covering layer.

For a metal to become passive its potential must exceed the passivation potential. This can happen in two ways: by anodic polarization or by reaction with an oxidizing agent. In a weakly oxidizing solution an anodic potential of $E > E_p$ must be applied by connecting the metal as an anode in an electrochemical cell. An anodically passivated metal generally loses its passivity as soon as the electrical circuit is turned off. In a strongly oxidizing solution, the oxidizing agent causes a spontaneous passivation of the metal. The corrosion potential in this case is located in the passive region: $E_p < E_{corr}$. Figure 21 illustrates how the presence of an oxidizing agent affects the observed polarization behavior of a metal. In the absence of an oxidizing agent, the corrosion potential is located in the active region. However, when the oxidizing agent is present, the corrosion potential is located in the passive region. It should be noted that the active-passive transition in the polarization curve of the steel and oxidizing agent is hidden by the cathodic partial current for the reduction of the oxidizing agent [21].

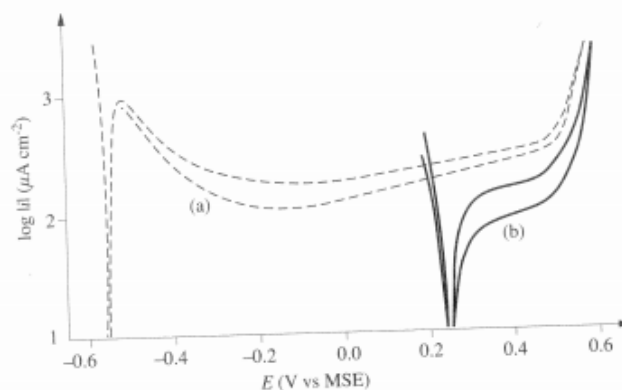


Figure 21 - Anodic polarization curve of Fe-66Ni-16Mo in 50% H₂SO₄ in absence (a) and in presence (b) of the oxidizing agent (Fe₂(SO₄)₃) [21].

In some cases the anodic and cathodic partial current densities may intersect at two points, as shown in Figure 22. In these situations the corrosion potential can be located in either the active or the passive region, depending on the preceding surface treatment. A surface that has been activated beforehand will remain active, while a surface that has been previously passivated will maintain its passive state. However, this is true only as long as the oxide film is not mechanically damaged. This phenomenon is called unstable passivity [21].

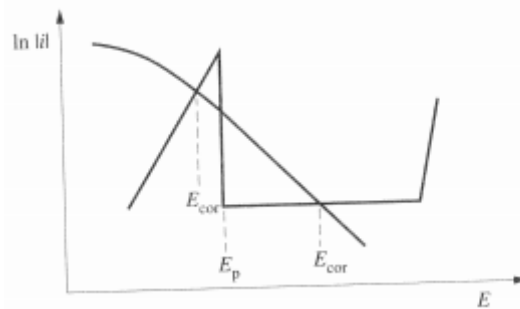


Figure 22 - Evans diagram showing a situation of unstable passivity. The corrosion potential can be located in either the active or passive region [21].

A metal that passivates spontaneously in a given environment will resist corrosion better than a metal exhibiting a corrosion potential in the active region. For a passivation to be spontaneous and stable, two conditions must be fulfilled:

$$E_p < E_{rev,ox}$$

$$i_p < |i_{c(E_p)}|$$

Where E_p is the passivation potential, $E_{rev,ox}$ is the reversible potential of the oxidizing agent, i_p is the passivation current density and $i_{c(E_p)}$ is the cathodic partial current density of the oxidizing agent at the passivation potential [21].

A metal's passivation potential will have an effect on the way in which a material will behave. In some situations a less noble metal may exhibit better corrosion resistance than a nobler metal. In Figure 23 the anodic partial current densities for two metals, whose only difference is the value of their passivation potential is shown. The corrosion potential of metal (a), having a lower passivation potential, is located in the passive region, while that for metal (b) is in the active region. Because of this metal (a) is expected to better resist corrosion. The passivation potential is affected by the pH. When the pH increases the passivation potential decreases. This is true for iron, but other metals show similar tendencies [21].

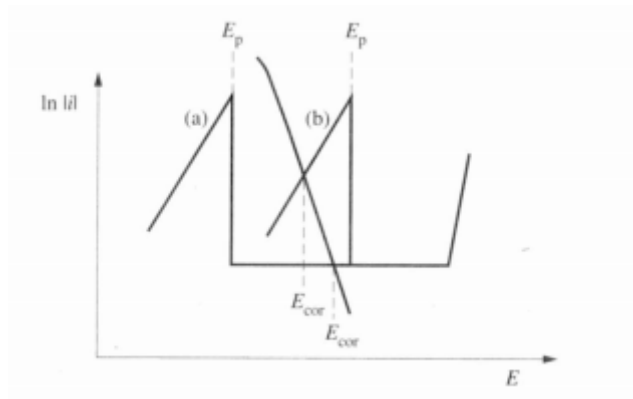


Figure 23 - Evans diagram showing the significance of the value of the passivation potential. The corrosion potential can be located in the passive (a) or active (b) region [21].

The significance of the passivation current density is illustrated in Figure 24. For metal (a) the passivation current density exceeds the current density of the cathodic partial reaction at the passivation potential : $i_p > |i_{c(E_p)}|$. In this case the corrosion potential may be located in either the passive or the active region, in other words the passivity is unstable. For metal (b) $i_p < |i_{c(E_p)}|$, which allows a state of stable passivity and therefore a low rate of corrosion [21].

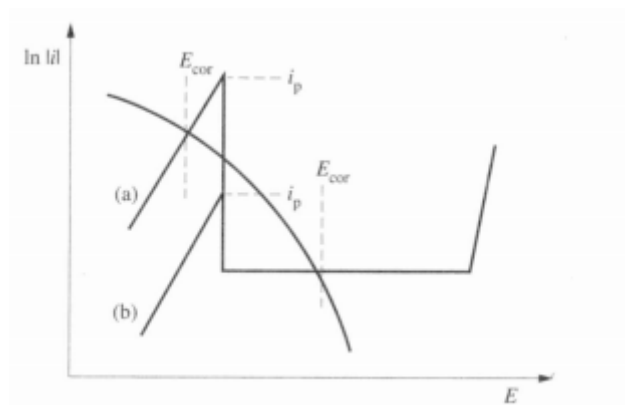


Figure 24 - Evans diagram showing the effect of passivation current density on corrosion behavior: (a) corrosion potential in the active region; (b) corrosion potential in the passive region [21].

There are four different factors which may affect the passivation current density [21]:

- the kinetics of active dissolution ;
- the mass transport of the dissolution products;
- the pH of the electrolyte;
- the water content of the electrolyte.

The exchange current density influences the value of the passivation current density more than any other kinetic parameter. If both of the anodic curves in Figure 24 were to belong to the same metal, the difference in i_p could be explained by a lower exchange current density for case (b). Certain adsorbed species inhibit or catalyze the dissolution of metals and thus affect the effective value of the exchange current density [21].

The mass transport may in some cases limit the passivation current density. If the metal does not dissolve at a sufficient speed the passivation current will be low [21].

The pH of the electrolyte is of importance to both passivation potential and passivation current density. This is because both the metal dissolution kinetics and the solubility of hydroxides depend on pH. Figure 25 shows the anodic polarization curves for iron at different pH. The higher the pH gets, the lower the passivation current density gets. This can be explained by a lowering of the solubility of ferrous hydroxide, which precipitates at the surface. Since both the passivation potential and the passivation current density decreases at increased values of pH, spontaneous passivation becomes possible in basic, aerated media [21].

The smaller the activity of water, the more difficult it becomes to passivate a metal. If there is no water, no passive film will be formed [21].

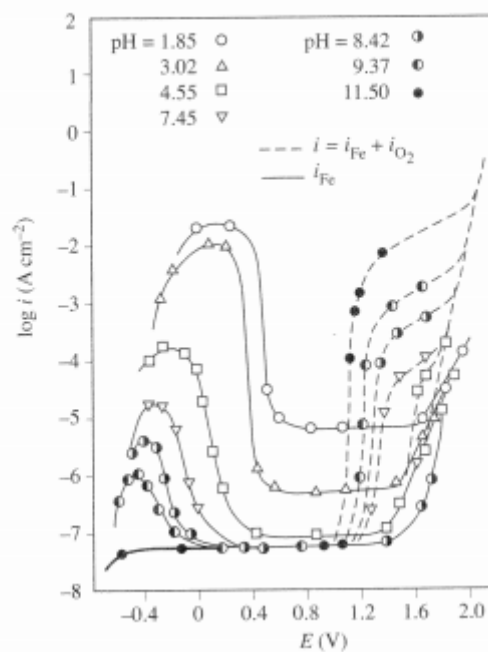


Figure 25 - Anodic partial current density for the dissolution of iron measured in 0.15 M phosphate solutions of different pH [21].

Passivity breakdown

In addition to low ionic conductivity and low solubility the passivating film should also have sufficient mechanical strength and adhesion to the surface of the metal so that it can properly withstand the formation of cracks, wear and spalling [17]. The passivating films can be decomposed by mechanical, chemical or electrochemical decomposition. Mechanical decomposition occurs by crack formation during deformation of the material, or by wear as a result of relative motion of the metal and the surrounding liquid, particles in the liquid, or other bodies in contact with the metal surface. This will be further discussed in chapter 2.4.1.4. Chemical decomposition occurs due to direct dissolution of the oxide film. Even in the passivated state, the oxide has a certain solubility. With a change in pH or

increase in temperature or concentration of aggressive compounds, the solubility can become so great that the passivity disappears to some extent or it may disappear completely. Electrochemical decomposition occurs when the potential changes to outside the area of passivation. This can happen by a decrease in the potential to the active area or by an increase to the transpassive area. When at the transpassive area, the oxide will decompose [17].

At the transpassive potential (where the transpassive region starts in Figure 20), the properties of the passive film change and a renewed increase in the rate of dissolution can be observed. This may be a result of film oxidation at high anodic potentials or of film breakdown favored by the presence of certain anions. There are three types of behavior observed in the transpassive potential region [21]:

- uniform transpassive dissolution at potentials below oxygen formation;
- localized dissolution by pitting;
- high rate transpassive dissolution above the potential of oxygen formation.

The uniform transpassive dissolution below the potential for oxygen formation occurs when the protecting passive film is oxidized to species having a higher solubility. This behavior is typically observed for metals in group VI of the periodic table. Upon passivation the metal forms a passive film which is barely soluble and provides an effective barrier that protects the metal against corrosion. However, at the transpassive potential, passive film oxidizes to a compound with a much higher solubility [21].

In the presence of certain aggressive anions, in particular chloride, metals lose their passivity above a critical potential called the pitting potential. When this happens, metal dissolution takes place from local sites where the passive film broke down. This localized dissolution leads to the formation of deep pits on an otherwise passivated surface. As explained earlier, this phenomenon is called pitting corrosion [21].

In absence of aggressive ions the transpassivation potential of metals such as iron is higher than the reversible potential of the oxygen electrode. As a result, when such a metal is anodically polarized to sufficiently high potentials, anodic oxygen evolution is observed. As the film breakdown potential is reached, oxygen gives way to anodic dissolution at high rate. The passive film breakdown is favored by high anion concentration on one hand, and by high local acidity at the anode surface which is a result of oxygen formation from water, which liberates protons [21].

2.4 Tribology

2.4.1 Wear mechanisms

Wear is “the progressive loss of substance from the operating surface of a body occurring as a result of relative motion at the surface” as defined by H. Czichos [22]. To explain this, one can imagine a simple tribo-mechanical system consisting of two metal bodies moving against each other. In this case there is no lubricant, only gaseous atmosphere. The material losses, on one of the materials, due to wear processes can occur in the following ways: Material transfer from one of the bodies to the other, material loss from the metal body to the atmosphere, or by formation of reaction products [22].

To properly characterize the type of wear occurring in a system the following characteristics should be specified [22]:

- I. The type of relative motion,
- II. The interacting elements,
- III. The dominant wear mechanism.

These three characteristics specify the type of wear. However, to get a more quantitative characterization, the following characteristics should be specified [22]:

- IV. The input work (normal load, friction coefficient, distance of motion),
- V. Material properties relevant to wear,
- VI. The appearance of the worn surfaces.

In Figure 26, a classification scheme which combines the characteristics of (I), (II) and (III) is shown. The types of wear are termed according to the type of relative motion in analogy to the classification of friction mode [22].

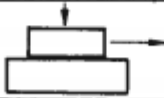

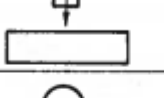
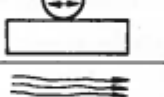
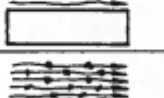
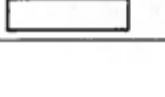
Interacting elements	Type of relative motion	Wear mechanisms	mainly stress interactions		stress + material interactions	
			surface fatigue	abrasion	adhesion	tribo-chemical
solid/solid (metals, polymers, minerals, etc.) without or with lubricants	 sliding		sliding wear			
	 rolling		rolling wear			
	 impact		impact wear			
	 oscillation		fretting wear			
solid/liquid	 flow		cavitation wear			
solid/fluid + particles	 flow		fluid erosion			

Figure 26 - Characterization of wear [22].

Wear mechanisms	Appearance of the worn surfaces
Surface fatigue	cracks, pits
Abrasion	scratches, grooves, striations
Adhesion	cones, flakes, pits
Tribochemical	reaction products (films, particles)

Figure 27 - Appearances of worn surfaces [22].

As shown in Figure 26, there are four basic types of relative motion: sliding, rolling, impact and oscillation. The wear occurring because of these motions can be classified into four groups, which are the four basic forms of wear: Fatigue, abrasion, adhesion and tribocorrosion (tribochemical). Determining what type of wear is occurring in a given system is not always easy. In any of the four types of relative motion, one or more of the four basic wear mechanisms may act. Therefore, it may be necessary to do a visual study of the materials. In Figure 27 some typical visual characteristics for the different types of wear mechanisms are listed. However, in general there is rarely only one wear mechanism acting in a tribo-mechanic system, in general, a combination of several wear mechanisms occurs. The Four basic wear mechanisms are described in more detail in the following chapters [22].

2.4.1.1 Surface fatigue mechanisms

Surface fatigue is a cause of surface stresses building up in a material. Repeating cycles of load may cause a stress-reverse effect, allowing fracture to develop under alternating stresses with a peak level which could be safe if applied with normal tension or compression [22].

Surface fatigue is the most common failure mode of rolling contact. However, surface fatigue in rolling contacts acts differently than surface fatigue of bulk material. Firstly, the fluctuations in the time to failure is more severe in rolling contact, and secondly the fatigue limit stress (under which fatigue does not occur) which is found in bulk material, has not been proven to exist in the surface fatigue cases [22].

According to the Hertzian theory of static elastic contact, the maximum compressive stress occurs at the surface and the maximum unidirectional shear stress is some distance below it. However, if the contact is subjected to considerable traction forces, then the positions of the maximum shear stress change and move towards the surface region [22].

There are a variety of factors to consider related to surface fatigue, factors which influence the stress and the likelihood of surface fatigue to occur [22]:

- Subsurface stress raisers: Oxides and other hard, brittle inclusions; sulfides, carbides and other second phase particles; grain boundaries, sub-boundaries, twins and other dislocation arrays.
- Surface character: Surface topography and texture, residual stresses, surface energy level, microstructure, contaminants.

- Surface flaws: Inclusions and second phase particles; nicks and dents including true and false brinelling; grooves and scratches; corrosion pits, rust and water etch; fretting damage; and skidding damage.
- Discontinuities in contact geometry; end of “line” contact geometry, debris particles in the contact area.
- Load distribution within the bearing
- Elastohydrodynamics
- Tangential forces: Without gross sliding, rolling plus sliding

Experiments indicate that the study of surface fatigue is basically a study of stress concentration effects that govern fatigue crack initiation along with crack propagation behavior. There are several possible mechanisms for crack initiation. The primary mechanisms for this are: Pile up of dislocations in slip band against grain boundary, coalescence of two slip dislocations to form a crack along a cleavage plane, and crack formation at tilt boundary. In addition to these three mechanisms, the effect of inclusion may initiate subsurface cracks. In steels, carbide inclusions are often present. The presence of such obstacles can cause dislocations coalescence and then initiation of subsurface crack nuclei [22].

By studying the stress fields in subsurface regions of sliding asperity contacts and the possible dislocation interaction a “delamination theory of wear” has been proposed. It starts with the generation of subsurface dislocations. After a while the dislocations will pile up and cause the formation of voids. Then coalescing voids will cause crack formation parallel to the surface. And finally, sheet-like particles will form as the crack reaches a certain critical length [22].

2.4.1.2 Abrasive wear mechanisms

As with surface fatigue, the main cause of abrasive wear mechanism is caused mainly by contact deformation processes. Abrasion occurs when two surfaces in direct contact moves relative to one another. In abrasive wear one of the materials is usually harder than the other. The harder surface asperities press into the softer surface, causing plastic flow of the softer surface in the areas around the asperities of the harder surface. If a tangential motion is imposed the harder surface will plough through and remove material of the softer surface [22].

Abrasive wear is very common in industrial situations and it has been estimated that about 50% of the wear encountered in industry is caused by abrasion mechanisms. Abrasive wear can occur in several different modes, and is therefore characterized in several ways [22]. Firstly it is distinguished between two-body abrasive wear and three-body abrasive wear [22, 23]. Two-body abrasion occurs when the wear is caused by asperities or firmly held grits sliding across the surface. Three-body abrasion occurs when free rolling particles slide over the surfaces of both components. According to Stchowiak et al. it has been found that three body abrasive wear is up to ten times slower than two-body abrasive wear [23]. Secondly, it is distinguished between: Gouging abrasion, as in hammers in impact pulverizes; grinding abrasion, as in grinding balls; and Erosion abrasion, as in sandblast nozzles [22].

A common mechanism which causes abrasive wear is cutting or ploughing. Cutting occurs when a sharp grit or hard asperity cuts into a softer surface as illustrated in Figure 28. The material that is cut is removed as wear debris. There are two basic mechanisms occurring when a material is pressed along another: A cutting mechanism and a wedge build up mechanism with flake-like debris. The latter mechanism is often referred to as ploughing, and is a far less efficient mode of removing metal than the microcutting [23].

The geometry of the grit plays an important role on the wear of a material. If the grit contains many sharp edges, it will remove far more material than a smoother rounder grit. Studies has also shown that in the presence of a lubricant a rapid microcutting form of abrasive wear is more likely to occur than without any lubricant. Beneath the surface of the abraded material, considerable plastic deformation will occur. And as a result of this strain hardening can take place which in some cases may reduce the abrasive wear [23].

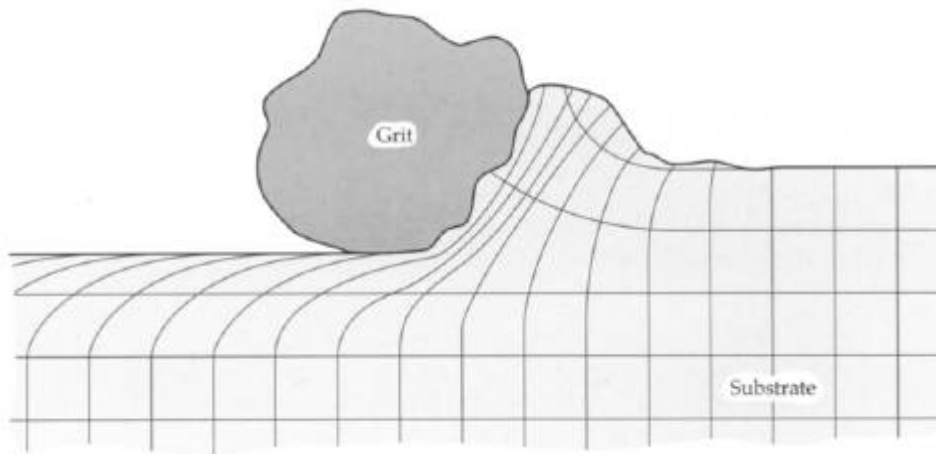


Figure 28 - Subsurface deformation during passage of a grit [23].

Abrasive wear is dependent on the hardness of the abrasive, H_a , and the hardness of the material H_m , which leads to three different wear regimes, as presented in Figure 29. If $H_a < H_m$, the system is within a low wear regime, (I). If $H_a = H_m$, the system is in a transition regime, (II). And if $H_a > H_m$, the system is in a high-wear regime, (III) [22].

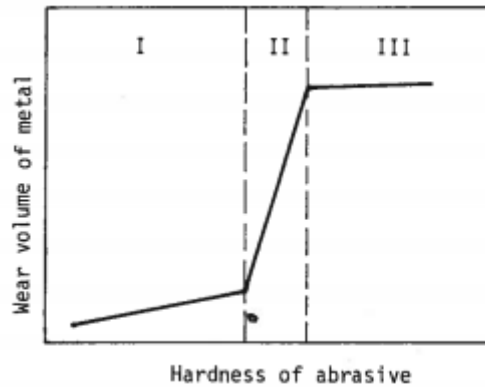


Figure 29 - Influence of the hardness of the abrasive on the wear of metals [22].

It could be concluded that in order to reduce an abrasive wear component, the hardness of the material, should be harder than that of the abrasive by a factor of about 1.3, in order to secure a low-wear abrasion rate [22].

$$H_m \approx 1.3 H_a \quad \text{Equation 7 [22]}$$

In region (III) it can be stated that the abrasion of a material is only dependent of the materials hardness, indicating that the wear resistance is proportionally dependent on the material hardness. However, if the abrasive wear processes only acts on the outer layer of the material, then the influence of surface contaminants and environmental atmosphere must additionally be taken into consideration [22].

2.4.1.3 Adhesive wear mechanisms

The wear mechanisms of surface fatigue and abrasion can be explained mainly in terms of forces, stresses and deformation process. However, in adhesive wear, the material interactions play an important role. Abrasive wear is when two bodies in close contact, connects, and then separates by the fracture of one or both of the materials, causing material failure in the system. While other wear mechanisms usually happen over time, adhesive wear can very suddenly lead to destructive failure [22].

When two solid bodies are brought into contact, they will first experience long-range van der Waals forces. When getting closer, at a distance of about 1 nm, stronger short-range surface forces comes into play at the real areas of contact. With assistance of the dispersal of surface contaminants this can cause strong adhesive junctions to be formed between the two bodies. If adhesive wear is to take place, then fracture must occur in one or both of the materials [22]. In Figure 30, the different adhesion bonding mechanisms is illustrated.

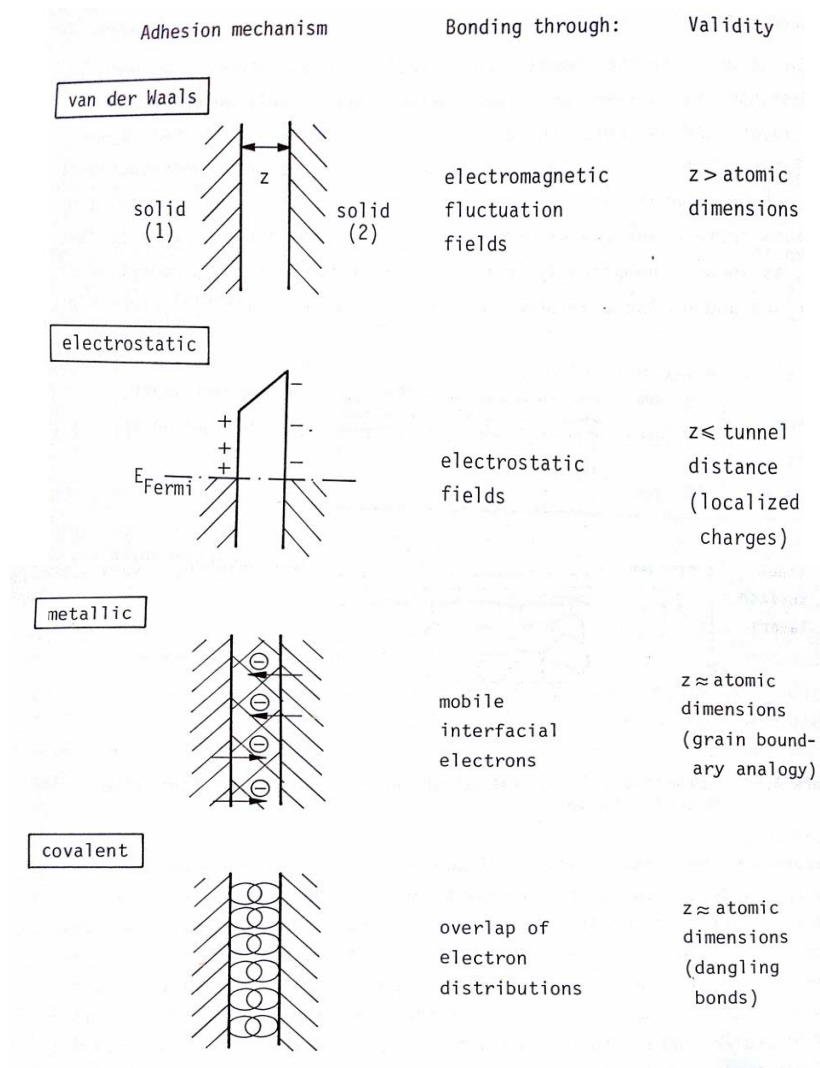


Figure 30 - Types of adhesion bonding mechanisms [22].

There are several different characteristics of contact adhesion and contact deformation processes that influence adhesive wear. Both adhesion and fracture are influenced by surface contaminants and effects of the environment. With this in mind, experiments, where these influences were eliminated, were carried out to determine other influences of adhesive wear. It was found that [22]:

- Interfacial metallic adhesion bonding occurs between any pair of metal and that there is no direct relation between the solubility of metal pairs and their adhesion bonding.
- Crystal structure influences the extent of adhesive wear. Hexagonal metals in general have lower adhesive wear characteristics than either body-centered cubic and face-centered cubic metals.
- The crystal orientation influences the adhesive wear behavior. In general high atomic density, low surface energy grain orientations exhibit lower adhesion and less adhesive wear than other orientations.
- When dissimilar metals are in contact the adhesive wear processes will generally result in the transfer of particles of the cohesively weaker of the two materials to the cohesively stronger.
- Small amounts of alloying elements such as carbon and sulfur are sufficient to inhibit appreciably the adhesion of metallic alloys thereby minimizing their adhesive wear.

Adhesive wear particles

The characteristics mentioned above along with the combined effects of adhesion and fracture influence the formation of loose adhesive particles. In Figure 31, mechanisms involved in the formation of adhesive wear particles are presented. At first, adhesion between the two bodies occurs. Then, with tangential motion, the fracture occurs along slip bands as the tangential force parts atomic planes. At some applied tangential force, the applied force exceeds the adhesive bonding and causes a fracture which in combination with motion creates a curl on the surface. A second pass over the surface will then shear off the curl, creating an adhesive wear particle [22].

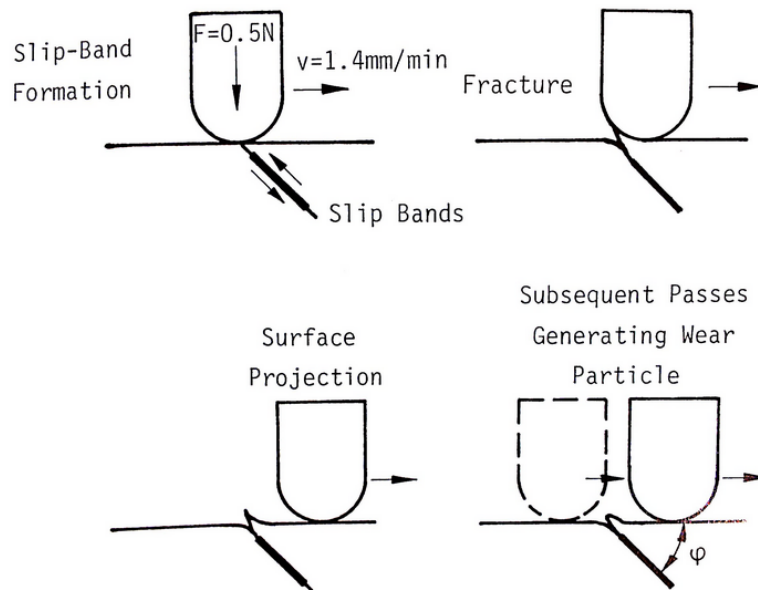


Figure 31 - Origin of surface fracture and formation of wear particles [22].

In Figure 32 the surface of a boron steel disc is shown. The disc was used in a pin on disc test. From the image one can see the occurrence of severe adhesive wear. The disc was tested against a pin of untreated tool steel at 500 °C [24]. From the image one can see that there is residual material from the second body on the disc.

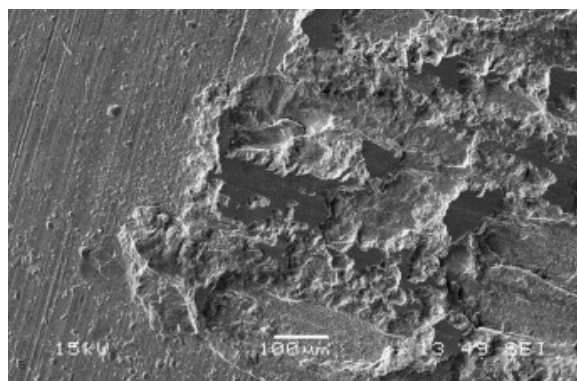


Figure 32 - SEM image of boron disc adhesive wear scar [24].

2.4.1.4 Corrosion wear: Tribocorrosion

Corrosive wear can occur in a wide variety of situations both lubricated and unlubricated. Corrosive wear is a result of chemical reactions between the worn material and a corroding medium which can be a chemical reagent, reactive lubricant or even air. A somewhat special characteristic of corrosive wear is that a rapid wear rate is usually accompanied by a diminished friction coefficient. This divergence between friction and wear is useful in identifying this type of wear [23]. As the components react with each other, movement of the bodies involved will result in continuous formation and removal of the reaction products and since the contents of the reaction products comes from the contacting bodies, material is removed from the surfaces, causing wear. This process may be described as a cyclic process [22]:

- (I) At the first stage the surfaces react with the environment. Either one of the surfaces react with the environment, or both, creating reaction products on the surface of the bodies.
- (II) Next, attrition of the reaction products as a result of crack formation and abrasion caused by the interaction of the bodies will occur. With the removal of reaction products, unreacted surface will appear, and stage (I) will start over, creating a cycle of wear.

If a metal corrodes and produces a film on its surface while it is simultaneously subjected to a sliding contact then one of the four following hypothetical processes may occur[23]:

1. A durable lubricating film which inhibits both corrosion and wear may be formed;
2. A weak film which has a short life-time under sliding contact may be produced and a high rate of wear may occur due to regular formation and destruction of the films. The friction coefficient may or may not be below in this instance;
3. The protective surface films may be worn (e.g. by pitting) and a galvanic coupling between the remaining films and the underlying substrate may result in rapid corrosion of worn area on the surface;
4. The corrosive and wear processes may act independently to cause a material loss which is simply the sum of these two processes added together.

The first process considers the formation of a full durable lubricating film. If the film prevails, good lubrication is ensured and the neither corrosion nor wear will occur. However, very few corrosion product films are durable enough, so this process rarely occurs in practice. The second process considers the formation of a sacrificial or short life-time corrosion product film. This is the most common form of corrosive wear considering that most corrosive films consist of brittle oxides or other ionic compounds. During this process, corrosion occurs on active areas, where active areas are the true contact area. Wear occurs because of the removal of corrosion products, which are regenerated after removal. The third process relates to wear in highly corrosive media while the fourth relates to extremely corrosive media where the corrosion products are very weak and probably even soluble in the liquid media [23].

As mentioned, process two is the most common form of corrosive wear. The corrosive film builds up gradually, but is nearly instantaneously removed after a certain number of sliding contacts is reached. Since most of the corrosion film passivate or stops growing beyond a certain thickness, this causes a greater rapidity of loss of material than corrosion alone [23].

Considering these facts, the chemistry of the reaction product formation and their properties must be considered [22]. It is highly unlikely that wear and corrosion, if occurring in the same system, can proceed independently since the heat and mechanical agitation of a sliding contact would almost inevitably accelerate corrosion [23]. The heat and the mechanical agitation will cause the asperities of the materials to undergo some changes. Firstly, the reactivity will increase due to the increased asperity temperature, and therefore the formation of surface layers is accelerated. Secondly, the mechanical properties of the surface asperity layers are changed, in general giving them a tendency to brittle fracture [22]. Heat increase has a great impact on corrosive wear. With an increase of 20°C in temperature, the corrosive wear rate may double. Therefore, it is important, that the surfaces are sufficiently cooled in order to suppress corrosive wear problems [23].

Effect of NaCl

Sodium chloride will cause the steel surface to corrode. However, according to the findings of Wang et al. [25] the corrosion of the steel may also lead to the formation of so-called “green rust” which may act as a lubricant causing a mixed lubricating effect from both the aqueous solution and the green rust. In their paper, a polymer sample of PTFE was pressed against a rotating steel ring in different solutions; among these, a solution of NaCl. Their experiments showed, as expected, corrosion forming on the steel. However, an unstable matter of green rust was also formed, which are iron(II-III) hydroxysalts. While the corrosion of the steel makes the steel surface rougher, causing a higher friction coefficient, the green rust creates a lubricating effect, which will be beneficial to reduce the friction coefficient. Depending on the presence of other components (as often found in sea water) like Mg^{2+} and Ca^{2+} , the green rust can be even more stable and allow even better lubrication [25].

2.4.2 Lubrication

The tribological processes discussed in the chapters above concerning wear and friction of two interacting bodies are explained as interactions between two bodies in physical contact. All these processes can be influenced or modified by the process of lubrication. Lubrication is needed to separate the moving surfaces with a film of a material which can be sheared with low force without causing damage to the surfaces. The lubrication in a wear process can act by different modes depending on several factors, such as the thickness of the lubricating film, the interfacial height distribution of the film and the degree of geometric conformity. The modes of lubrication can be discussed by using the Stribeck curve. The Stribeck curve represents the general characteristics of lubricated moving surfaces as a function of the lubricant viscosity η , the velocity v and the normal load F_N . In Figure 33 the Stribeck curve is shown as a function of the parameter $\eta \cdot v \cdot F_N^{-1}$ [22].

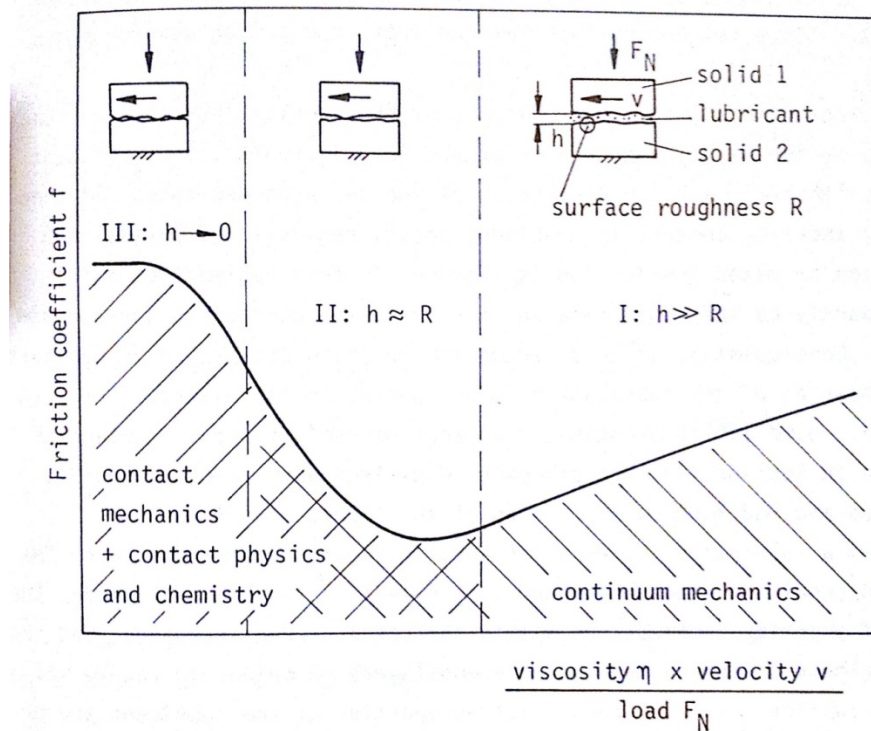


Figure 33 - Stribeck Curve and lubrication regimes [22].

According to the Stribeck curve there are three main lubricating modes which should be discussed [22]:

- I) Hydrodynamic lubrication (and Elastohydrodynamic lubrication)
- II) Partial EHL lubrication or mixed lubrication
- III) Boundary lubrication

In regime I, the rigid surfaces are separated by a continuous film, whose thickness is much larger than the combined surface roughness measure R of the surfaces. The friction resistance is due to the internal friction of the lubricant. The tribological behavior is determined by the rheology of the lubricant and can be calculated or estimated by the methods of fluid dynamics. If the lubricated system under consideration consists of non-conformal concentrated contacts, the elastic deformation of the surfaces and the pressure dependence of the lubricants viscosity must also be considered. In regime I there is no direct physical contact between the surfaces and therefore wear processes cannot take place, except for surface fatigue, cavitation wear or fluid erosion [22].

During hydrodynamic or EHL lubrication, if the lubricant viscosity or the velocity decreases, or the load increases, the lubricant film will get thinner and the separation of the surfaces decreases. If the film gets thin enough and asperity contact interaction occur, then region II is reached, where partial EHL lubrication or mixed lubrication mode is the occurring lubrication mode. In this regime, the load is carried partly by the fluid film, and partly by the contacting surface asperities making the friction coefficient dependent partly on the shearing of the lubricant film and partly on the asperity interactions. All wear mechanisms may occur in this regime, but they will be influenced and modified by the lubricating film [22].

If the lubricant viscosity or velocity decreases or the load increases even more, the amount of asperity interactions within the contact area will increase and the film thickness decreases down to some monolayers or below. In regime III, where boundary lubrication occurs, the bulk rheological properties of the lubricant are of less importance and the load is carried almost entirely through the deformation of asperities. The different modes of lubrication will be discussed in more detail in the following chapters [22].

2.4.2.1 Hydrodynamic lubrication

In this form of lubrication, a continuous fluid film is brought between the moving surfaces to minimize the friction and to eliminate wear. According to Czichos, the behavior of a system with this lubrication mode is determined by two features [22]:

- I) The resistance to motion is given by the “internal friction” of the fluid, i.e., the shear resistance or “viscosity” of the fluid film.
- II) The effects of wear are eliminated if the geometry of the surface is such that a load-carrying pressure is set up in the lubricant film during the motion of the surfaces leading to a complete separation of the surfaces.

2.4.2.2 Elastohydrodynamic lubrication

It is important to consider the lubrication in cases with poor geometrical conformity as in the cases of Hertzian concentrated contact situations, and the deformation of the surfaces must therefore be taken into account. Because of the high pressure found in lubricated Hertzian contact, the pressures effect on the properties of the lubricant (especially the viscosity), must be considered, which leads to the concept of elastohydrodynamic lubrication [22]. In elastohydrodynamic lubrication, both the deformation of the bodies and the change in viscosity play a significant role. The film thickness can be as low as 0.1 - 1 μm thick. Even with such a thin layer, it manages to separate the interacting surfaces resulting in a significant reduction in wear and friction [23]. But with a film layer so thin, the effect of surface roughness and the possibility of asperity contacts cannot be neglected. The inclusion of these factors has led to the concept of partial EHL lubrication.

2.4.2.3 Mixed lubrication

When mixed lubrication occurs, one can assume that the total applied load is carried partly by the hydrodynamic action of the lubricant film, and partly by asperity contacts. The models of mixed lubrication can be broadly classified in two groups: Models of mixed lubrication, in which the (classical) hydrodynamic lubrication theory is used as a starting point, and models of mixed lubrication, which start from the EHL lubrication theory taking into account the asperity contact component [22].

2.4.2.4 Boundary lubrication

The lubrication mode of the left most side of the Stribeck curve is boundary lubrication. This lubrication mode is characterized by the following features:

- a) The solid surfaces are so close together that appreciable contact takes place between the asperities.
- b) Hydrodynamic effects and influences of the bulk rheological properties of the lubricants are of little or no importance.
- c) The tribological behavior is determined by surface interactions between thin layers of boundary lubricants and the solid surface.

Because of these features, the processes which determine the tribological behavior of solid surfaces are valid also for boundary lubrication conditions. All of these solid/solid interactions are modified through the action of the boundary lubricant, so that the tribological behavior of a boundary lubricated system is determined by the processes at the solid/lubricant/solid interface influenced by the environmental atmosphere. The case of boundary lubrication is a lot more complex than the dry state and the other lubrication modes of the Stribeck curve which is because of the variety of interactions and parameters involved [22].

2.4.3 Aqueous Lubrication

In tribological processes the water can act as a coolant and a lubricant. It reduces the workpiece thermal deformation, assures longer tool life and lowers the friction between the tool and the workpiece, and flushes away wear products from the cutting zone [26]. Aqueous solutions as lubricants are drawing attention because of their ecological advantages, fire-resistance, high-thermal conductivity, non-toxicity, accessibility, biodegradability, environmental friendliness, and good solvency [27]. Though water is low cost and high cooling capacity its low viscosity and corrosive properties makes it unsuitable for most tribological applications. However, by the addition of high quality additives, its properties and performance as a lubricant can be greatly improved. The function of the additives depends on the application of the lubricant, but in general they are used to improve the areas where water falls short as an efficient lubricant. Among these areas are: prevention of corrosion and adhesion between the tool and the workpiece, reduction of tool wear and prevention of fungal and microbial growth, which is a health and safety hazard [26].

The mechanisms of aqueous lubrication are still not well known because of the diversity and complexity of aqueous solutions. The unique and complex physical and chemical properties of water renders some of the traditional lubrication theories invalid [27].

As previously discussed the formation of elastohydrodynamic lubrication between two surfaces is crucial to the lubrication efficiency. Pure water has poor film formation ability because of its low viscosity. When rubbing two surfaces together in a water lubricated system, the thickness of the lubrication film is only at 10 nm at rolling speeds above 5 m/s [27].

Since water itself is not an efficient lubricant, various additives are needed to improve its film formation ability. This can be polymers, surfactants, oils, etc. Both the lubrication mechanisms and behaviors are different for different types of aqueous liquids [27].

Surfactants

Surfactants have a unique amphiphilic molecular structure with hydrophobic tails and hydrophilic heads. By migrating to the water surface, the alignment and aggregation of surfactant molecules will alter the surface properties. In doing this the surfactant influences the performance of aqueous lubrication. The film formation of aqueous lubricants containing surfactants depend upon both the type and concentration of the surfactant and also the pH value of the surfactant solutions [27].

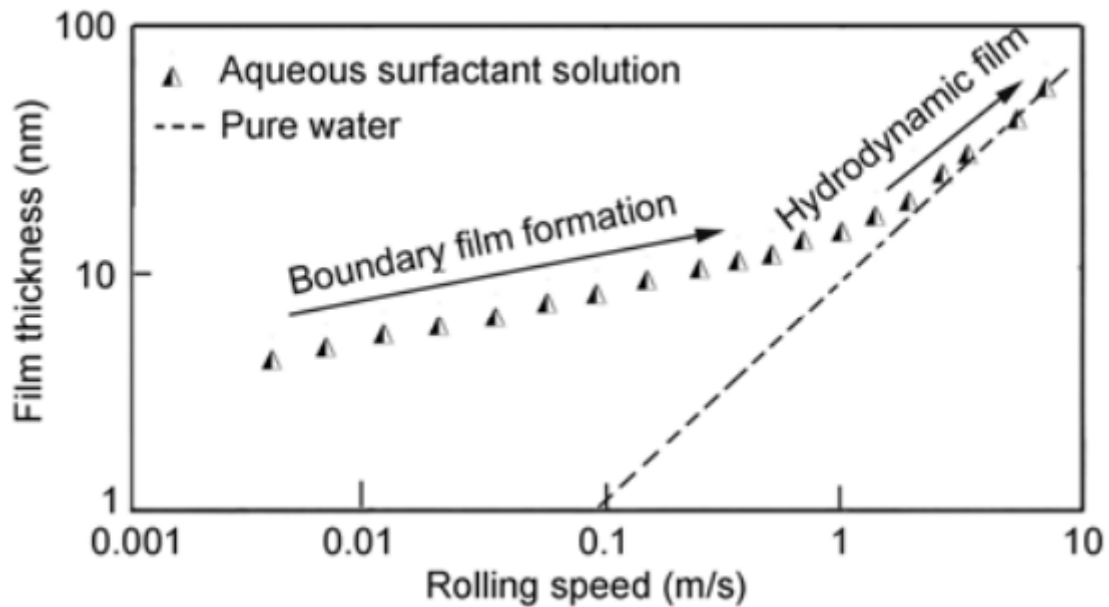


Figure 34 - Film-forming properties of different types of aqueous surfactant solutions [27].

The film formation of an aqueous surfactant solution is shown in Figure 34. This shows that the boundary film formation is due to the absorption on the solid surfaces of mono- or bi-layers of surfactant at low speeds, and the film is enhanced by the hydrodynamic entrainment of water solutions at high speed. Studies have also shown that surfactants will adsorb at surfaces forming either monolayers or multi-(liquid crystalline) layers. Packing of surfactants resulted in good film-forming capability and load-carrying capability, which is affected by the length of the spacer group. The film formation of an aqueous solution is obviously improved by the adsorption of the surfactants on the solid surface [27].

Polymers

Polymers separate two rubbing surfaces by forming a protective layer on the surfaces and improving both the load carrying and lubrication capability of water. S. Lee et al. [28] performed studies on the addition of the polymer PLL-g-PEG to improve the lubrication capability of water in metal-oxide based tribo systems. The polymer addition helped the formation of a protective layer on iron oxide thus effectively improving load-carrying and boundary lubrication properties of water. The Experiments by Raviv et al. [29] obtained a coefficient of friction of 0.0006-0.001 using poly electrolytes (PMMA-b-PSGMA). The results show that brushed of charged polymers attached to

surfaces result in superior lubrication ability. This good lubrication performance is because of the strong resistance to interpenetration of compressed brushes, combined with the fluidity of the hydration layers surrounding the charged polymer segments. Plaza et al. [30] explored the tribological properties of polyethoxyglycol esters of dithiophosphate acid derivative aqueous solutions using four-ball and ball on disk machines. The solutions showed excellent load-carrying capabilities and strongly reduced friction coefficients at different sliding speeds, solution concentrations and loads, compared to that of pure water [27].

3. Experimental setup

3.1 Test materials

The rock used in this project was Iddefjord granite. The composition of the stone was analyzed using XRD.

The steel used in this project was the steel used in a hard rock cutter disc. The steel is referred as *H13* by the cutter disc manufacturer (The Robbins Company) and has a martensitic structure.

Two steel pieces cut from a cutter ring was used to perform XRF analysis of the steel to find its composition, and to measure the hardness of the steel. The hardness was measured using a MicroWiZhard hardness testing machine produced by Mitutoyo, with an applied force of 0.3 N on the steel surface.

Three different foam additives were used in the testing. All of the foams were produced and supplied by BASF. The foams used in this project were ABR5, SLF41 and SLF47B. Their properties are listed in Table 3 as stated by BASF.

Table 3 - Physical properties of the foams.

Foam	ABR5	SLF41	SLF47B
Form	Liquid	Liquid	Liquid
Colour	Yellow to brown	Transparent	Light brown
pH value	7.5-8.4	6.5-7.5	6-7
Density (g/cm ³)	1.02-1.04	1.035-1.045	1.035-1.045
Viscosity cP (mPas)	<500	N/A	N/A
Type of TBM	Hard Rock	Soft Soil	Soft Soil

3.2 Test procedures

3.2.1 Corrosion performance

The corrosion performance of the steel was evaluated by means of polarization curves. The steel was exposed to different electrolytes and the polarization curves were measured using an AUTOLAB potentiostat (302N) and the Nova version 1.5 software. The potentiostat and the cell setup are shown in Figure 35 and Figure 36 respectively. The polarization curves were obtained by applying a voltage of ± 700 mV with a speed of 5 mV/min, in both the anodic and cathodic area. A Ag/AgCl 3M KCl reference electrode and a platinum counter electrode was used in the experiment. The different conditions in which the steel was tested are given in Table 4. All the tests were performed twice for repeatability purposes.

Table 4 - Test matrix for polarization tests.

Electrolyte additive	Electrolyte
100% ABR5	-
3% ABR5	water
3% ABR5	1.4% NaCl
3% ABR5	3.4% NaCl
100% SLF41	-
3% SLF41	water
3% SLF41	1.4% NaCl
3% SLF41	3.4% NaCl
100% SLF47B	-
3% SLF47B	water
3% SLF47B	1.4% NaCl
3% SLF47B	3.4% NaCl

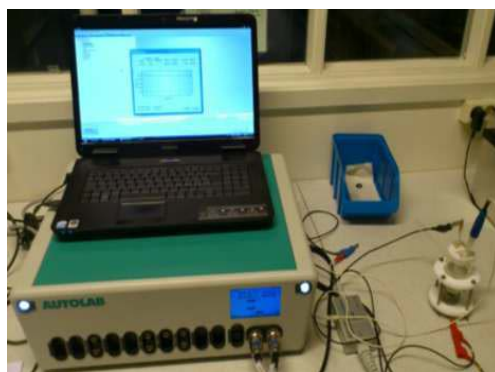


Figure 35 - The potentiostat



Figure 36 - The cell setup

Corrosion is a serious cause of degradation of cutter ring steel, therefore the foams were tested in different concentrations of NaCl to see how the foam and steel reacts in a saline environment which may be encountered during tunnel boring.

3.2.2 pH measurements

The pH was measured using a PHM210 STANDARD pH METER from MeterLab. A picture of the setup is presented in Figure 37. The lubricants were measured at room temperature under the following conditions: 100% lubricant, 3% lubricant, 3% lubricant + 1.4% NaCl and 3% lubricant + 3.4% NaCl.



Figure 37 - PHM210 pH meter

3.2.3 Viscosity

The viscosity measurements were done by using a Hakee III Rheometer. The fluids were put in a sample holder and by using a rotational device in the fluid, the viscosity was measured. The lubricants were measured at room temperature under the following conditions: 100% lubricant, 3% lubricant, 3% lubricant + 1.4% NaCl and 3% lubricant + 3.4% NaCl. The rheometer allowed for several different measurement methods. In this thesis the viscosity was measured by a constant increase in the rotational speed of the rotational device for 180 seconds. After this the rotational speed was kept constant at 500 RPS for 15 seconds, and then it was slowly decreased for 180 seconds until it stopped. The viscosity measurements from the area of constant speed were used as the viscosity values. The measured viscosity, was the dynamic viscosity of the fluid.

3.2.4 Reciprocal ball-on-plate

To determine the tribocorrosion properties of the steel, a reciprocal ball-on-plate test was executed. The machine used in this project was a ResMat Tribocorr, see Figure 38. In this test a steel ball (made of H13 steel) with a diameter of 6 mm was rubbed back and forth on to a rock surface with a stroke length of 10 mm repeatedly. The frequency of the sliding was 1 Hz and the duration of the sliding was 3600 seconds. This corresponds to a linear sliding speed of 0.02 m/s. The steel was loaded at a normal load of 5 N. A simplified schematic of the test is illustrated in Figure 39.

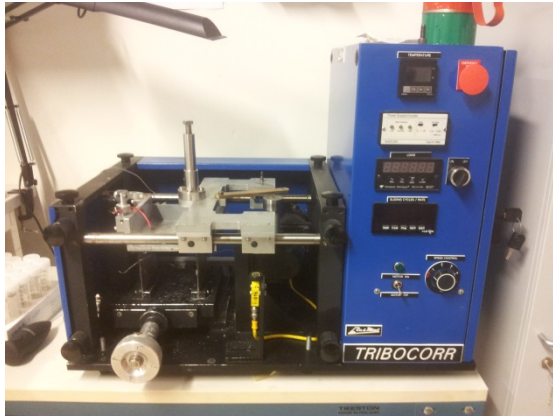


Figure 38 - ResMat Tribocorr test machine.

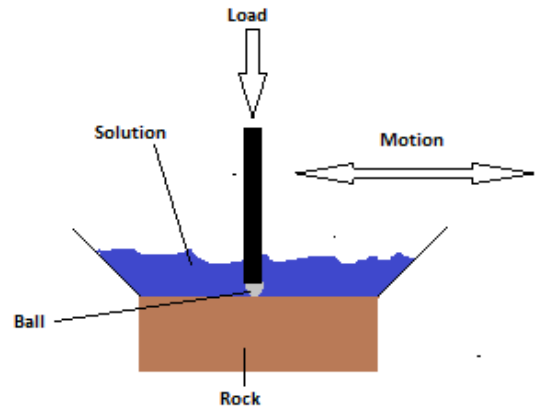


Figure 39 - Simplified model of the test method.

All the tests were performed twice under the following conditions:

Table 5 - Test matrix for the reciprocal ball-on-plate test.

Condition	Surface Material	Sliding Material	Lubricant
Dry	Iddefjord Granite	Steel	-
Water	"	"	-
"	"	"	3% ABR5
"	"	"	3% SLF41
"	"	"	3% SLF47B
Water + 1.4% NaCl	"	"	-
"	"	"	3% ABR5
"	"	"	3% SLF41
"	"	"	3% SLF47B
Water + 3.4% NaCl	"	"	-
"	"	"	3% ABR5
"	"	"	3% SLF41
"	"	"	3% SLF47B

The concentration of the foam in distilled water was 3 volume%. A mechanical stirrer was used to generate a foam. When the foam was used the tests were stopped every 20 minutes for removing and replacing of the foam. This was done to ensure that the lubricant always was in the form of a “foam” as it after some time tends to recover the initial liquid state.

During each test, the friction coefficient between the rock and the steel ball was measured.

After the ball-on-plate test, the rock and steel samples were examined using a Scanning Electron Microscope (SEM). The rocks had to be pre-treated with carbon sputtering in order to make them visible in the SEM. The SEM pictures were taken using a Hitachi S-3400N. The rocks and steel balls were also examined using a confocal microscope developed by Alicona.

4. Results

4.1 Rock characterization

The composition of the rock samples used in the tests was found using XRD. The results are presented in Table 6 below.

Table 6 - Composition of Iddefjord granite (including Moh's hardness values as stated in the theory section of this thesis).

Mineral Group	Mineral	Wt.%	Moh's Hardness
Quartz	Quartz	25	7
Feldspar	Plagioclase	32	6-6.5
	K-feldspar	35	6
Mica	Mica	8	2-4
Chlorite	Chlorite	<1	2-2.5

From Table 6 it can be seen that the minerals of largest composition are also the hardest minerals.

4.2 Steel Characterization

The composition of the steel was found by performing XRF analysis on a cutter disc piece. Each piece was cut from the outer part of the cutter ring (the part in contact with the rock) and each piece was measured in three different spots. The results of the analysis are presented in Table 7 below. The numbers are given in weight%.

Table 7 - Composition of the H13 steel.

H13	1-3			1-8			Average
Carbon	0.526	0.540	0.628	0.579	0.493	0.521	0.57
Manganese	0.286	0.295	0.298	0.288	0.264	0.327	0.29
Silicon	1.034	0.982	0.989	1.04	0.939	0.9	0.98
Chromium	4.806	5.027	4.765	4.798	4.84	4.82	4.84
Vanadium	0.904	0.931	0.914	0.913	0.917	0.912	0.92
Molybdenum	1.341	1.35	1.358	1.346	1.344	1.342	1.35
Sulphur	-	-	-	-	-	-	-
Phosphorus	-	-	-	-	-	-	-
Copper	0.112	0.115	0.115	0.116	0.126	0.124	0.12
Nickel	0.12	0.115	0.12	0.118	0.131	0.128	0.12
Iron	90.871	90.645	90.813	90.802	90.946	90.926	90.83
Sum	100.00	100.00	100.00	100.00	100.00	100.00	100.00

The steel hardness of the steel was also measured. The hardness of part 1-3 was 639.5 HV while the hardness for part 1-8 was 636.2 HV.

4.3 Polarization curves

Figure 40 to Figure 51 show the polarization curves of the steel exposed to ABR5, SLF41 and SLF47B at different conditions. The graphs are plotted with the potential on the x-axis and the logarithm of the current density on the y-axis. The potential in all the curves has been calculated to be against the standard hydrogen electrode (SHE) which difference with Ag/AgCl 3 M KCl is 0.224 V.

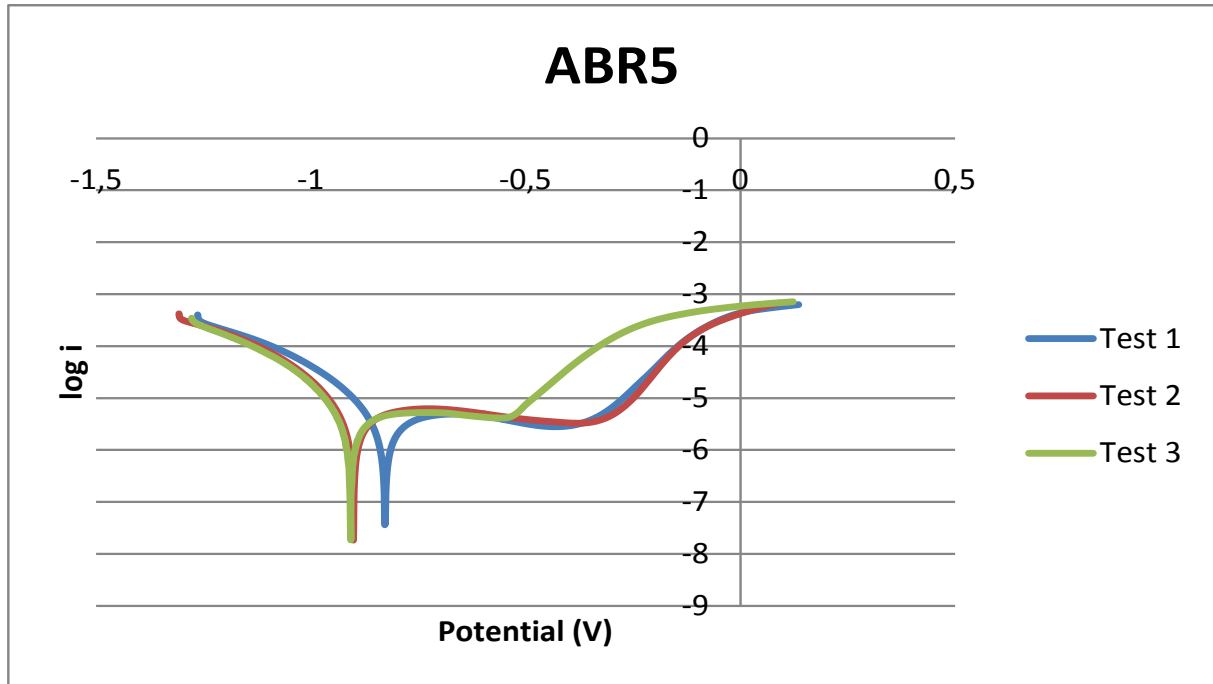


Figure 40 - Polarization curves for ABR5.

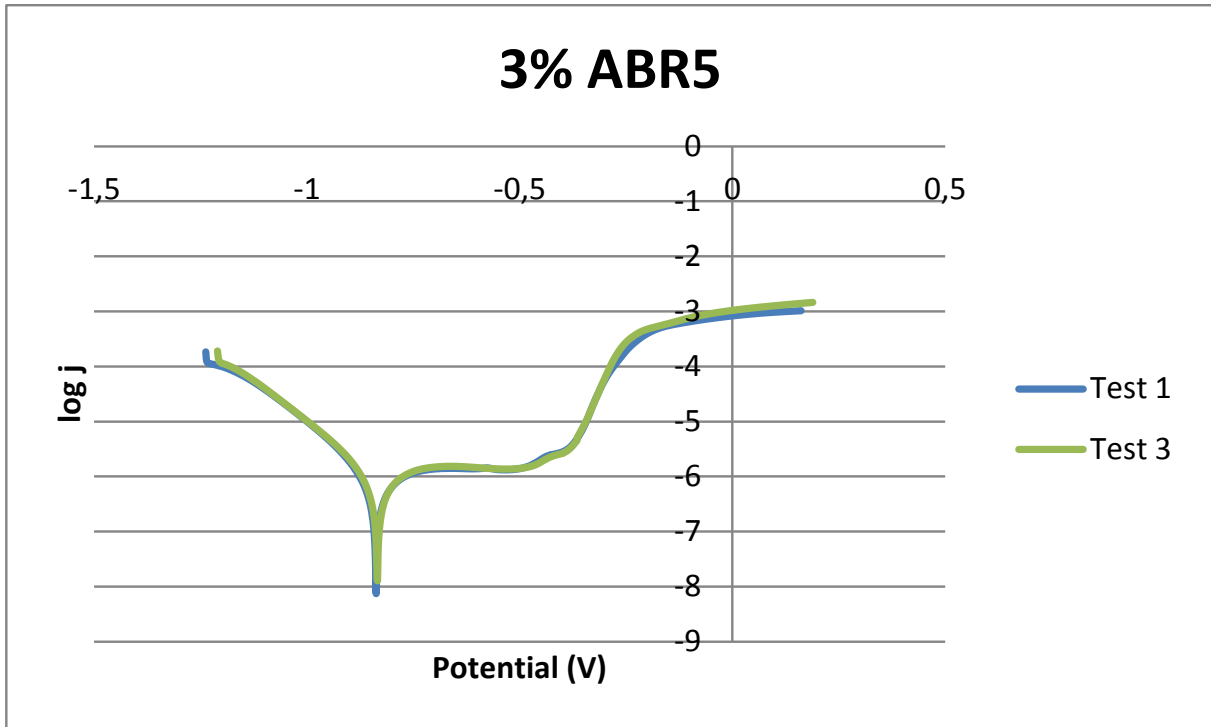


Figure 41 - Polarization curves for 3% ABR5

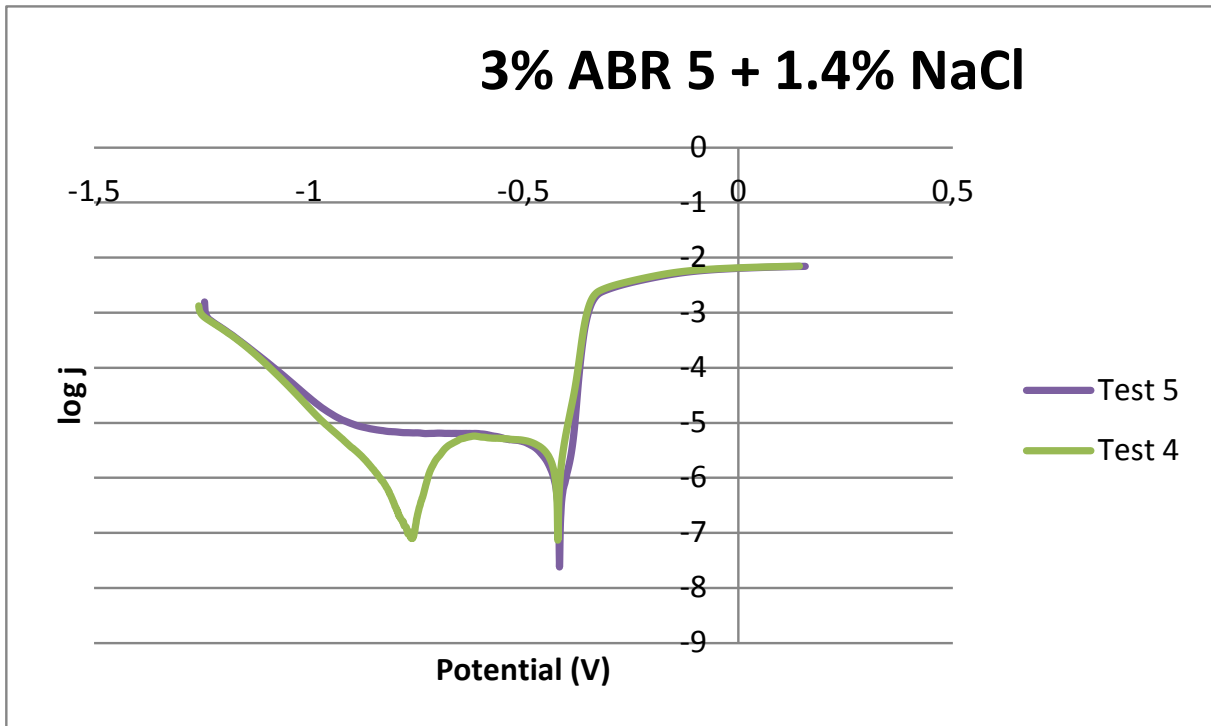


Figure 42 - Polarization curves for 3% ABR5 + 1.4% NaCl

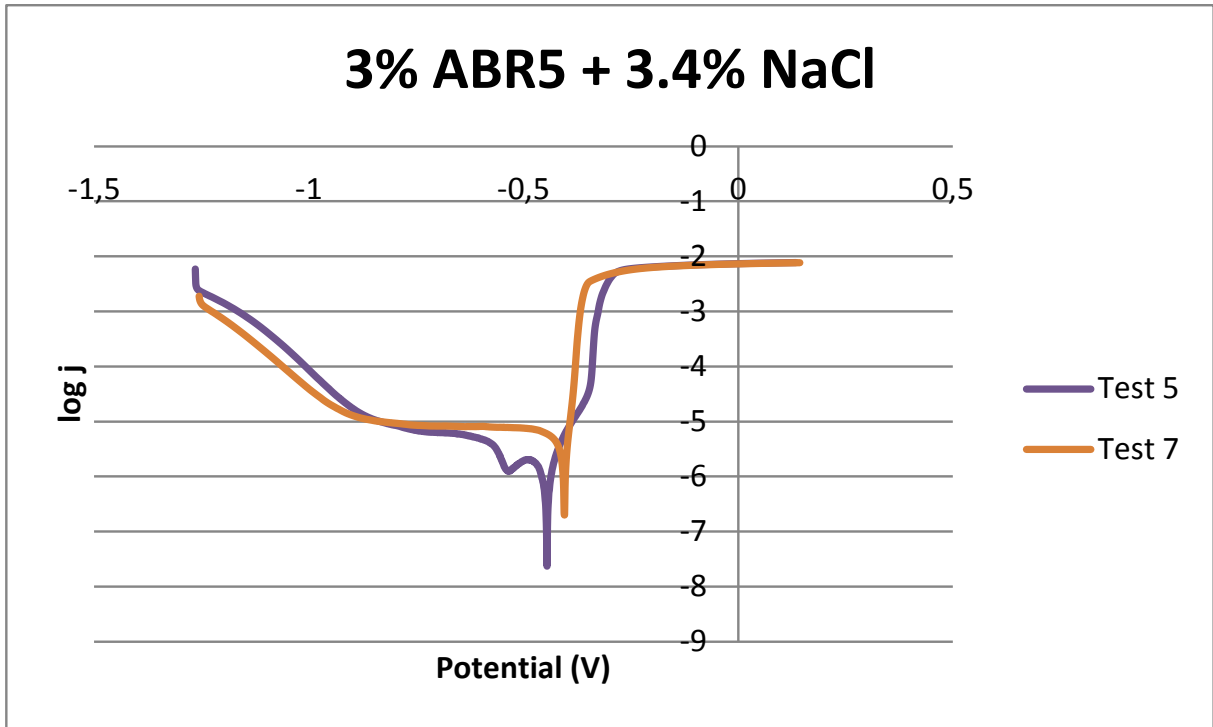


Figure 43 - Polarization curves for 3% ABR5 + 3.4% NaCl

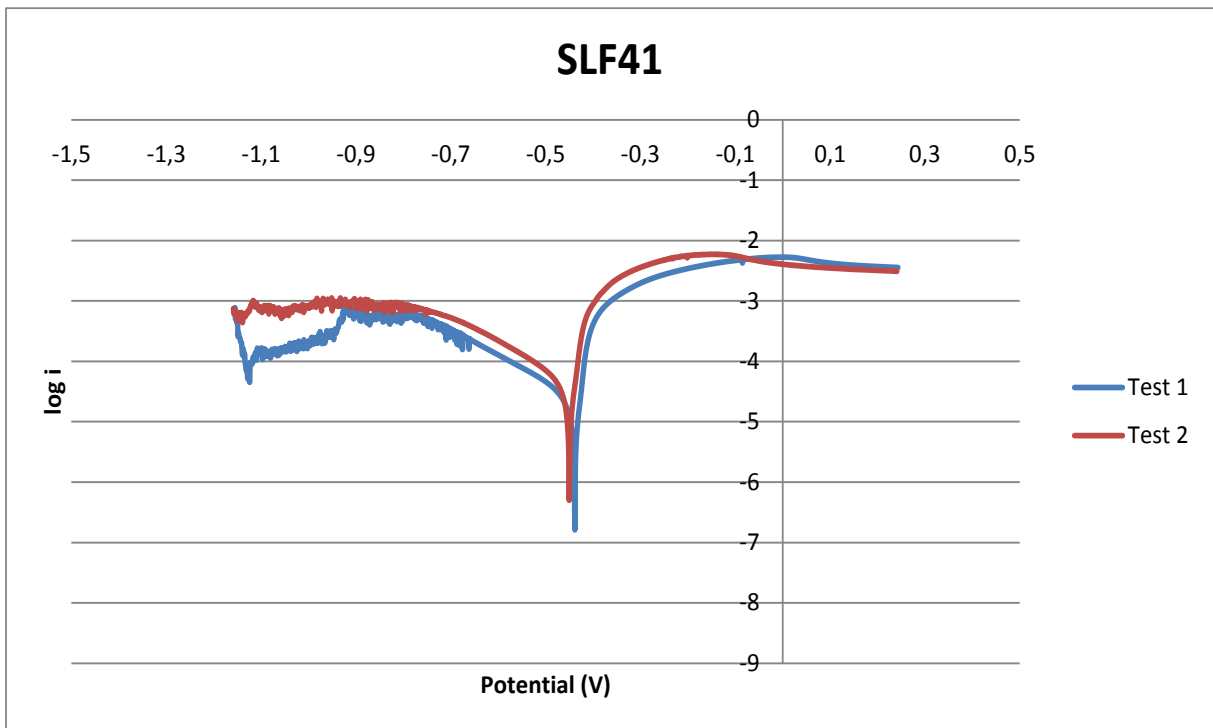


Figure 44 - Polarization curves for SLF41.

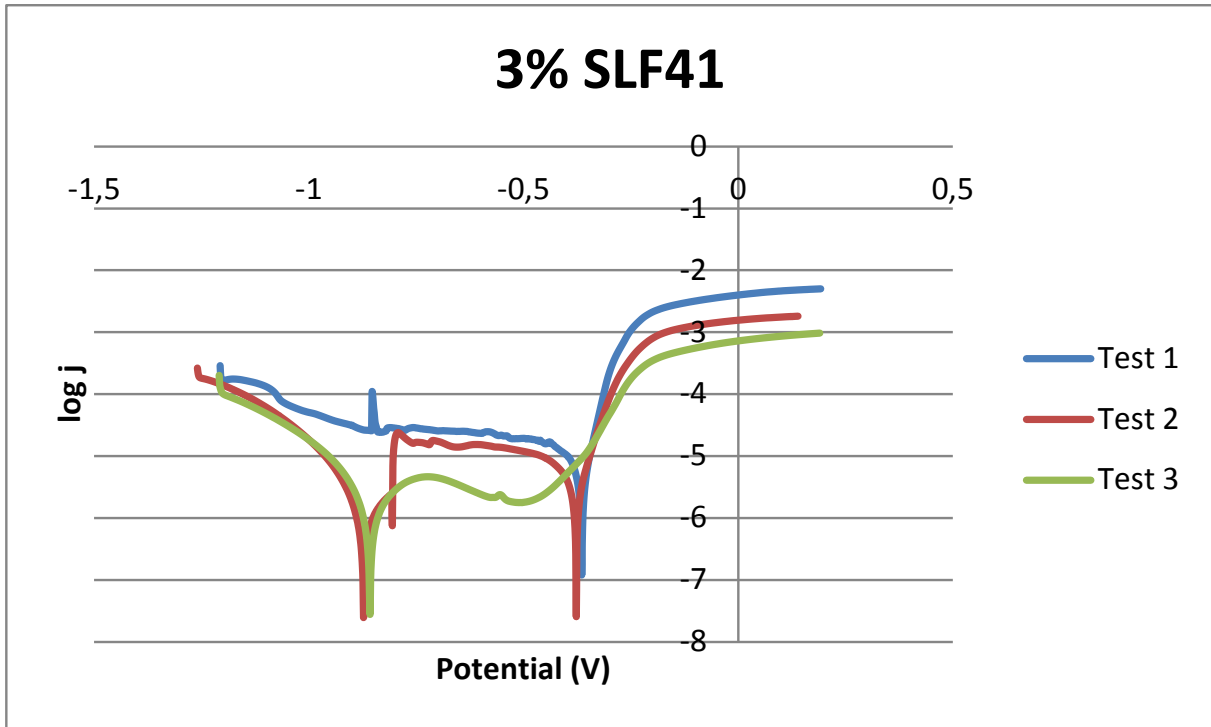


Figure 45 - Polarization curves for 3% SLF41

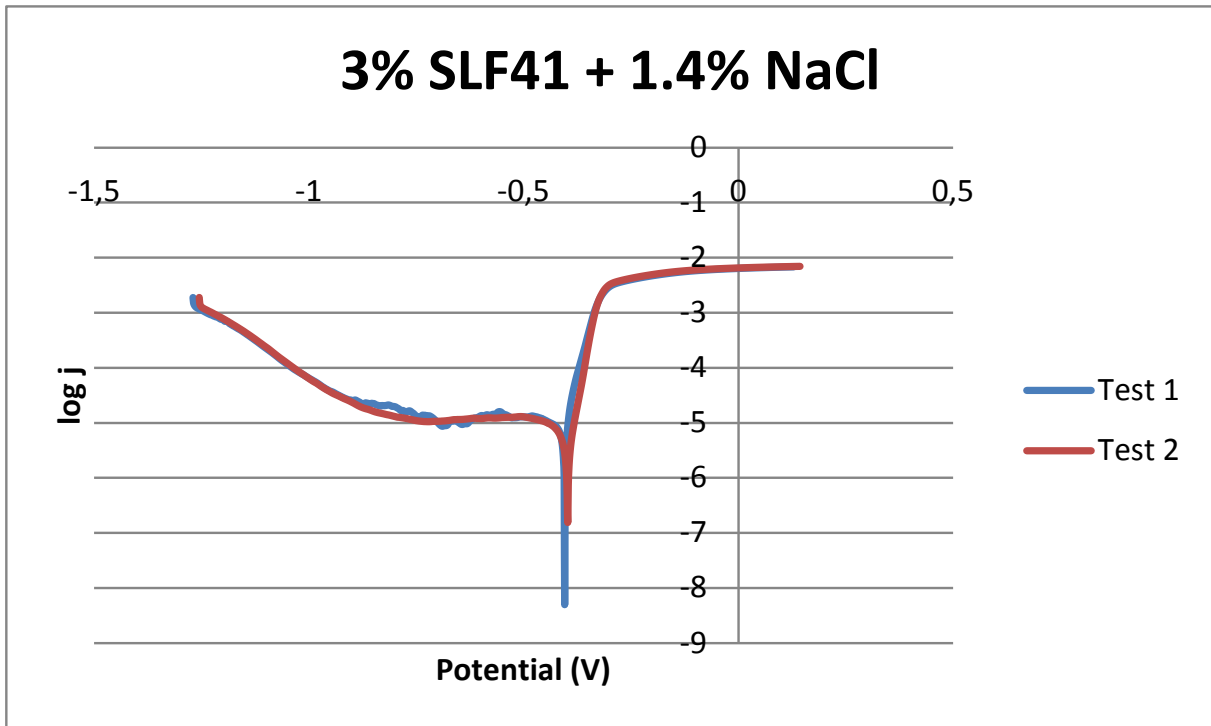


Figure 46 - Polarization curves for 3% SLF41 + 1.4% NaCl

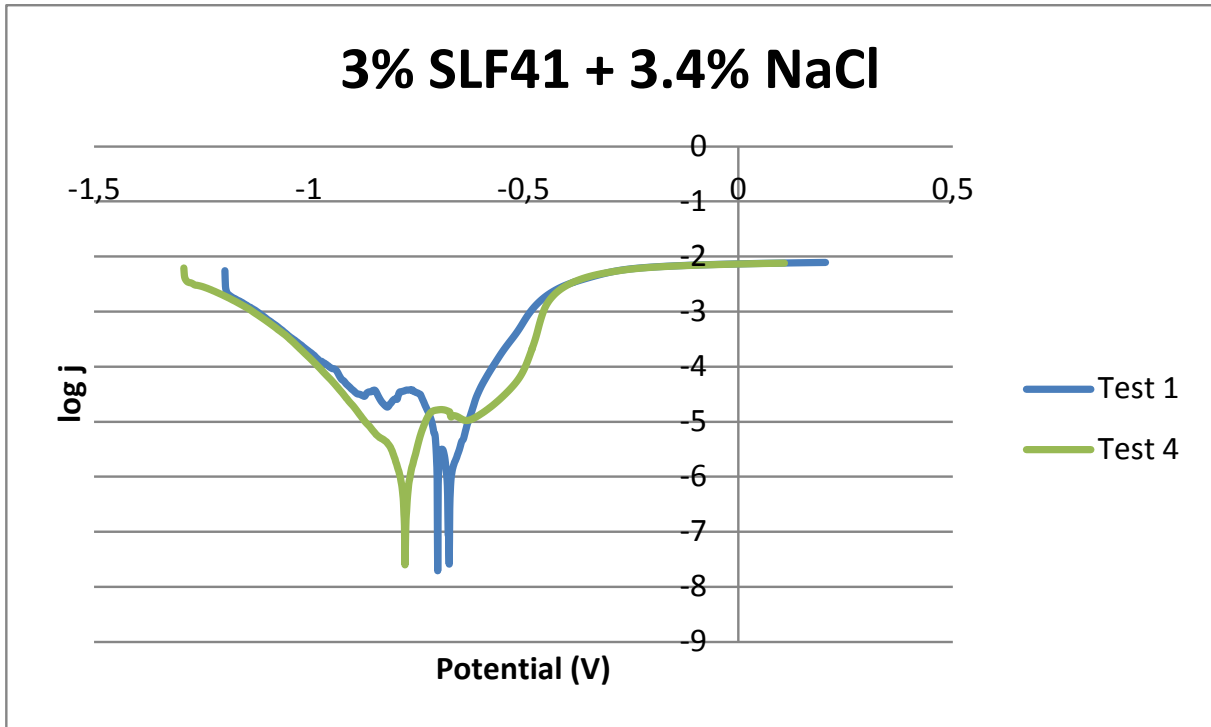


Figure 47 - Polarization curves for 3% SLF41 + 3.4% NaCl

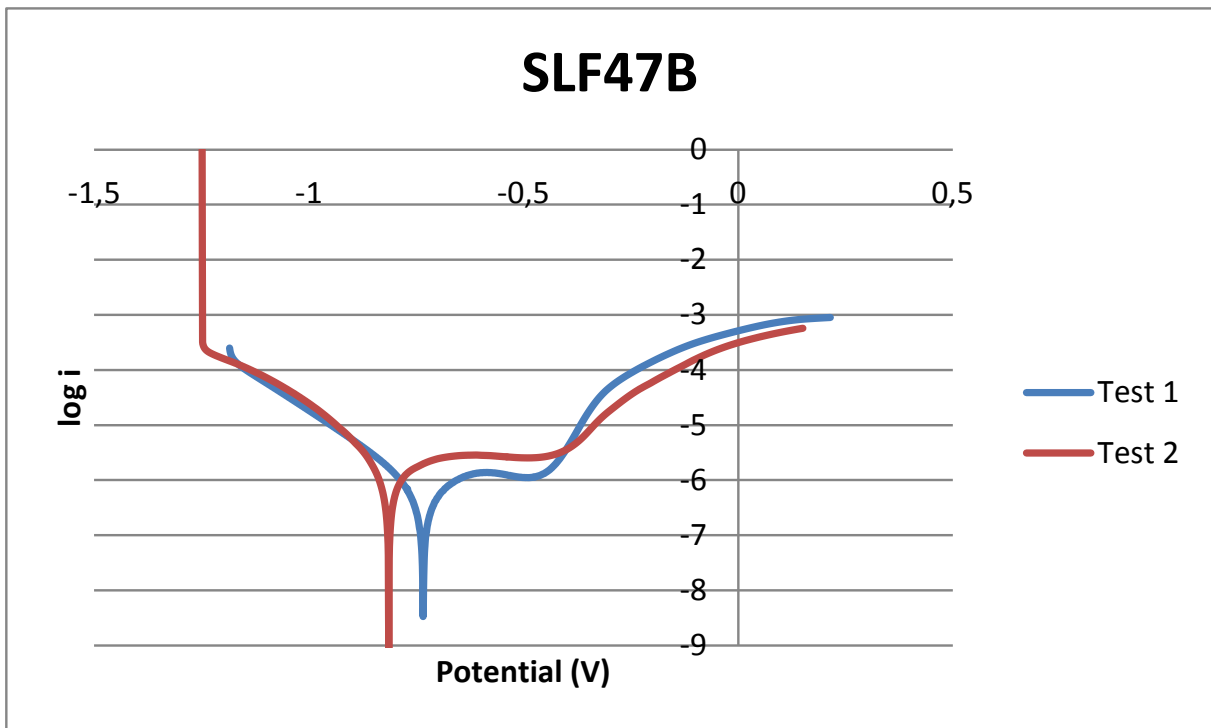


Figure 48 - Polarization curves for SLF47B.

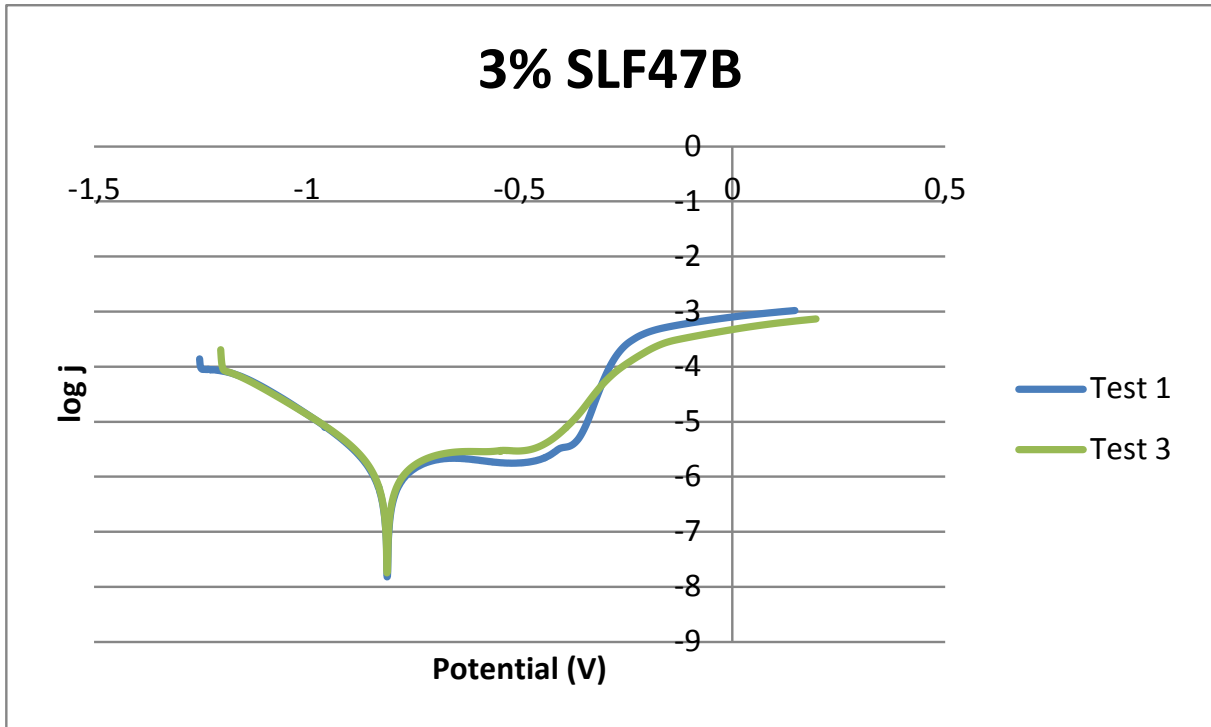


Figure 49 - Polarization curves for 3% SLF47B

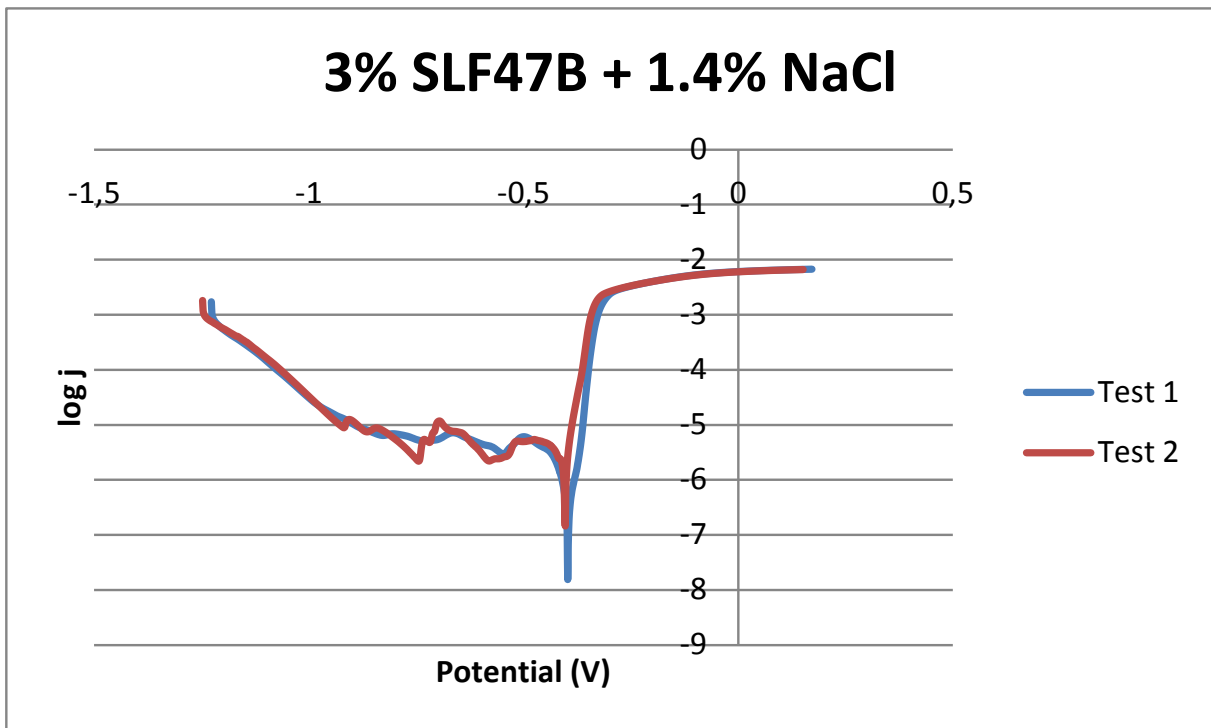


Figure 50 - Polarization curves for 3% SLF47B + 1.4% NaCl

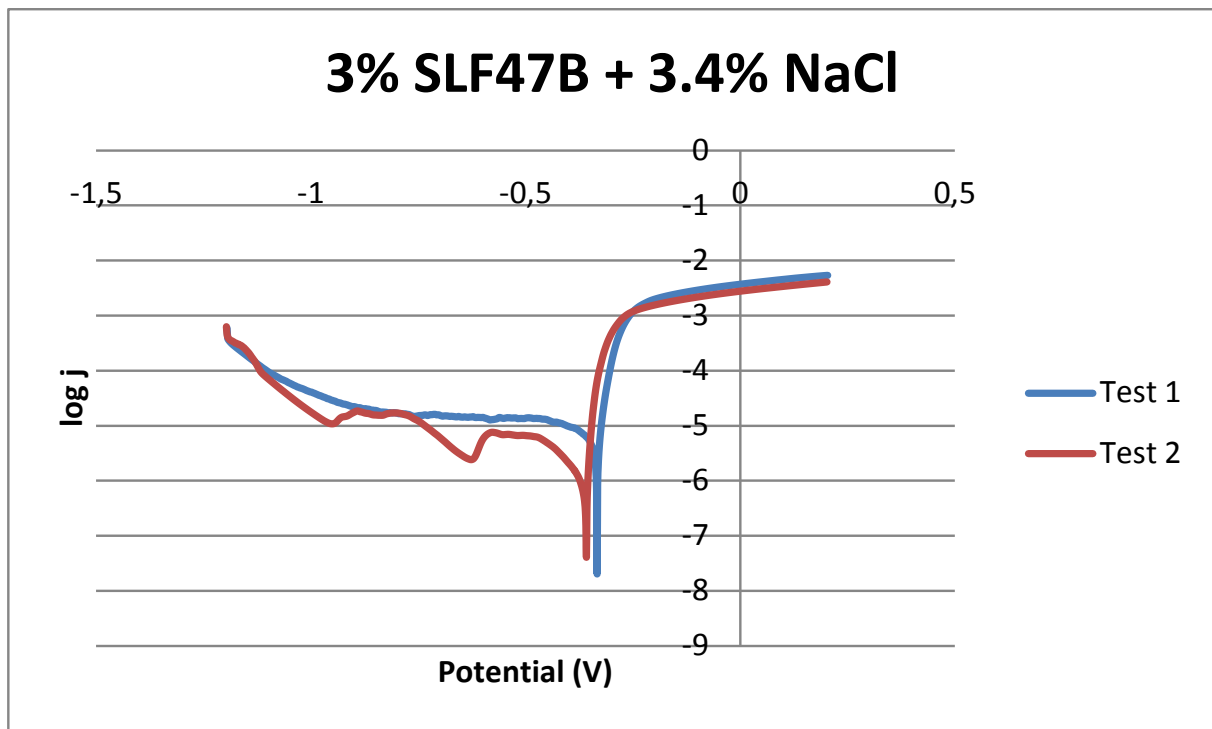


Figure 51 - Polarization Curves for 3% SLF47B + 3.4% NaCl

At 100% foam concentration SLF41 seems to be the most corrosive foam. Its corrosion potential is the highest and the current density is the lowest. ABR5 and SLF47B show the least corrosive properties, and they both cause passivation. However, SLF47B has the lowest current density while ABR5 has the lowest corrosion potential.

At 3% concentration, ABR5 shows little variation from 100% concentration. SLF41 however, shows passivating ability, which it did not do at 100% concentration. SLF47B does not change very much except for a slight decrease in the corrosion potential.

At 1.4% NaCl concentration ABR5 goes from passivating to unstable passivation. SLF41 loses its unstable passivating ability and becomes fully corrosive. SLF47B loses its passivation completely.

At 3.4% NaCl concentration ABR5 loses its unstable passivity and is now fully corrosive. SLF41, has exhibits a major decrease in corrosion potential suggesting less corrosive behavior at 3.4% NaCl concentration. SLF47B shows similar behavior as with 1.4% NaCl except for a slight increase in the corrosion potential.

4.4 pH Measurements

The pH values of the lubricants were measured and are presented in Table 8 below. In Figure 52 the pH-values are presented in a graph for easier comparison of the effect of water and salt on the lubricant. In Figure 53 the pH-values are presented again, but for easier comparison of the lubricants in the different testing scenarios.

Table 8 - pH-values of the lubricants

Lubricant	pH-value (Test 1)	pH-value (Test 2)
ABR5	7.16	7.23
3% ABR5	6.85	6.85
3% ABR5 + 1.4% NaCl	6.32	6.30
3% ABR5 + 3.4% NaCl	6.22	6.18
SLF41	8.98	8.94
3% SLF41	6.40	6.40
3% SLF41 + 1.4% NaCl	7.25	7.26
3% SLF41 + 3.4% NaCl	7.25	7.28
SLF47B	7.60	7.63
3% SLF47B	6.74	6.79
3% SLF47B + 1.4% NaCl	6.94	6.96
3% SLF47B + 3.4% NaCl	6.73	6.72

pH-values of lubricants

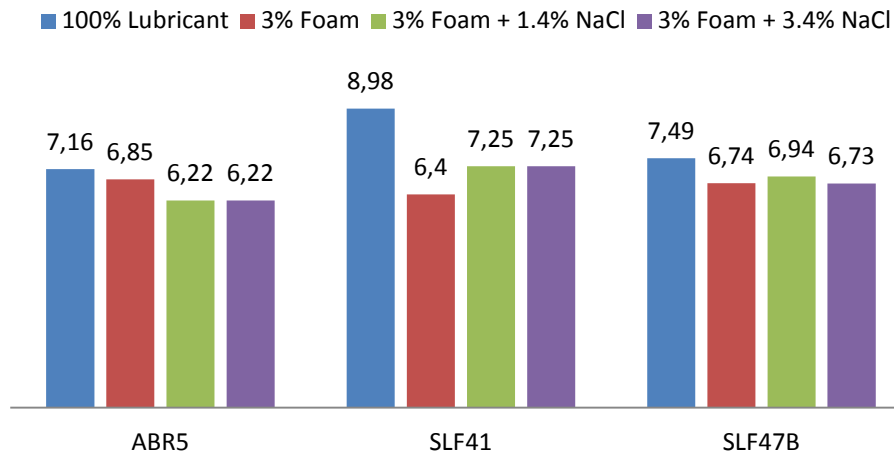


Figure 52 - pH-values of the lubricants.

pH-values of lubricants

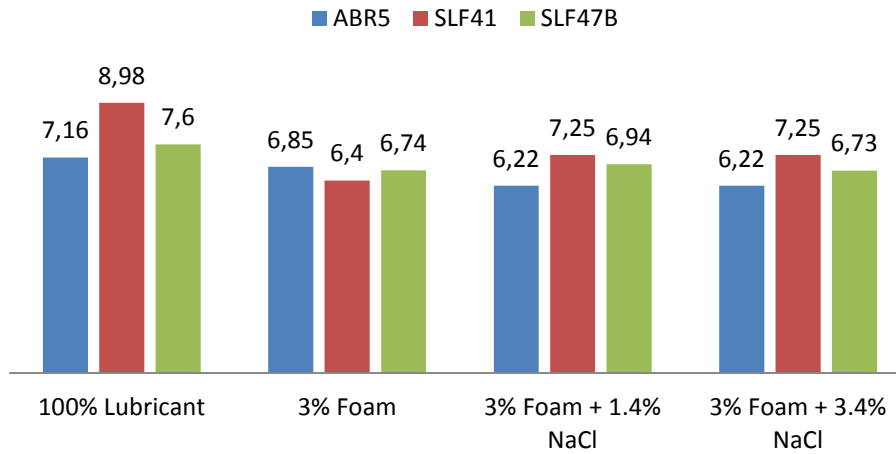


Figure 53 - pH values of the lubricants in the different electrolytes.

4.5 Viscosity

The results of the viscosity measurements are presented in Table 9 below. The values are also presented in Figure 54 and Figure 55 for easier comparison.

Table 9 - Viscosity of lubricants.

Lubricant	Dynamic viscosity (Pa·s) [10 ⁻³]
ABR5	29.14
3% ABR5	1.47
3% ABR5 + 1.4% NaCl	1.61
3% ABR5 + 3.4% NaCl	1.49
Lubricant	SLF41
SLF41	45.82
3% SLF41	1.80
3% SLF41 + 1.4% NaCl	1.68
3% SLF41 + 3.4% NaCl	1.68
Lubricant	SLF47B
SLF47B	2.95
3% SLF47B	1.17
3% SLF47B + 1.4% NaCl	1.41
3% SLF47B + 3.4% NaCl	1.41

Viscosity of lubricants

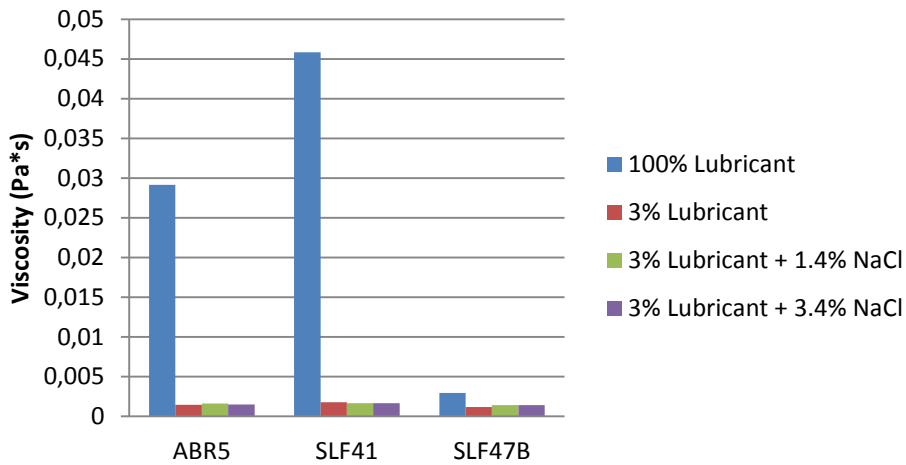


Figure 54 - Viscosity of lubricants.

Viscosity of lubricants

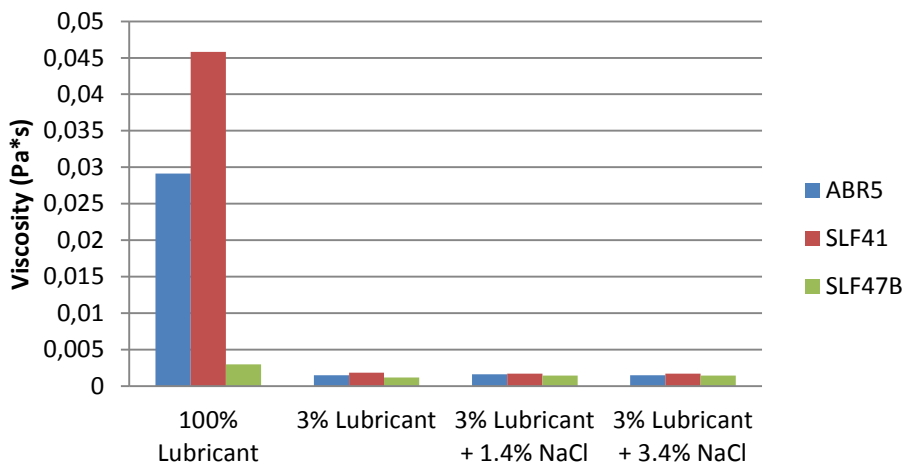


Figure 55 - Viscosity of lubricants.

From the figures once can see that ABR5 and SLF41 are their most viscous in their pure form, SLF47B on the other hand, is not. The addition of water, makes the foams a lot less viscous. With the addition of 1.4% NaCl, the viscosity increases for ABR5. However, at 3.4% NaCl, the viscosity drops to a value fairly similar to that without NaCl. SLF41 experiences a drop in viscosity with the addition of 1.4% NaCl and its viscosity remains unchanged at 3.4% NaCl concentration. SLF47B shows opposite behavior. With the addition of 1.4% NaCl, the viscosity increases, but same as SLF41, it remains unchanged at 3.4% NaCl concentration.

4.6 Reciprocal Ball-on-Plate

Table 10 shows the average coefficient of friction (COF) for the steel ball sliding against the rock surface. The number in parenthesis which is given for some values indicates the “real” test number of the test, e.g. ABR5 +3.4% NaCl (2) have test number two. In Figure 56 the average COF is presented in a column chart. Figure 57 to Figure 69 shows the variations in the COF as function of time during the different test scenarios.

Table 10 - Average COF for the ball-on-plate tests.

Test conditions	Average COF*
Dry	1.02 ± 0.06
	0.98 ± 0.05
Wet	0.85 ± 0.10
	0.80 ± 0.08
Wet + 1.4% NaCl	0.77 ± 0.05
	0.76 ± 0.05
Wet + 3.4 % NaCl	0.76 ± 0.06
	0.76 ± 0.06
ABR5	0.11 ± 0.04
	0.19 ± 0.11
ABR5 + 1.4% NaCl	0.13 ± 0.03
	0.15 ± 0.05
ABR5 + 3.4 % NaCl	0.41 ± 0.05 (2)
	0.21 ± 0.06 (3)
SLF41	0.62 ± 0.18
	0.51 ± 0.07
SLF41 + 1.4% NaCl	0.86 ± 0.09 (1)
	0.80 ± 0.10 (3)
SLF41 + 3.4 % NaCl	0.72 ± 0.09
	0.80 ± 0.11
SLF47B	0.16 ± 0.04
	0.22 ± 0.20
SLF47B + 1.4% NaCl	0.35 ± 0.12 (3)
	0.46 ± 0.13 (4)
SLF4B + 3.4 % NaCl	0.14 ± 0.03 (2)
	0.24 ± 0.04 (3)

*The results of the two repetitions of each test are shown in the table

Average COF

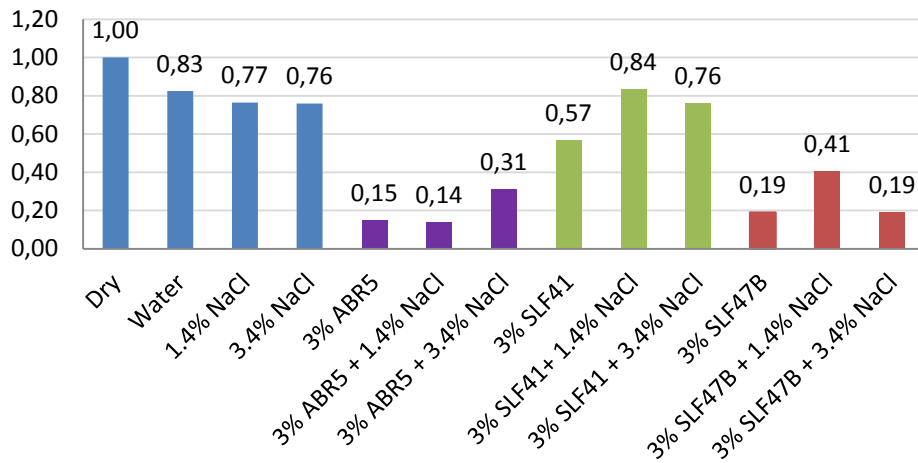


Figure 56 - Average COF for the different test scenarios.

The COF is reduced when using water as a lubricant. The addition of NaCl lowers the COF a little bit more, but the concentration has little effect. An even lower COF is achieved when adding a foam lubricant. Further the results show that the COF increases when testing in NaCl. ABR5 and SLF47B achieve the lowest COF of the tested foams. Adding 1.4% NaCl to the foam increases the COF, except for when using ABR5. Increasing the NaCl concentration to 3.4% causes a lower COF for SLF41B and SLF41, for ABR it increases.

In Figure 57 to Figure 69 the COF evolution with times is shown for all the tests performed.

Dry

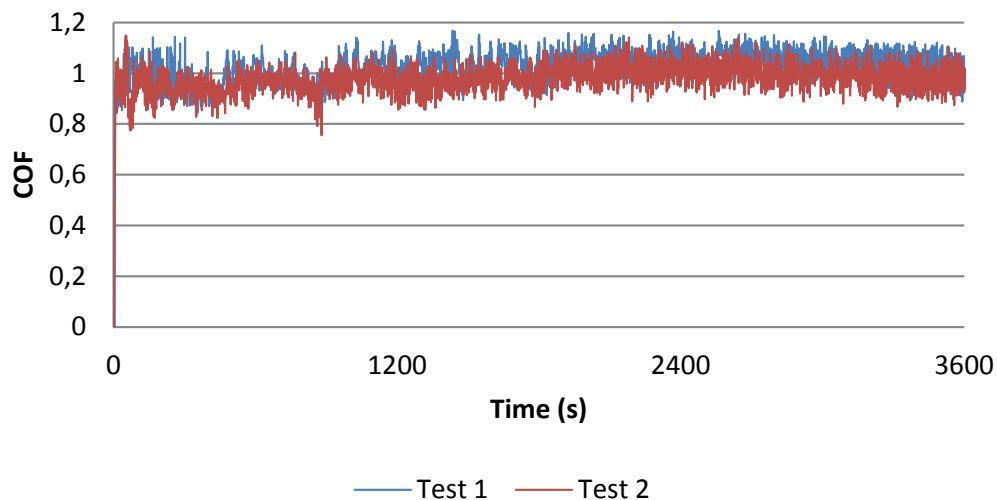


Figure 57 - Coefficient of friction for dry rubbing.

Water

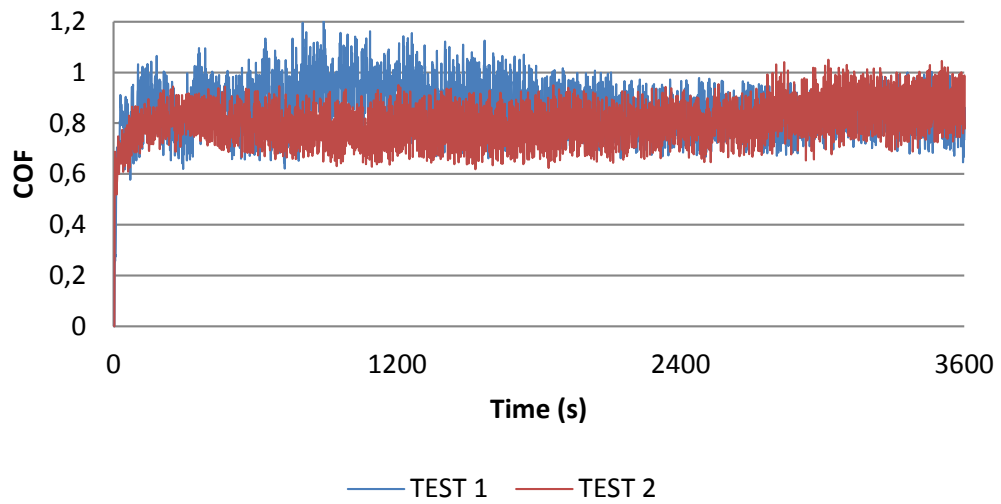


Figure 58 – Coefficient of friction for wet rubbing.

1.4% NaCl

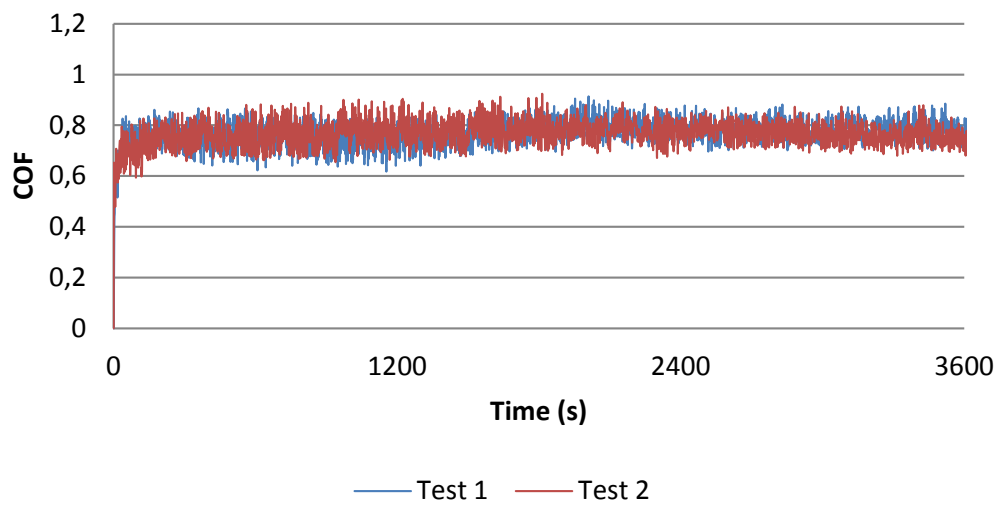


Figure 59 - Coefficient of friction for wet rubbing with 1.4% NaCl.

3.4% NaCl

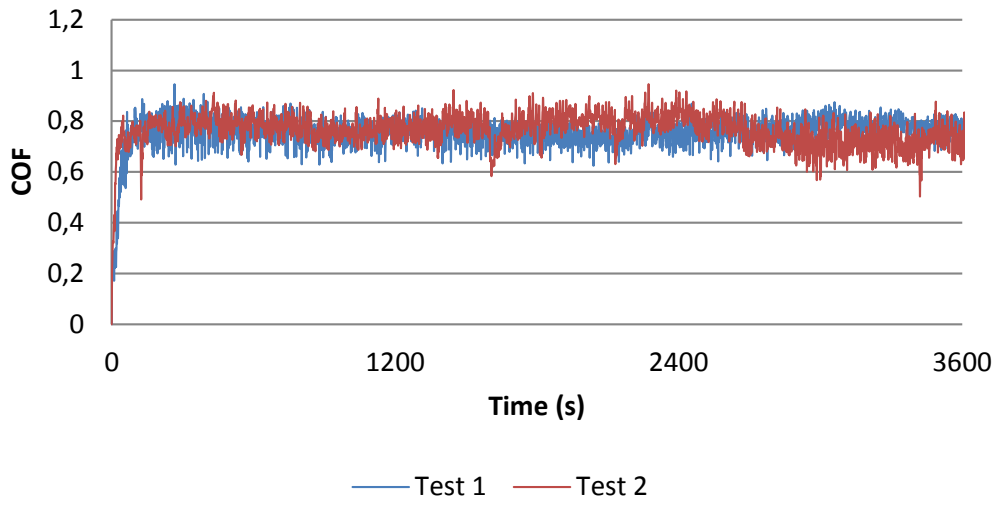


Figure 60 - Coefficient of friction for wet rubbing with 3.4% NaCl.

3% ABR5

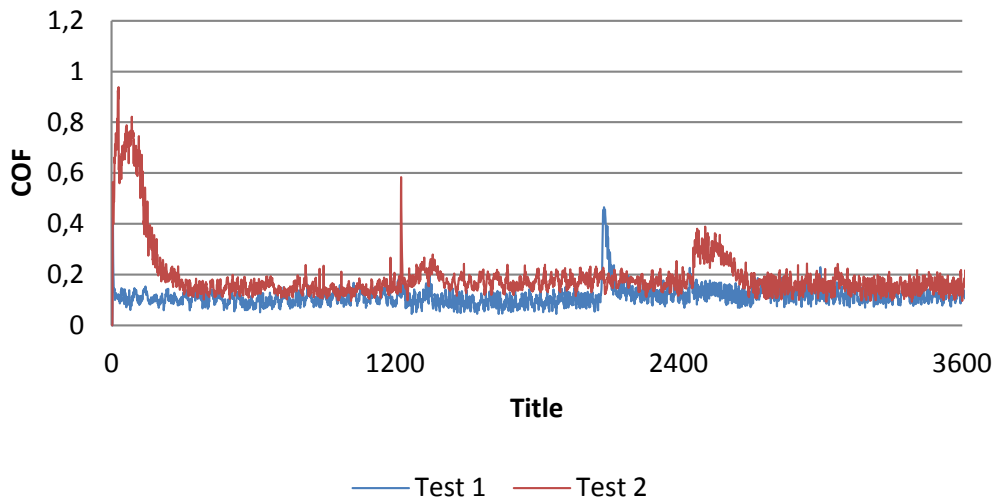


Figure 61 - Coefficient of friction for wet rubbing with 3% ABR5 foam.

3% ABR5 + 1.4% NaCl

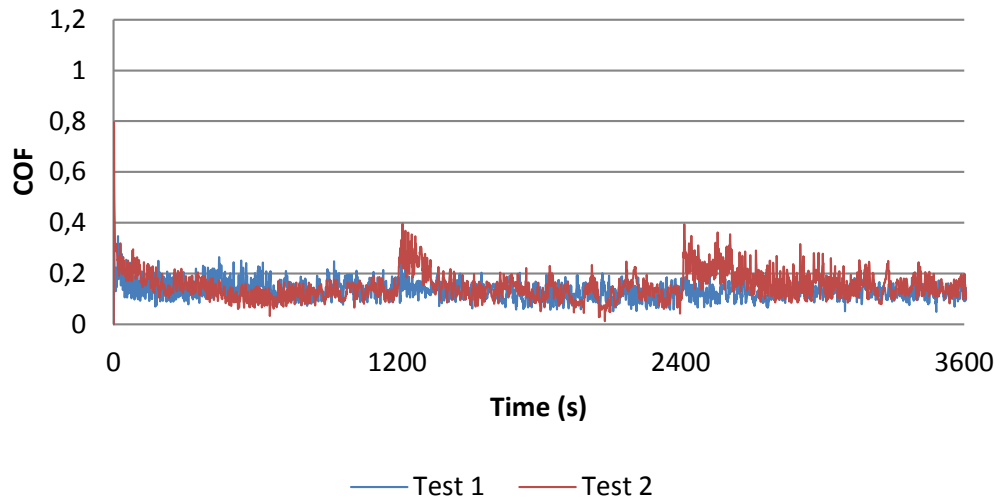


Figure 62 - Coefficient of friction for wet rubbing with 3% ABR5 foam and 1.4% NaCl.

ABR5 + 3.4% NaCl

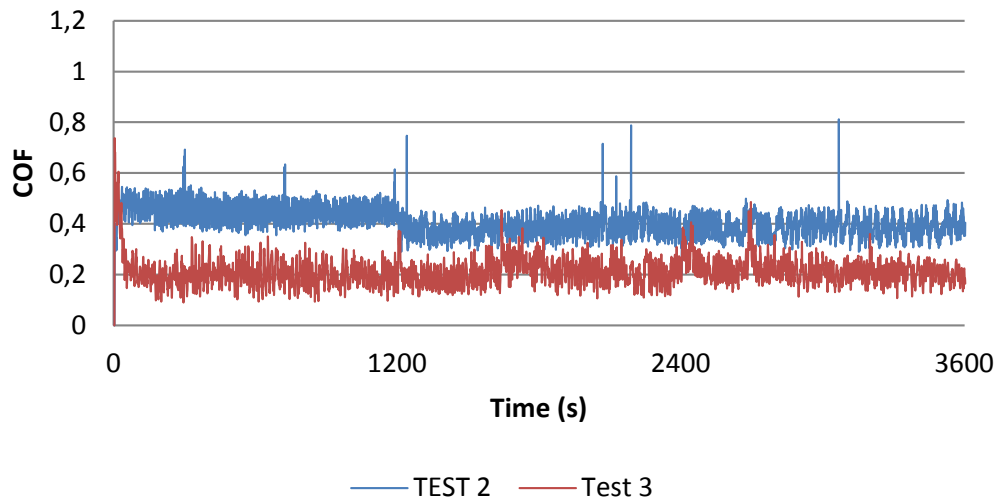


Figure 63 - Coefficient of friction for wet rubbing with 3% ABR5 Foam and 3.4% NaCl.

3% SLF41

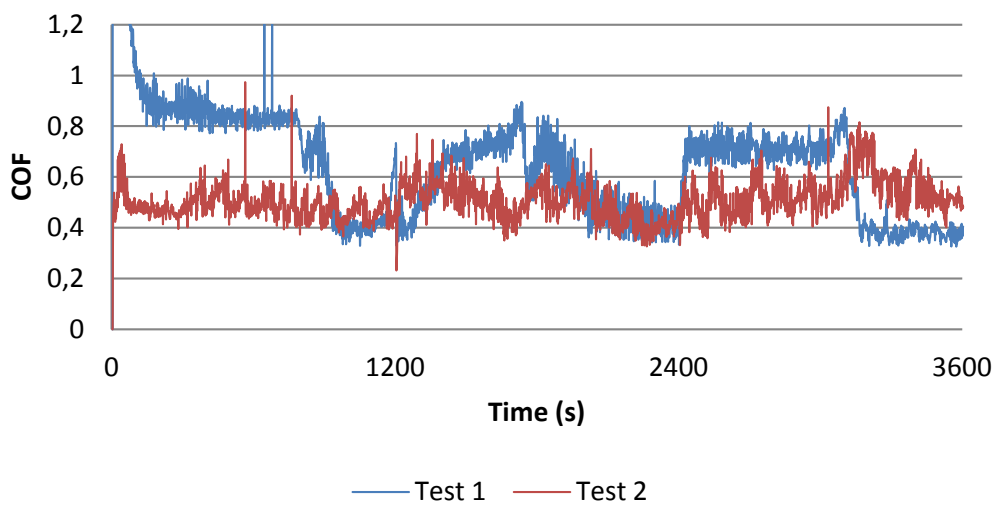


Figure 64 - Coefficient of friction for wet rubbing with 3% SLF41 Foam.

3% SLF41 + 1.4% NaCl

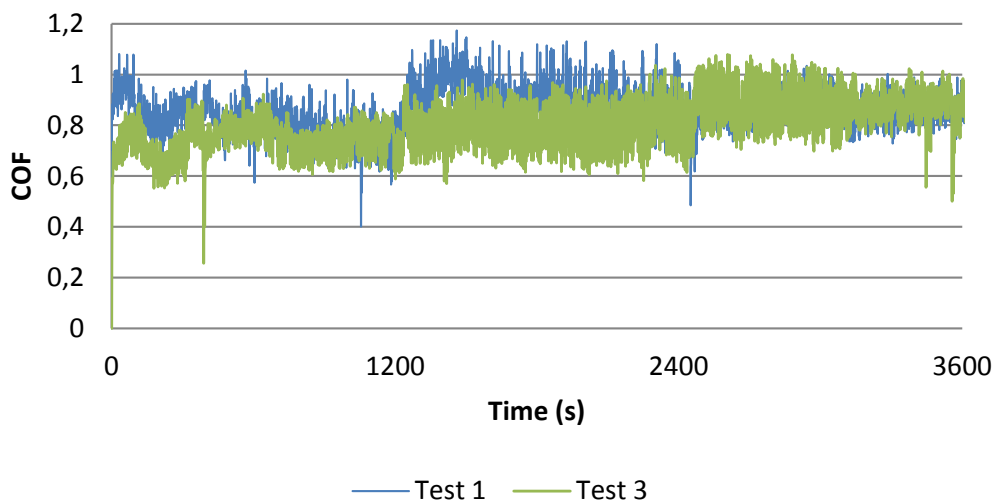


Figure 65 - Coefficient of friction for wet rubbing with 3% SLF41 and 1.4% NaCl.

3% SLF41 + 3.4% NaCl

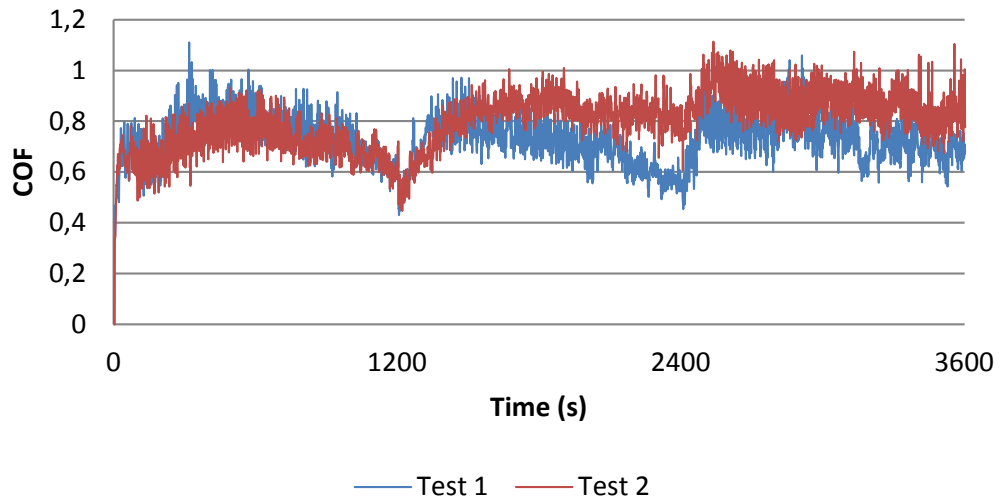


Figure 66 - Coefficient of friction for wet rubbing with 3% SLF41 foam and 3.4% NaCl.

3% SLF47B

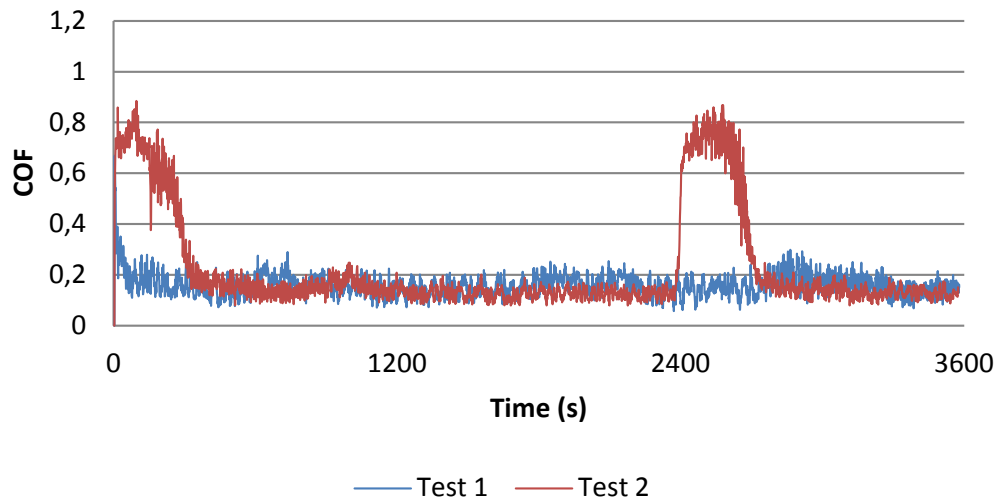


Figure 67 - Coefficient of friction for wet rubbing with 3% SLF47B foam.

3% SLF47B + 1.4% NaCl

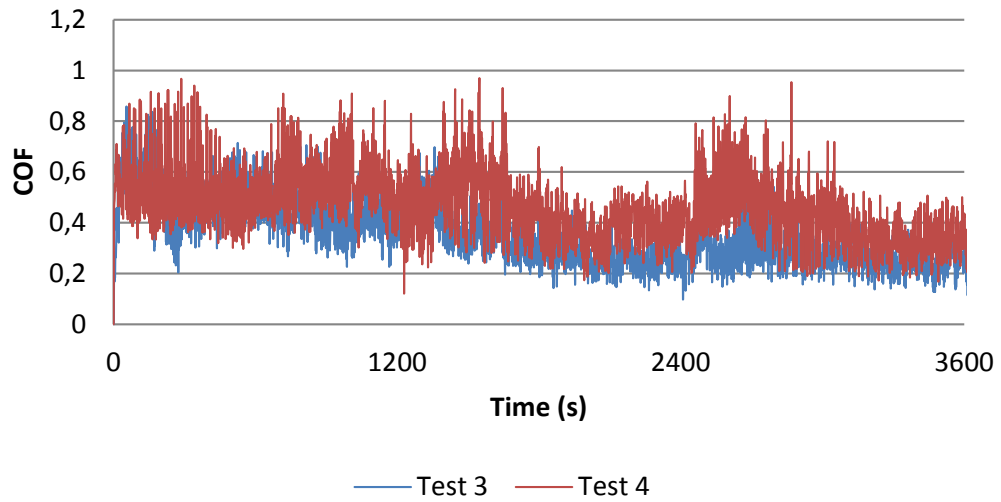


Figure 68 - Coefficient of friction for wet rubbing with 3% SLF47B and 1.4% NaCl.

3% SLF47B + 3.4% NaCl

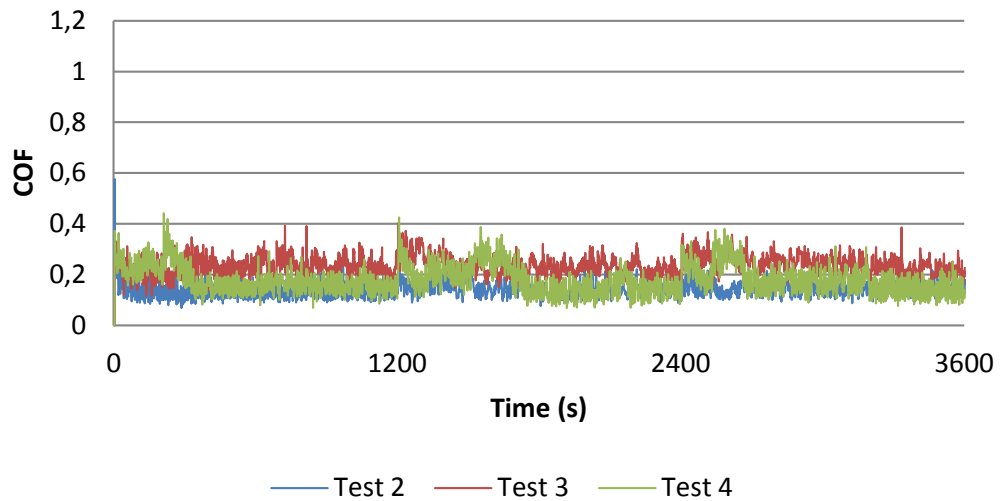


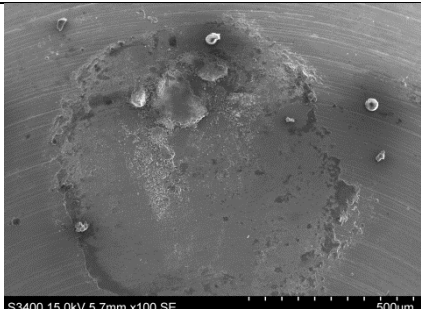
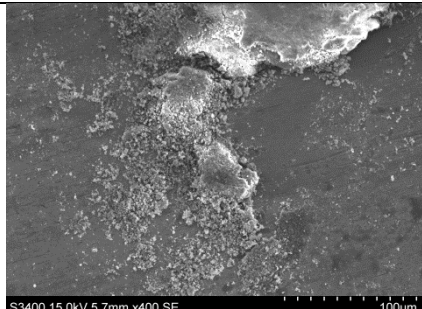
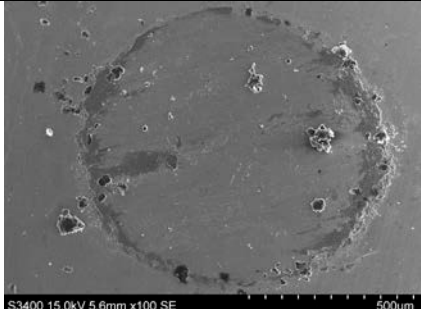
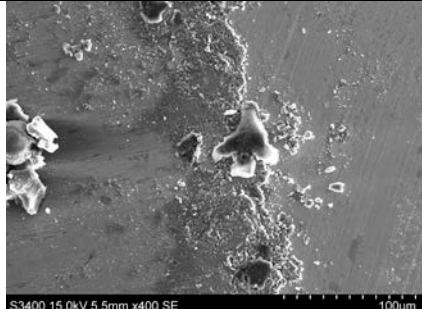
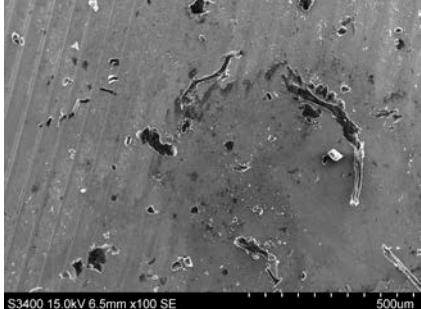
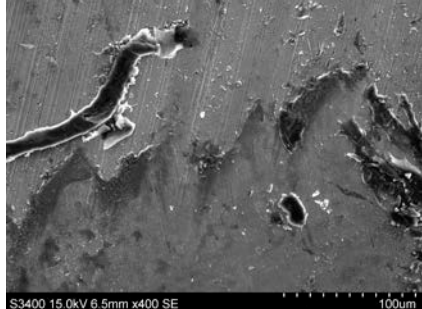
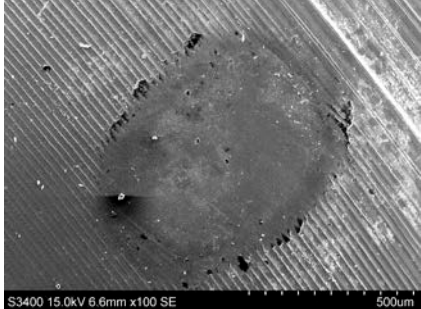
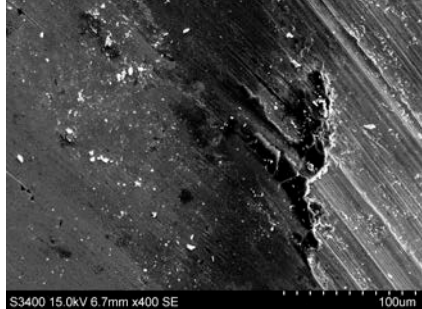
Figure 69 - Coefficient of friction for wet rubbing with 3% SLF47B foam and 3.4% NaCl.

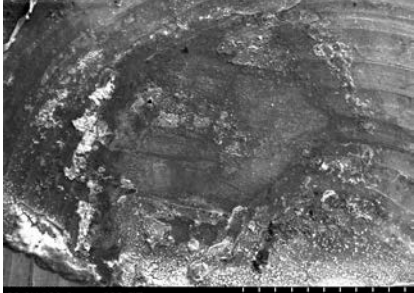
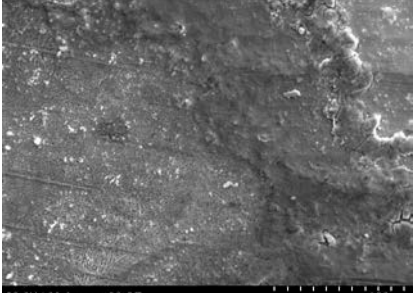
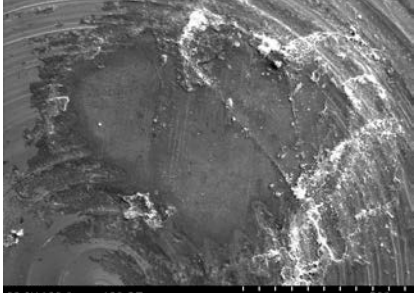
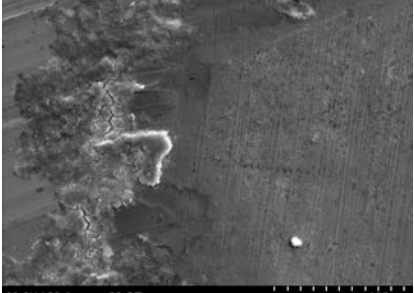
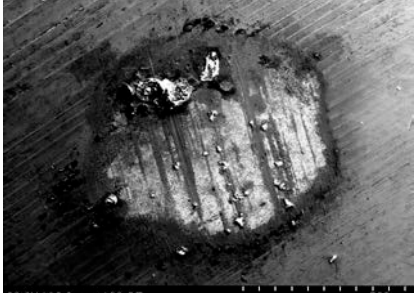


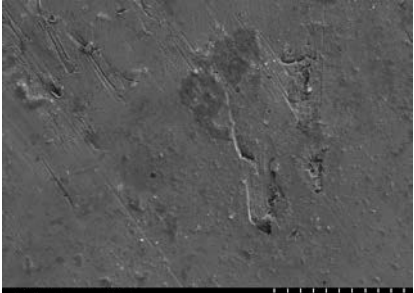
4.6.1 Topography of the steel balls

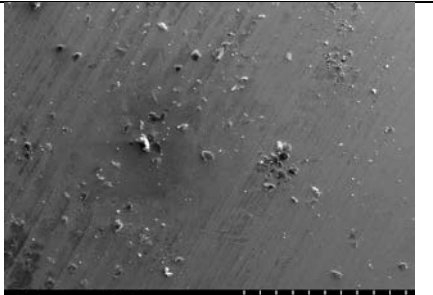
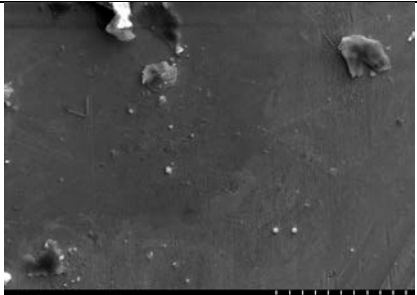
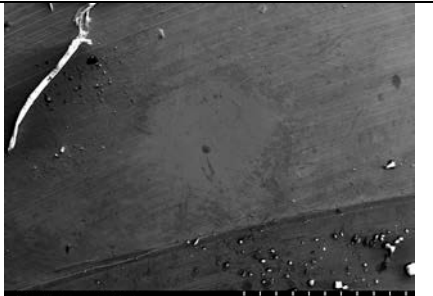
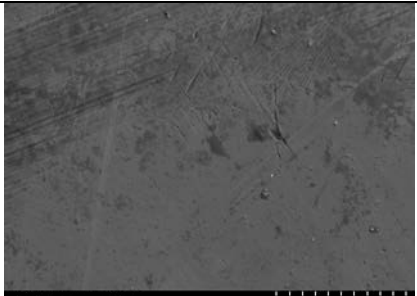

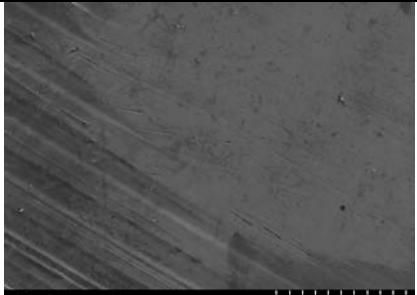
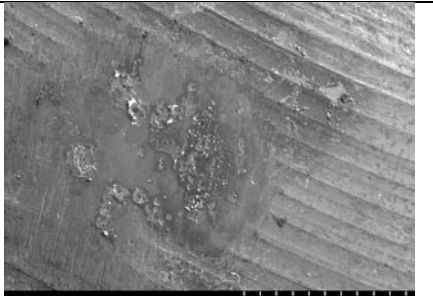
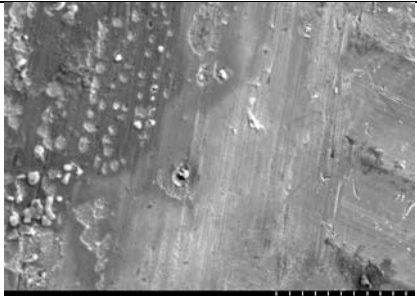
SEM



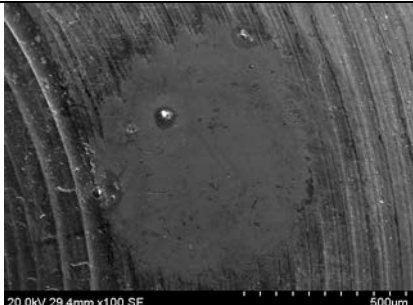



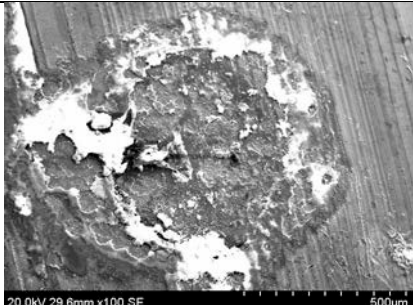
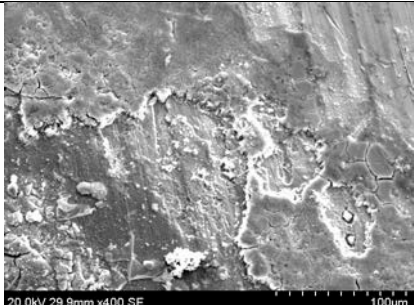
The wear on the steel ball under the different scenarios from the ball-on-plate test is presented in Figure 70 to Figure 77 in Table 11 below.

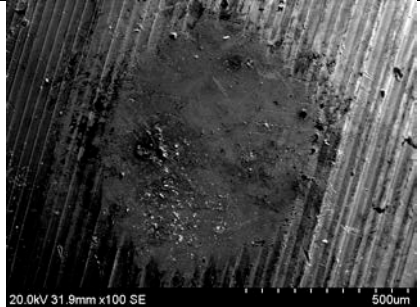

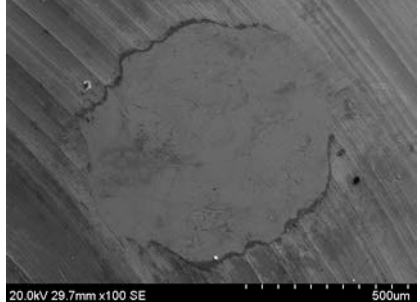

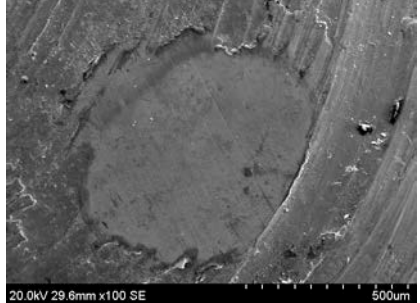

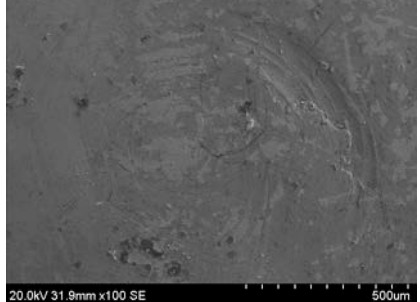
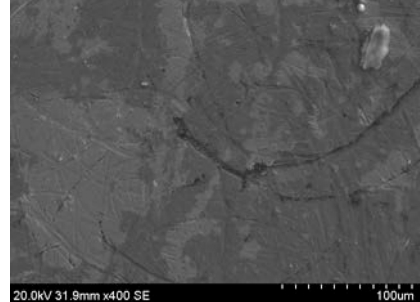
Table 11 - SEM pictures of the steel surface after reciprocal ball-on-plate test.

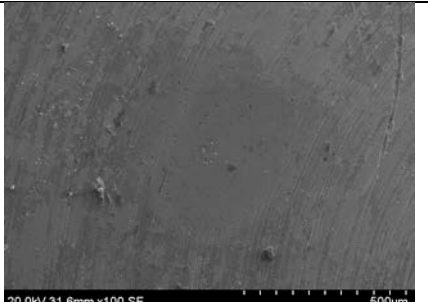
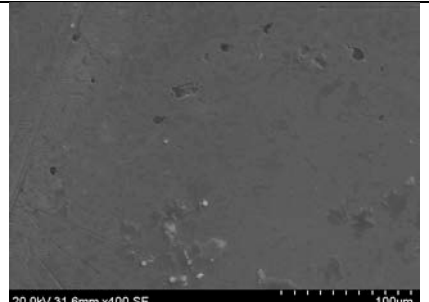
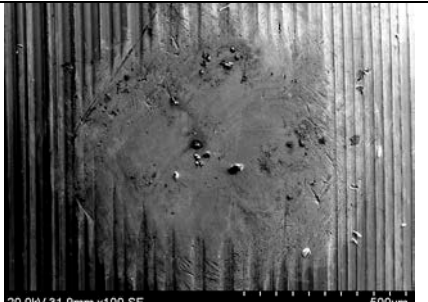
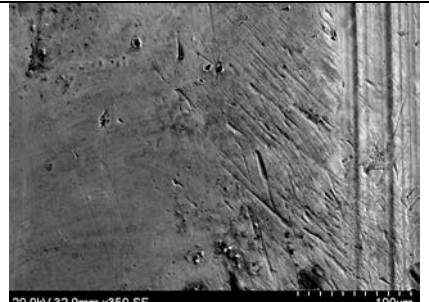



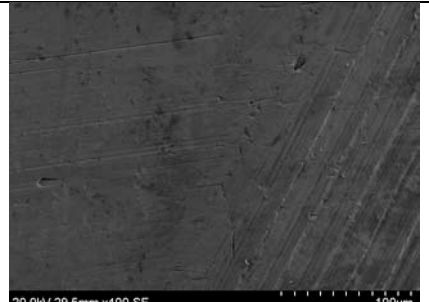
Condition	Magnification	
	100x	400x
Dry wear Test 1	 <p>S3400 15.0kV 5.7mm x100 SE 500um Figure 70 - Wear track on the steel ball from dry wear at 100x magnification.</p>	 <p>S3400 15.0kV 5.7mm x400 SE 100um Figure 71 - Wear track on the steel ball from dry wear at 400x magnification.</p>
Dry wear Test 2	 <p>S3400 15.0kV 5.6mm x100 SE 500um Figure 72 - Wear track on the steel ball from dry wear at 100x magnification.</p>	 <p>S3400 15.0kV 5.5mm x400 SE 100um Figure 73 - Wear track on the steel ball from dry wear at 400x magnification.</p>
Wet wear Test 1	 <p>S3400 15.0kV 6.5mm x100 SE 500um Figure 74 - Wear track on the steel ball from wet wear at 100x magnification.</p>	 <p>S3400 15.0kV 6.5mm x400 SE 100um Figure 75 - Wear track on the steel ball from wet wear at 400x magnification.</p>
Wet wear Test 2	 <p>S3400 15.0kV 6.6mm x100 SE 500um Figure 76 - Wear track on the steel ball from wet wear at 100x magnification.</p>	 <p>S3400 15.0kV 6.7mm x400 SE 100um Figure 77 - Wear track on the steel ball from wet wear at 400x magnification.</p>

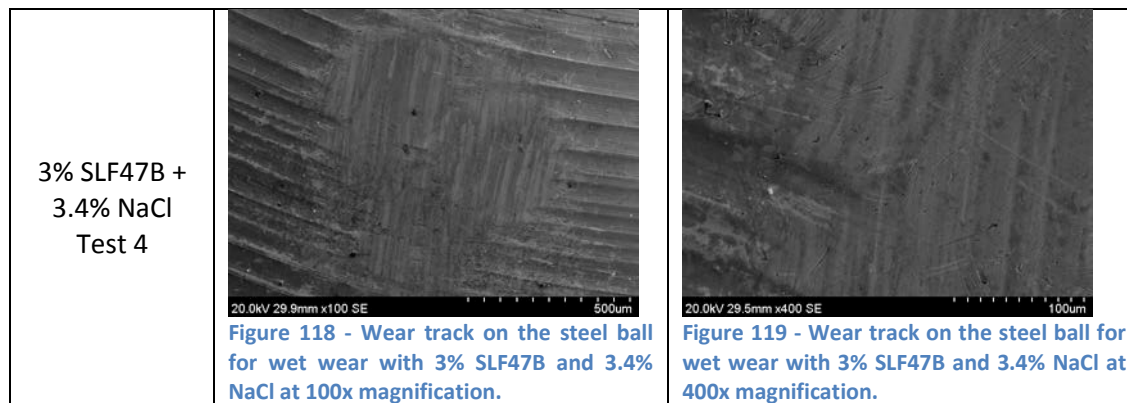
<p>1.4% NaCl Test 1</p>	 <p>20.0kV 29.6mm x100 SE 500µm</p> <p>Figure 78 - Wear track on the steel ball from 1.4% NaCl at 100x magnification.</p>	 <p>20.0kV 29.6mm x400 SE 100µm</p> <p>Figure 79 - Wear track on the steel ball from 1.4% NaCl at 400x magnification.</p>
<p>1.4% NaCl Test 2</p>	 <p>20.0kV 29.6mm x100 SE 500µm</p> <p>Figure 80 - Wear track on the steel ball from 1.4% NaCl at 100x magnification.</p>	 <p>20.0kV 29.6mm x400 SE 100µm</p> <p>Figure 81 - Wear track on the steel ball from 1.4% NaCl at 400x magnification.</p>
<p>3.4% NaCl</p>	 <p>20.0kV 32.0mm x100 SE 500µm</p> <p>Figure 82 - Wear track on the steel ball for wet wear with 3.4% NaCl at 100x magnification.</p>	 <p>20.0kV 32.0mm x400 SE 100µm</p> <p>Figure 83 - Wear track on the steel ball for wet wear with 3.4% NaCl at 400x magnification.</p>
<p>3% ABR5 Test 1</p>	 <p>20.0kV 31.4mm x80 SE 500µm</p> <p>Figure 84 - Wear track on the steel ball for wet wear with 3% ABR5 at 100x magnification.</p>	 <p>20.0kV 31.4mm x400 SE 100µm</p> <p>Figure 85 - Wear track on the steel ball for wet wear with 3% ABR5 at 400x magnification.</p>

<p>3% ABR5 Test 2</p>	 <p>20.0kV 31.4mm x100 SE</p> <p>Figure 86 - Wear track on the steel ball for wet wear with 3% ABR5 at 100x magnification.</p>	 <p>20.0kV 31.4mm x400 SE</p> <p>Figure 87 - Wear track on the steel ball for wet wear with 3% ABR5 at 400x magnification.</p>
<p>3% ABR5 + 1.4% NaCl Test 1</p>	 <p>20.0kV 29.4mm x100 SE</p> <p>Figure 88 - Wear track on the steel ball for wet wear with 3% ABR5 and 1.4% NaCl at 100x magnification.</p>	 <p>20.0kV 29.4mm x400 SE</p> <p>Figure 89 - Wear track on the steel ball for wet wear with 3% ABR5 and 1.4% NaCl at 400x magnification.</p>
<p>3% ABR5 + 1.4% NaCl Test 2</p>	 <p>20.0kV 29.5mm x100 SE</p> <p>Figure 90 - Wear track on the steel ball for wet wear with 3% ABR5 and 1.4% NaCl at 100x magnification.</p>	 <p>20.0kV 29.5mm x400 SE</p> <p>Figure 91 - Wear track on the steel ball for wet wear with 3% ABR5 and 1.4% NaCl at 400x magnification.</p>
<p>3% ABR5 + 3.4% NaCl Test 2</p>	 <p>20.0kV 29.8mm x100 SE</p> <p>Figure 92 - Wear track on the steel ball for wet wear with 3% ABR5 and 3.4% NaCl at 100x magnification.</p>	 <p>20.0kV 29.8mm x400 SE</p> <p>Figure 93 - Wear track on the steel ball for wet wear with 3% ABR5 and 3.4% NaCl at 400x magnification.</p>

<p>3% ABR5 + 3.4% NaCl Test 3</p>	 <p>20.0kV 29.6mm x100 SE 500µm</p> <p>Figure 94 - Wear track on the steel ball for wet wear with 3% ABR5 and 3.4% NaCl at 100x magnification.</p>	 <p>20.0kV 29.5mm x400 SE 100µm</p> <p>Figure 95 - Wear track on the steel ball for wet wear with 3% ABR5 and 3.4% NaCl at 400x magnification.</p>
<p>3% SLF41 Test 1</p>	 <p>20.0kV 29.4mm x100 SE 500µm</p> <p>Figure 96 - Wear track on the steel ball for wet wear with 3% SLF41 at 100x magnification.</p>	 <p>20.0kV 29.4mm x400 SE 100µm</p> <p>Figure 97 - Wear track on the steel ball for wet wear with 3% SLF41 at 400x magnification.</p>
<p>3% SLF41 Test 2</p>	 <p>20.0kV 29.6mm x100 SE 500µm</p> <p>Figure 98 - Wear track on the steel ball for wet wear with 3% SLF41 at 100x magnification.</p>	 <p>20.0kV 29.8mm x400 SE 100µm</p> <p>Figure 99 - Wear track on the steel ball for wet wear with 3% SLF41 at 400x magnification.</p>
<p>3% SLF41 + 1.4% NaCl Test 1</p>	 <p>20.0kV 29.6mm x100 SE 500µm</p> <p>Figure 100 - Wear track on the steel ball for wet wear with 3% SLF41 and 1.4% NaCl at 100x magnification.</p>	 <p>20.0kV 29.9mm x400 SE 100µm</p> <p>Figure 101 - Wear track on the steel ball for wet wear with 3% SLF41 and 1.4% NaCl at 400x magnification.</p>

<p>3% SLF41 + 1.4% NaCl Test 3</p>	 <p>20.0kV 31.9mm x100 SE 500µm</p> <p>Figure 102 - Wear track on the steel ball for wet wear with 3% SLF41 and 1.4% NaCl at 100x magnification.</p>	 <p>20.0kV 31.8mm x400 SE 100µm</p> <p>Figure 103 - Wear track on the steel ball for wet wear with 3% SLF41 and 1.4% NaCl at 400x magnification.</p>
<p>3% SLF41 + 3.4% NaCl Test 1</p>	 <p>20.0kV 29.7mm x100 SE 500µm</p> <p>Figure 104 - Wear track on the steel ball for wet wear with 3% SLF41 and 3.4% NaCl at 100x magnification.</p>	 <p>20.0kV 29.5mm x400 SE 100µm</p> <p>Figure 105 - Wear track on the steel ball for wet wear with 3% SLF41 and 3.4% NaCl at 400x magnification.</p>
<p>3% SLF41 + 3.4% NaCl Test 2</p>	 <p>20.0kV 29.6mm x100 SE 500µm</p> <p>Figure 106 - Wear track on the steel ball for wet wear with 3% SLF41 and 3.4% NaCl at 100x magnification.</p>	 <p>20.0kV 29.6mm x400 SE 100µm</p> <p>Figure 107 - Wear track on the steel ball for wet wear with 3% SLF41 and 3.4% NaCl at 400x magnification.</p>
<p>3% SLF47B Test 1</p>	 <p>20.0kV 31.9mm x100 SE 500µm</p> <p>Figure 108 - Wear track on the steel ball for wet wear with 3% SLF47B at 100x magnification.</p>	 <p>20.0kV 31.9mm x400 SE 100µm</p> <p>Figure 109 - Wear track on the steel ball for wet wear with 3% SLF47B at 400x magnification.</p>

<p>3% SLF47B Test 2</p>	 <p>Figure 110 - Wear track on the steel ball for wet wear with 3% SLF47B at 100x magnification.</p>	 <p>Figure 111 - Wear track on the steel ball for wet wear with 3% SLF47B at 400x magnification.</p>
<p>3% SLF47B + 1.4% NaCl Test 3</p>	 <p>Figure 112 - Wear track on the steel ball for wet wear with 3% SLF47B and 1.4% NaCl at 100x magnification.</p>	 <p>Figure 113 - Wear track on the steel ball for wet wear with 3% SLF47B and 1.4% NaCl at 400x magnification.</p>
<p>3% SLF47B + 1.4% NaCl Test 4</p>	 <p>Figure 114 - Wear track on the steel ball for wet wear with 3% SLF47B and 1.4% NaCl at 100x magnification.</p>	 <p>Figure 115 - Wear track on the steel ball for wet wear with 3% SLF47B and 1.4% NaCl at 400x magnification.</p>
<p>3% SLF47B + 3.4% NaCl Test 2</p>	 <p>Figure 116 - Wear track on the steel ball for wet wear with 3% SLF47B and 3.4% NaCl at 100x magnification.</p>	 <p>Figure 117 - Wear track on the steel ball for wet wear with 3% SLF47B and 3.4% NaCl at 400x magnification.</p>



The dry tests show more wear debris than the wet tests. Though the wet test show less wear, some corrosion products seem to be present. The addition of salt at both 1.4% and 3.4% NaCl concentration causes a severe increase in corrosion products.

In Figure 84 to Figure 87 one can see that 3% ABR5 greatly reduces the wear on the steel ball. The wear track is very difficult to spot. In Figure 88 to Figure 91 one can see that the addition of 1.4% NaCl, the wear track is easier to spot, however, the wear track is very small. No corrosion can be spotted. When 3.4% NaCl is used, the wear is a lot more visible and so is the corrosion. From Figure 92 and Figure 95 one can see that the ABR5 in 3.4% NaCl causes pitting in the steel as well as normal corrosion.

From Figure 96 to Figure 99 one can see that the wear of the steel ball from a test using SLF41 is greater than when ABR5 was used. At 1.4% NaCl concentration the SLF41 foam caused corrosion in test 1, while on test 2 there is little visible corrosion as seen in Figure 100 to Figure 103. With 3.4% NaCl the wear track seems to be bigger and deeper. No corrosion can be spotted, Figure 104 to Figure 107.

The pictures for the 3% SLF47B tests show wear tracks that are barely visible as seen in Figure 108 to Figure 111. No corrosion can be seen. The pictures in Figure 112 to Figure 115 show that the addition of 1.4% NaCl causes the wear to increase. The wear track is more visible, and scratches can be seen. No corrosion is spotted. At 3.4% NaCl concentration the wear track is barely visible and no corrosion can be spotted as seen in Figure 116 to Figure 119.

Optical Microscopy

The wear track on the steel ball analyzed by optical microscopy is presented in Figure 120 to Figure 145 in Table 12 below. It is important to note that the magnification is not the same for all the images. This is because of lighting issues which made the images hard to analyze. However, for the measurements of the wear track, the magnification differences were accounted for.

Table 12 - Optical microscope pictures of steel surface after reciprocal ball-on-plate test.

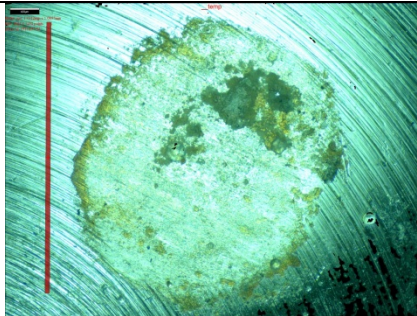
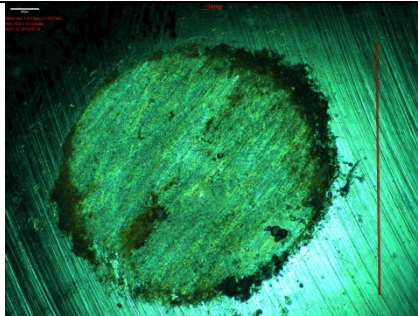
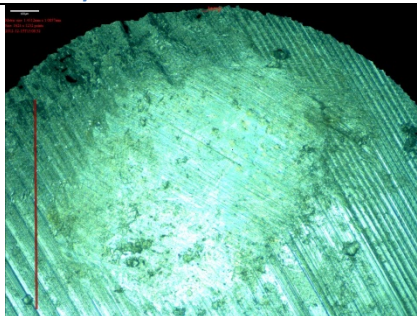
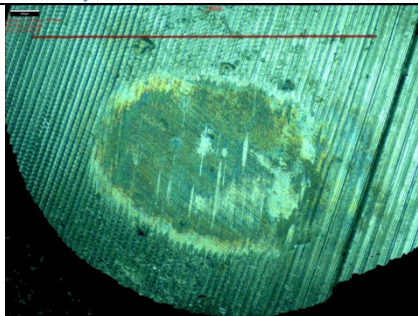
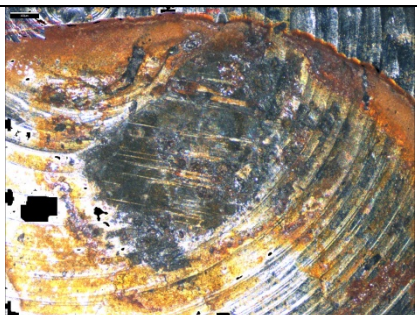
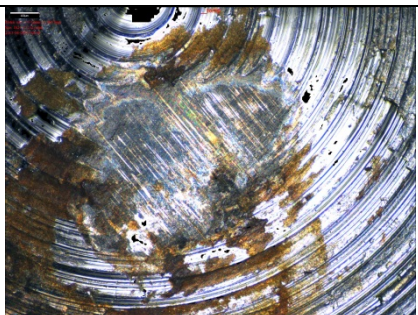
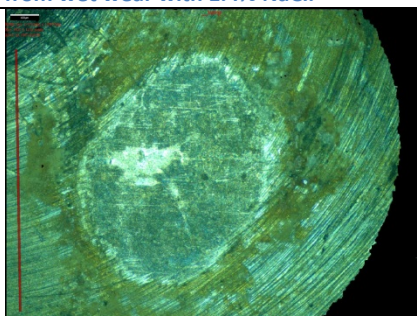
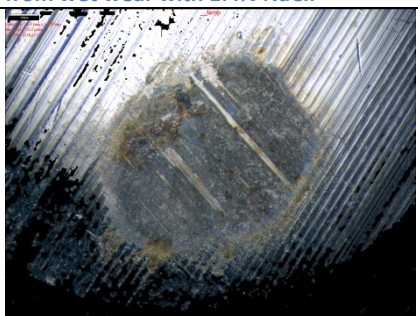
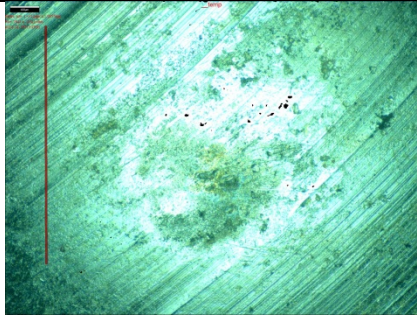
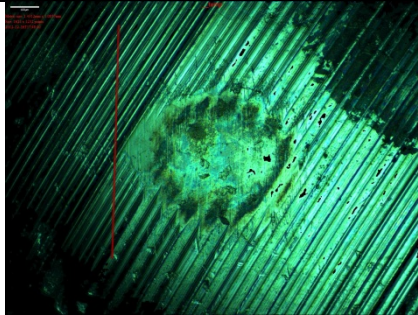
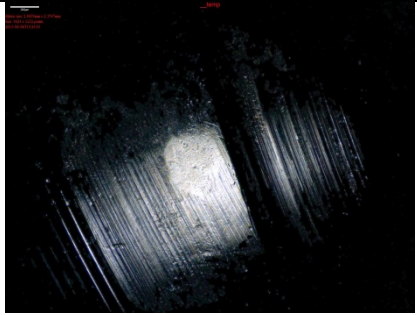
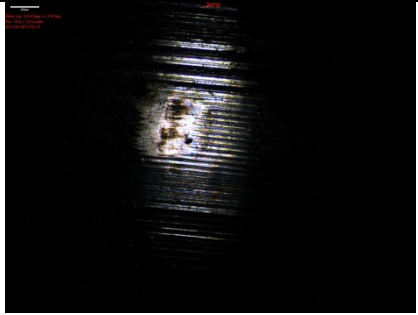
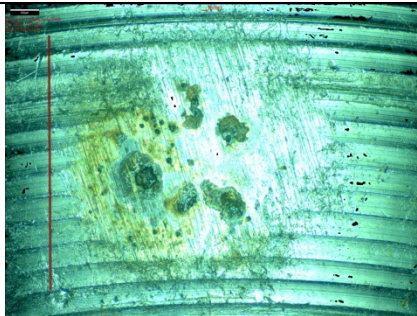
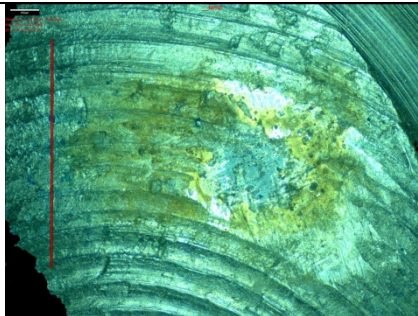
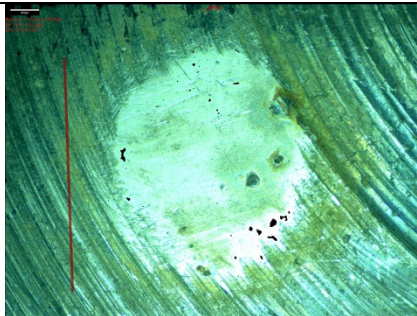
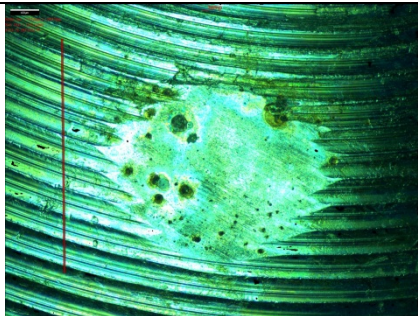
Condition	Test 1	Test 2
Dry wear	 <p data-bbox="544 853 962 909">Figure 120 - Wear track on the steel ball from dry wear.</p>	 <p data-bbox="987 853 1406 909">Figure 121 - Wear track on the steel ball from dry wear.</p>
Wet wear	 <p data-bbox="544 1223 962 1279">Figure 122 - Wear track on the steel ball from wet wear.</p>	 <p data-bbox="987 1223 1406 1279">Figure 123 - Wear track on the steel ball from wet wear.</p>
Wet wear + 1.4% NaCl	 <p data-bbox="544 1592 962 1648">Figure 124 - Wear track on the steel ball from wet wear with 1.4% NaCl.</p>	 <p data-bbox="987 1592 1406 1648">Figure 125 - Wear track on the steel ball from wet wear with 1.4% NaCl.</p>
Wet wear + 3.4% NaCl	 <p data-bbox="544 1962 962 2027">Figure 126 - Wear track on the steel ball from wet wear with 3.4% NaCl.</p>	 <p data-bbox="987 1962 1406 2027">Figure 127 - Wear track on the steel ball for wet wear with 3.4% NaCl.</p>

Table 13 - Optical microscope pictures of steel surface after reciprocal ball-on-plate test continued.

Condition	Test 1	Test 2
Lubricated wear 3% ABR5	 <p data-bbox="544 595 962 651">Figure 128 - Wear track on the steel ball from lubricated wear with 3% ABR5</p>	 <p data-bbox="987 595 1406 651">Figure 129 - Wear track on the steel ball from lubricated wear with 3% ABR5</p>
Lubricated wear 3% ABR5 with 1.4% NaCl	 <p data-bbox="544 967 962 1050">Figure 130 - Wear track on the steel ball from lubricated wear with 3% ABR5 and 1.4% NaCl</p>	 <p data-bbox="987 967 1406 1050">Figure 131 - Wear track on the steel ball from lubricated wear with 3% ABR5 and 1.4% NaCl</p>
Lubricated wear 3% ABR5 with 3.4% NaCl	 <p data-bbox="544 1366 962 1487">Figure 132- Wear track on the steel ball from lubricated wear with 3% ABR5 and 3.4% NaCl (2).</p>	 <p data-bbox="987 1366 1406 1487">Figure 133 - Wear track on the steel ball from lubricated wear with 3% ABR5 and 3.4% NaCl (3).</p>
Lubricated wear 3% SLF41	 <p data-bbox="544 1803 962 1856">Figure 134 - Wear track on the steel ball from lubricated wear with 3% SLF41.</p>	 <p data-bbox="987 1803 1406 1856">Figure 135 - Wear track on the steel ball from lubricated wear with 3% SLF41.</p>

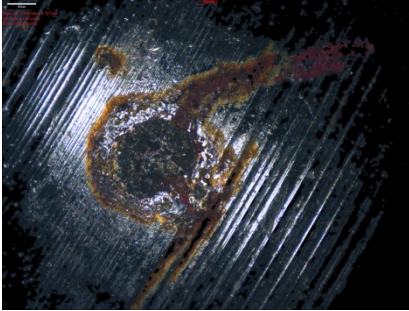
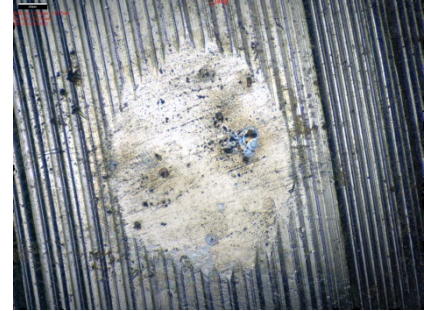
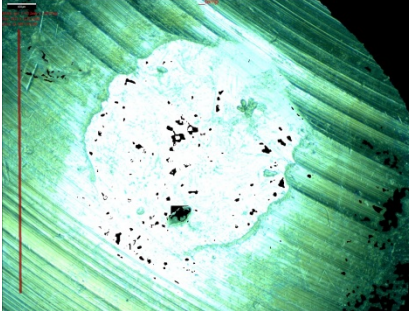
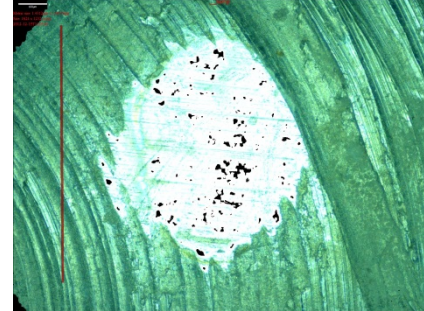
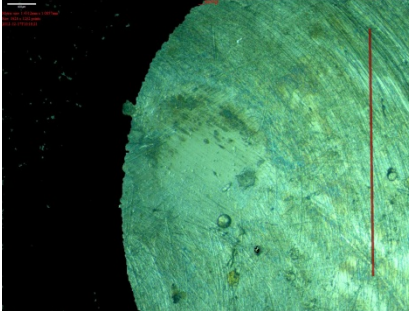
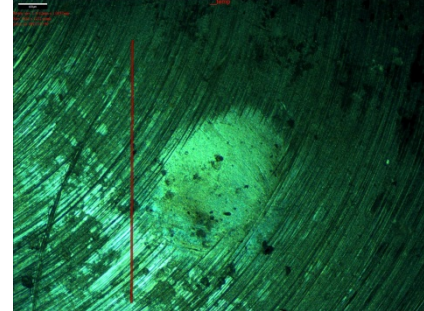
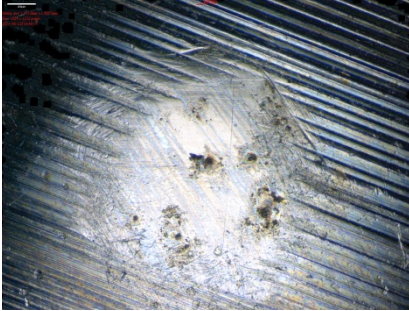
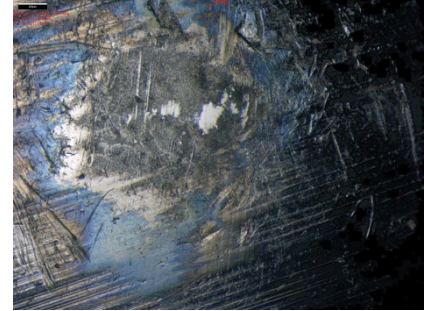
<p>Lubricated wear 3% SLF41 with 1.4% NaCl</p>		
<p>Lubricated wear 3% SLF41 with 3.4% NaCl</p>		
<p>Lubricated wear 3% SLF47B</p>		
<p>Lubricated wear 3% SLF47B with 1.4% NaCl</p>		

Figure 136 - Wear track on the steel ball from lubricated wear with 3% SLF41 and 1.4% NaCl (1).

Figure 137 - Wear track on the steel ball from lubricated wear with 3% SLF41 and 1.4% NaCl (3).

Figure 138 - Wear track on the steel ball from lubricated wear with 3% SLF41 and 3.4% NaCl.

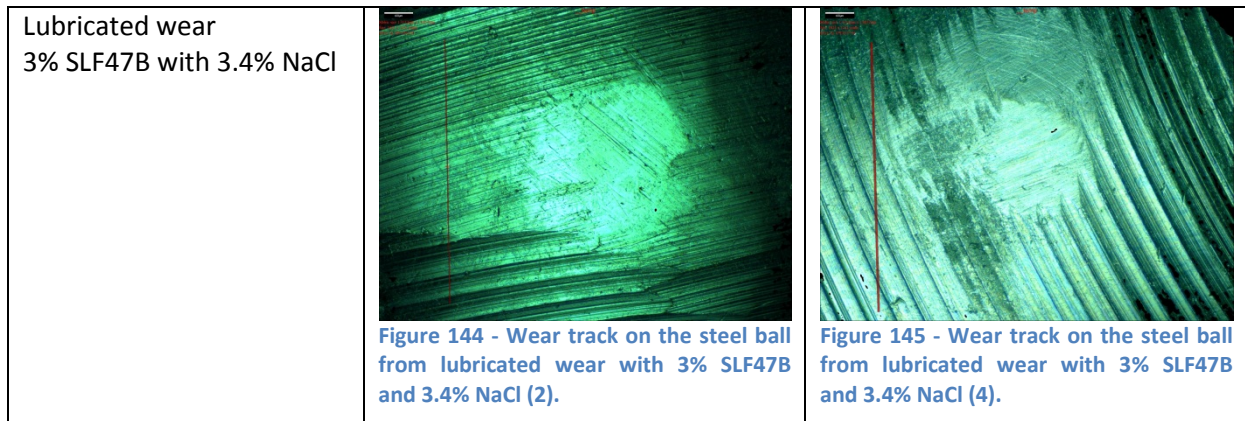
Figure 139 - Wear track on the steel ball from lubricated wear with 3% SLF41 and 3.4% NaCl.

Figure 140 - Wear track on the steel ball from lubricated wear with 3% SLF47B.

Figure 141 - Wear track on the steel ball from lubricated wear with 3% SLF47B.

Figure 142 - Wear track on the steel ball from lubricated wear with 3% SLF47B and 1.4% NaCl (3).

Figure 143 - Wear track on the steel ball from lubricated wear with 3% SLF47B and 1.4% NaCl (4).



Using the acquired images from the optical microscope, the diameter of the wear track was measured and used to calculate the area of the wear track. The average wear track area is presented in Figure 146.

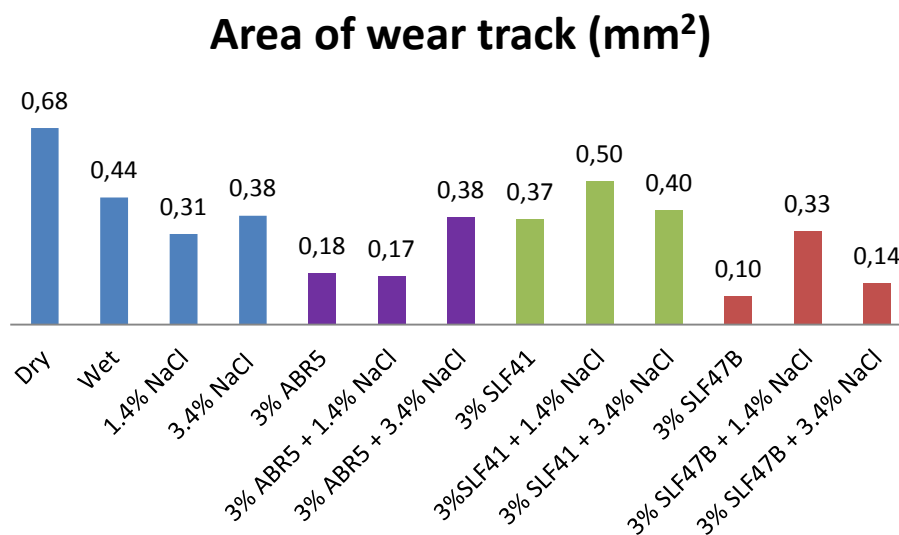


Figure 146 - Average area of wear track after ball-on-plate testing.

The dry wear tests exhibits a lot more wear than the rest of the tests. The wet wear test shows less wear but some corrosion products can be spotted, and in salt water, an even larger amount of corrosion products can be seen.

When ABR5 was used, the wear track was noticeably reduced. The wear track area did not change much with the addition of 1.4% NaCl compared to 3% ABR5. However, at 3.4% NaCl concentration, the wear track area significantly increased and corrosion and pitting could be spotted.

SLF41 also has a reduced wear track, but not as much as ABR5 and in addition large pits could be spotted. At 1.4% NaCl concentration the wear track increases and more corrosion can be spotted.

When the NaCl concentration increased, the wear track decreased and corrosion could no longer be spotted.


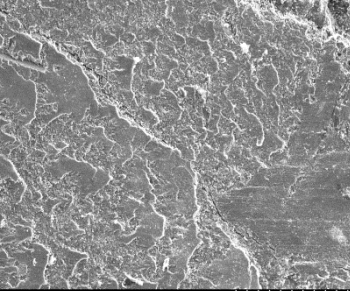
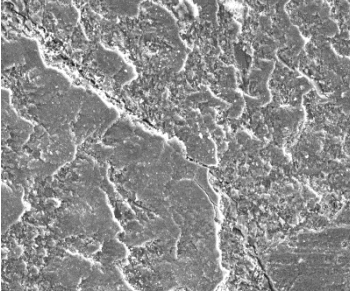
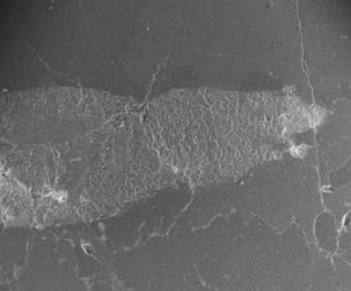
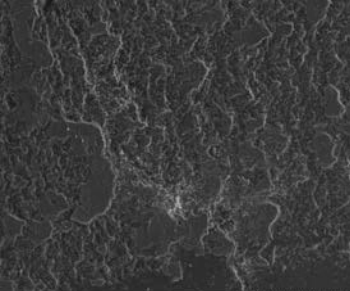
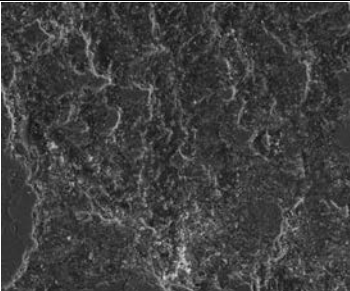
SLF47B shows a greatly reduced wear track, but show some signs of pitting (test 2), see Figure 141. The addition of 1.4% NaCl caused a severe increase of the area of the wear track. However, the wear track area decreases with the addition of 3.4% NaCl.

4.6.2 Wear on the rocks

SEM

The wear on the rocks under the different scenarios from the ball-on-plate test is presented in Figure 147 to Figure 152 in Table 14 below.

Table 14 - SEM pictures of the rock surface after reciprocal ball-on-plate test.

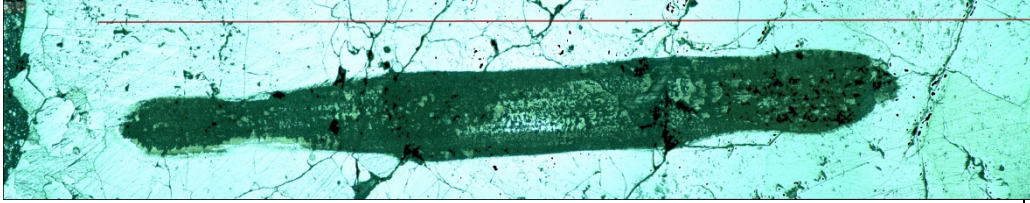
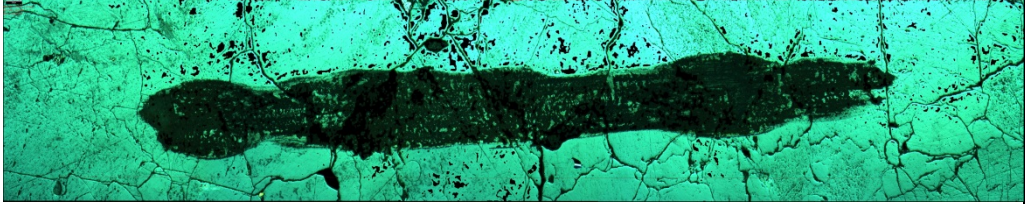
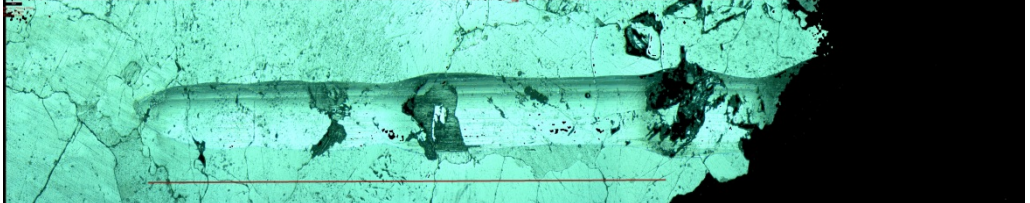
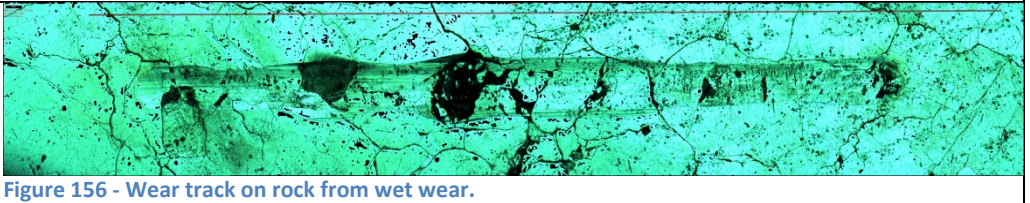
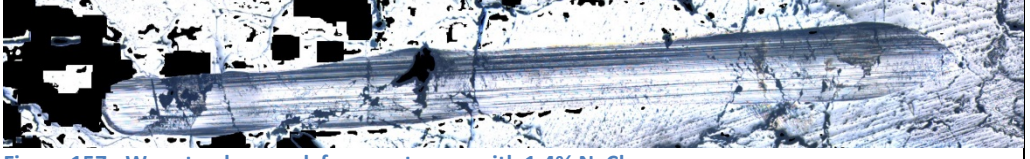
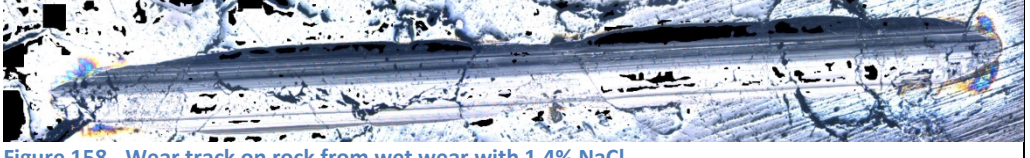
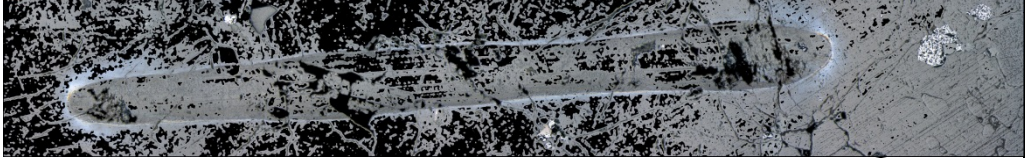
Condition	Magnification		
	50x	200x	450x
Dry wear Test 1	 <p>Figure 147 - Wear track on the rock from dry wear 50x magnification.</p>	 <p>Figure 148 - Wear track on the rock from dry wear 200x magnification.</p>	 <p>Figure 149 - Wear track on the rock from dry wear 450x magnification.</p>
Dry wear Test 2	 <p>Figure 150 - Wear track on the rock from wet wear 50x magnification.</p>	 <p>Figure 151 - Wear track on the rock from wet wear 200x magnification.</p>	 <p>Figure 152 - Wear track on the rock from wet wear 450x magnification.</p>

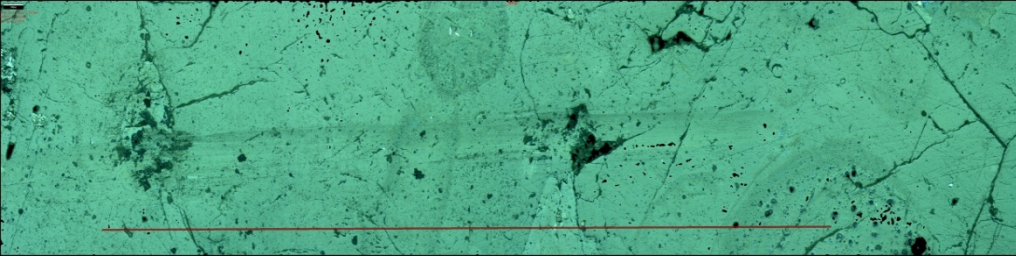
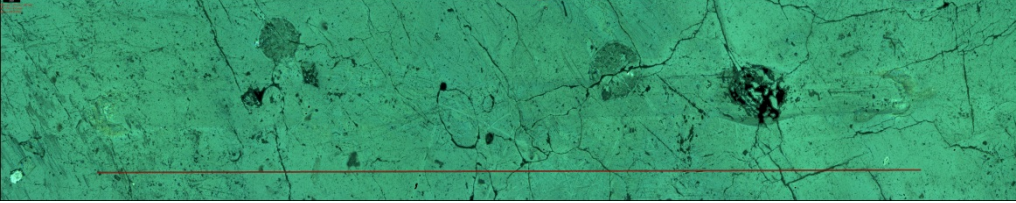
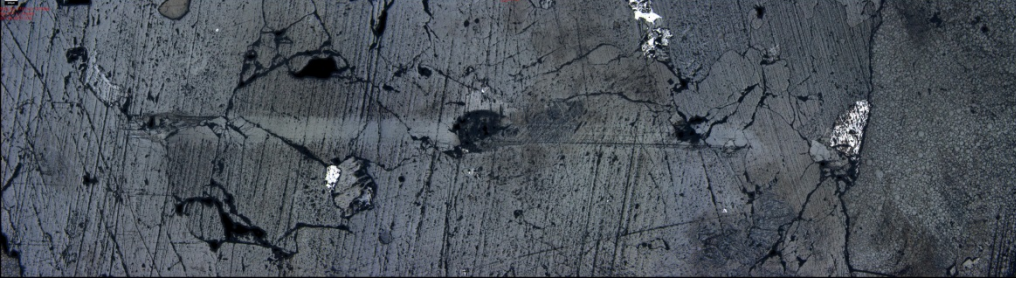

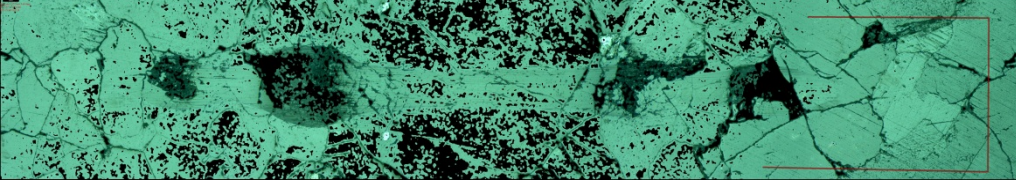
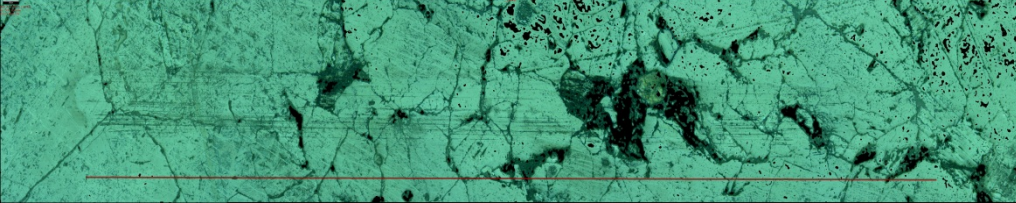
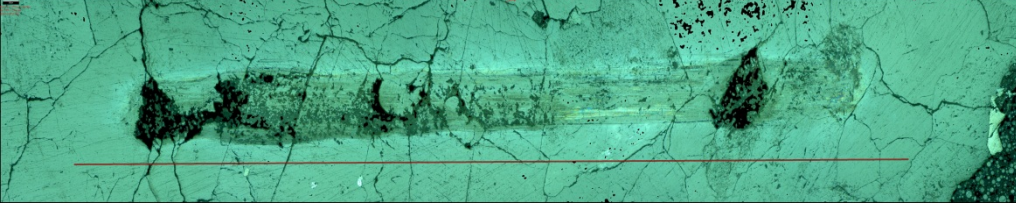
From the dry wear tests the wear track is easily spotted due to a significant amount of wear. However, for the lubricated wear tests, the wear track was too small to be found and therefore no further SEM images were taken.

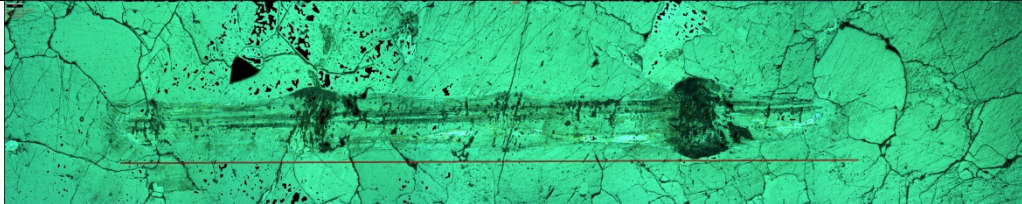


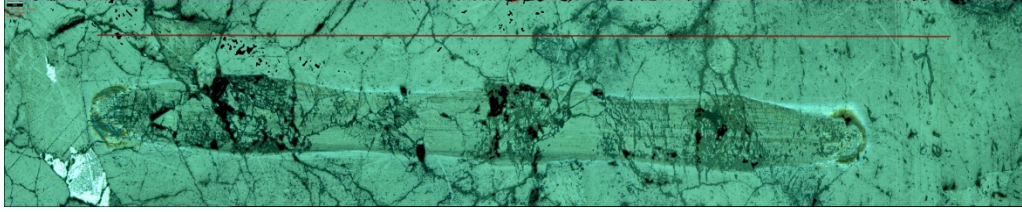
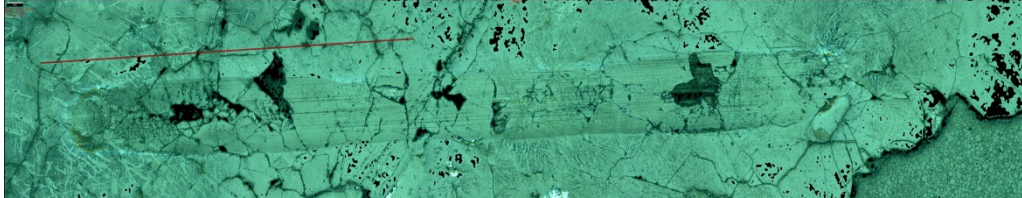
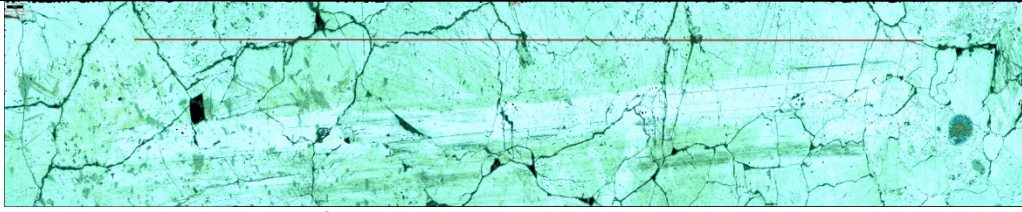
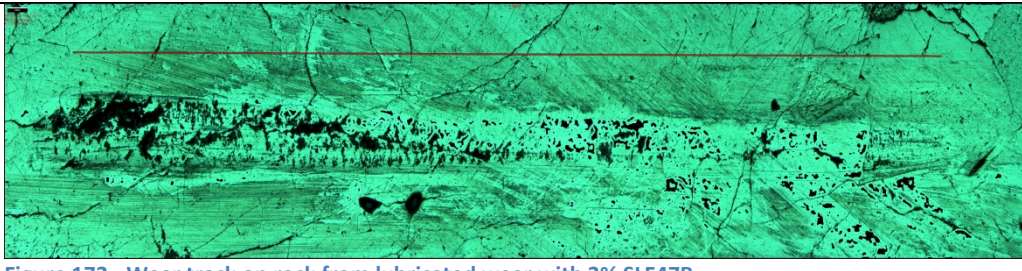
Optical Microscopy

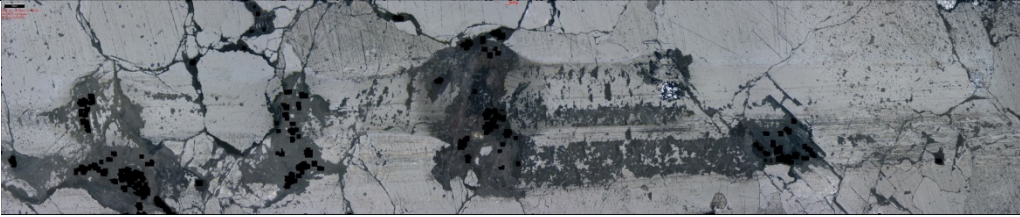
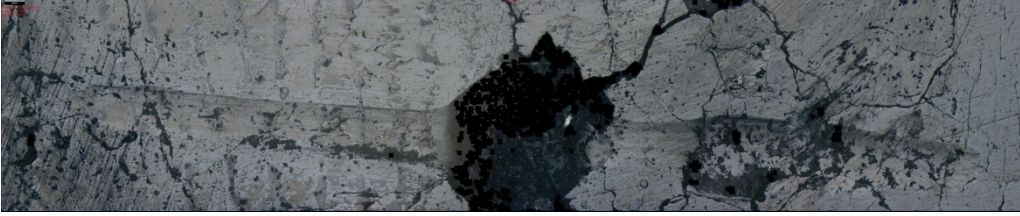
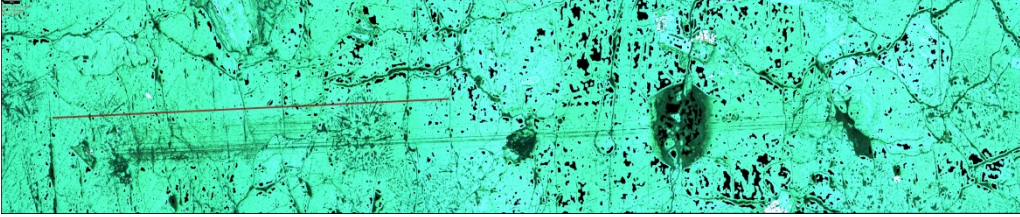
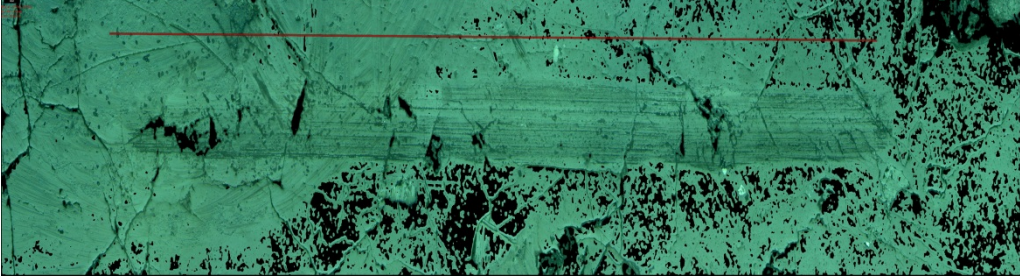
The wear track on the steel ball analyzed by optical microscopy is presented in Figure 153 to Figure 177 in Table 15 below.

Table 15 - Optical microscope pictures of steel surface after reciprocal ball-on-plate test.

Conditions	
Dry wear Test 1	 <p data-bbox="392 667 861 689">Figure 153 - Wear track on rock from dry wear.</p>
Dry wear Test 2	 <p data-bbox="392 900 861 922">Figure 154 - Wear track on rock from dry wear.</p>
Wet wear Test 1	 <p data-bbox="392 1133 861 1155">Figure 155 - Wear track on rock from wet wear.</p>
Wet wear Test 2	 <p data-bbox="392 1366 861 1388">Figure 156 - Wear track on rock from wet wear.</p>
Wet wear 1.4% NaCl Test 1	 <p data-bbox="392 1554 1021 1576">Figure 157 - Wear track on rock from wet wear with 1.4% NaCl.</p>
Wet wear 1.4% NaCl Test 2	 <p data-bbox="392 1742 1021 1765">Figure 158 - Wear track on rock from wet wear with 1.4% NaCl.</p>
Wet wear 3.4% NaCl	 <p data-bbox="392 1930 1021 1953">Figure 159 - Wear track on rock from wet wear with 3.4% NaCl.</p>

<p>Lubricated wear 3% ABR5 Test 1</p>	 <p>Figure 160 - Wear track on rock from lubricated wear with 3% ABR5.</p>
<p>Lubricated wear 3% ABR5 Test 2</p>	 <p>Figure 161 - Wear track on rock from lubricated wear with 3% ABR5.</p>
<p>Lubricated wear 3% ABR5 with 1.4% NaCl Test 2</p>	 <p>Figure 162 - Wear track on rock from lubricated wear with 3% ABR5 and 1.4% NaCl.</p>
<p>Lubricated wear 3% ABR5 with 1.4% NaCl Test 2</p>	 <p>Figure 163 - Wear track on rock from lubricated wear with 3% ABR5 and 1.4% NaCl.</p>
<p>Lubricated wear 3% ABR5 with 3.4% NaCl Test 2</p>	 <p>Figure 164 - Wear track on rock from lubricated wear with 3% ABR5 and 3.4% NaCl.</p>
<p>Lubricated wear 3% ABR5 with 3.4% NaCl Test 3</p>	 <p>Figure 165 - Wear track on rock from lubricated wear with 3% ABR5 and 3.4% NaCl.</p>
<p>Lubricated wear 3% SLF41 Test 1</p>	 <p>Figure 166 - Wear track on rock from lubricated wear with 3% SLF41.</p>

<p>Lubricated wear 3% SLF41 Test 2</p>	 <p>Figure 167 - Wear track on rock from lubricated wear with 3% SLF41.</p>
<p>Lubricated wear 3% SLF41 with 1.4% NaCl Test 1</p>	 <p>Figure 168 - Wear track on rock from lubricated wear with 3% SLF41 and 1.4% NaCl.</p>
<p>Lubricated wear 3% SLF41 with 1.4% NaCl Test 3</p>	 <p>Figure 169 - Wear track on rock from lubricated wear with 3% SLF41 and 1.4% NaCl.</p>
<p>Lubricated wear 3% SLF41 with 3.4% NaCl Test 1</p>	 <p>Figure 170 - Wear track on rock from lubricated wear with 3% SLF41 and 3.4% NaCl.</p>
<p>Lubricated wear 3% SLF41 with 3.4% NaCl Test 2</p>	 <p>Figure 171 - Wear track on rock from lubricated wear with 3% SLF41 and 3.4% NaCl.</p>
<p>Lubricated wear 3% SLF47B Test 1</p>	 <p>Figure 172 - Wear track on rock from lubricated wear with 3% SLF47B.</p>
<p>Lubricated wear 3% SLF47B Test 2</p>	 <p>Figure 173 - Wear track on rock from lubricated wear with 3% SLF47B.</p>

Lubricated wear 3% SLF47B with 1.4% NaCl Test 3	 <p data-bbox="394 409 1418 432">Figure 174 - Wear track on rock from lubricated wear with 3% SLF47B and 1.4% NaCl.</p>
Lubricated wear 3% SLF47B with 1.4% NaCl Test 4	 <p data-bbox="394 658 1418 680">Figure 175 - Wear track on rock from lubricated wear with 3% SLF47B and 1.4% NaCl.</p>
Lubricated wear 3% SLF47B with 3.4% NaCl Test 2	 <p data-bbox="394 907 1418 929">Figure 176 - Wear track on rock from lubricated wear with 3% SLF47B and 3.4% NaCl.</p>
Lubricated wear 3% SLF47B with 3.4% NaCl Test 4	 <p data-bbox="394 1216 1418 1238">Figure 177 - Wear track on rock from lubricated wear with 3% SLF47B and 3.4% NaCl.</p>

As seen in Figure 153 and Figure 154 the wear track in the dry tests are easily spotted because of its deep grooves. The wet tests shows smaller wear tracks but is still significant; see Figure 155 and Figure 156. The saltwater solution does not change the wear track of the stones very much. The different concentration does not show much difference.

The addition of ABR5 caused a significant drop in wear as the wear track is barely visible. The addition of NaCl to ABR5 makes the wear track slightly more visible. SLF41 had less wear than the wet and dry, but still not as little as with ABR5. The addition of NaCl caused an increase in wear, most so at 1.4% concentration. With SLF47B there is very little wear. At 1.4% NaCl concentration the wear increases with some significance. However, at 3.4% NaCl concentration, the wear is less. For all the foams it seems as though the use of salt water increased the wear track slightly. However, for SLF41 and SLF47B it seems that 1.4% NaCl concentration causes the most wear.

5. Discussion

5.1 Rock and steel characterization

The XRD of the Iddefjord granite shows relatively high contents of K-feldspar, quartz and plagioclase and only minor levels of Mica and Chlorite. As seen in Table 6 the hardness for quartz, K-feldspar and plagioclase are higher than that of the lesser present minerals.

The hardness of the steel can be converted to Mohs hardness for easier comparison. In Figure 178 a hardness conversion chart is shown with the hardness measurements of the steel plotted.

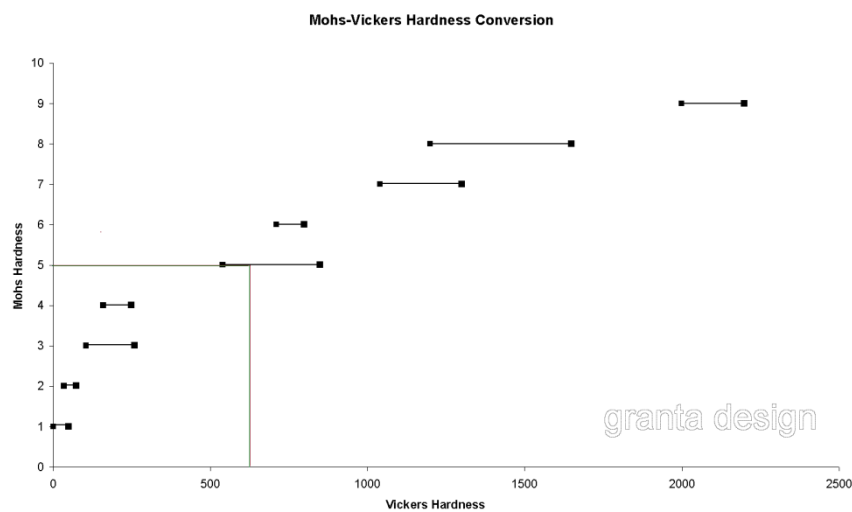


Figure 178 - Mohs-Vickers Hardness Conversion Chart [31].

From the graph we can see that the steel balls hardness converts to a Mohs hardness of about 5. As the rock contains mainly elements that are much harder than the steel, the wear on the steel will be more severe. As discussed in the theory the hardness of the steel should be 1.3x the hardness of the rock to efficiently reduce the wear of the steel. However, this would likely make the steel to brittle to withstand fracture in real tunnel boring application. Because the rock is harder than the steel, this may cause more wear on the steel balls than if the rock was of a composition with lower hardness. The rock is very brittle, and will easily crack at high enough pressures. This creates wear particles which are very hard and will abrade the softer steel ball.

The steel that was used in this thesis was a H13 type steel. It had been die forged and heat treated. Die forging should make the steel harder. The heat treatment of the steel is likely annealing to the first stage, recovery. It is also likely, that some recrystallization was done to make the steel a little more ductile to avoid cracking of the steel, but not full recrystallization which would make the steel too ductile. From the hardness values of the steel and from a datasheet for a typical H13 steel [32] it is possible to assume that the steel was air cooled from a high temperature of about 1000°C and then tempered at a temperature of about 500 – 550 °C, however, these are assumptions based on the steel properties, not exact information.

The chromium content of the steel allows for some corrosion protection, but the chromium content is not as high as it is for stainless steels. The steel also contains some molybdenum which protects against chloride penetration and increases the hardenability of the steel. There is also some vanadium present which increases both the strength and hardness of the steel and its resistance to impact. The nickel will also help the impact strength. The carbon and manganese will make the steel harder, but less ductile and the silicon improves the strength. Considering the heat treatment and the alloying elements the H13 steel should have a good balance between hardness and ductility/toughness which should be beneficial in this particular application area. It should also exhibit some protection against corrosion and penetration of chloride.

5.2 Polarization curves

In Figure 179 the polarization curves for all the foams at a 100% concentration has been gathered for easier comparison between them.

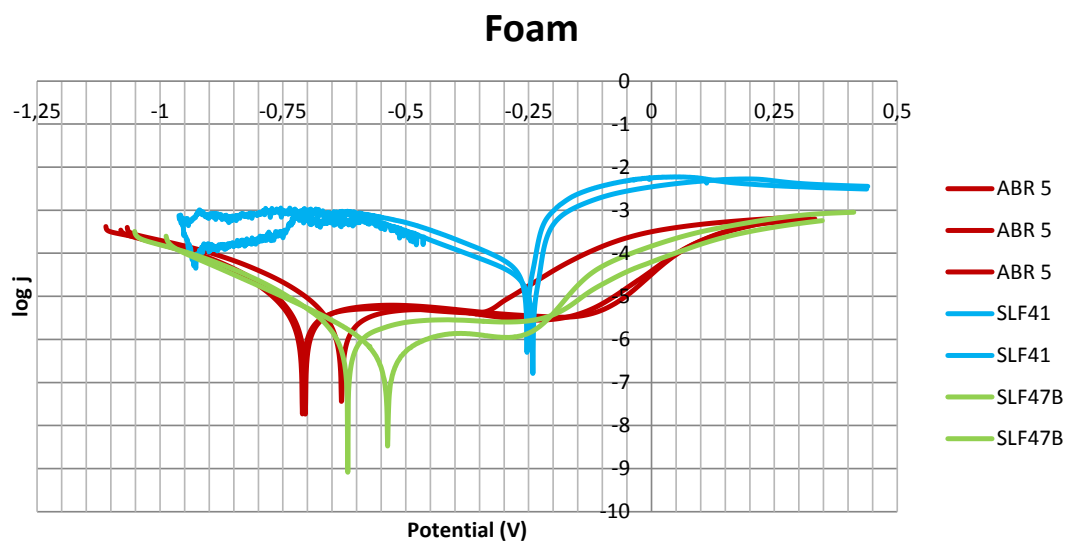


Figure 179 - Polarization curves of all the foams with 100% concentration.

By studying Figure 179 one can see that SLF41 has the highest value of j_{corr} , in other words, SLF41 is likely to have the fastest corrosion rate. ABR5 and SLF47B on the other hand, have a lower j_{corr} , indicating a slower rate of corrosion. They also have a plateau, indicating it that they passivate the steel, which will inhibit corrosion. SLF41 has the highest value of E_{corr} at about -0,25 V, while ABR5 and SLF47B has an E_{corr} value of about -0.70 and -0.575 respectively. The pitting potential for both ABR5 and SLF47B seem to be fairly similar but arguments can be made that ABR5 shows the most resistance to pitting.

3% Foam

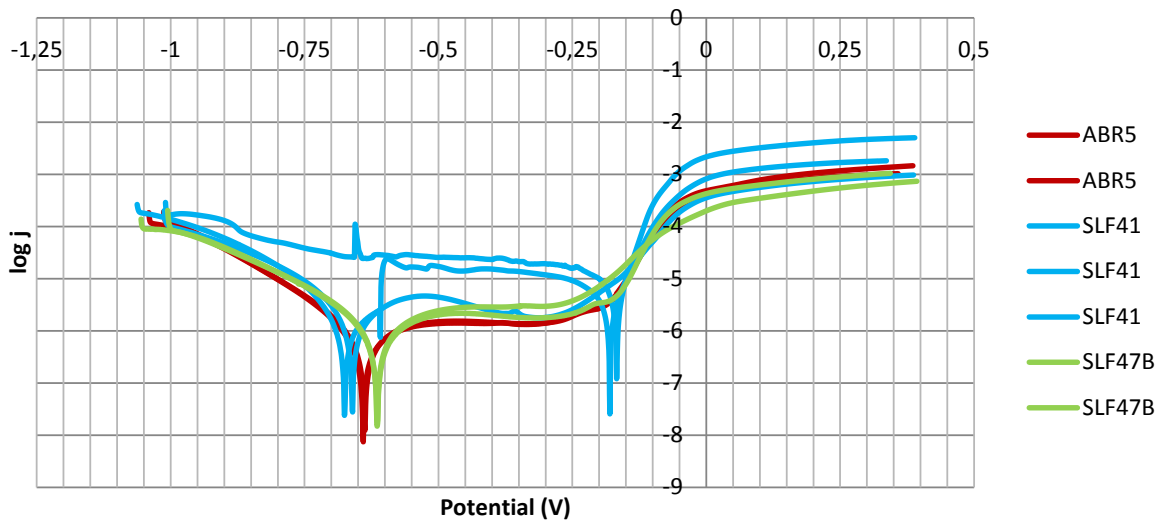


Figure 180 - Polarization curves for all the foams with 3% concentration.

In Figure 180 all the foams at 3% concentration are shown together. From the figure, one can see that ABR5 and SLF47B show quite similar behavior. They both have a corrosion potential at about -0.625, they passivate similarly and the pitting potential is equal. By studying the Pourbaix diagram for iron in water, Figure 181, one can see that the steel is in the immune area when used in ABR5 and SLF47B. However, it is important to note that the Pourbaix diagram in Figure 181 is for pure iron in water, so the effects of alloying elements, and the effects of the foam composition, is not taken into account. SLF41 shows strange behavior. By taking a closer look at Figure 45 one can see that in test 1, the foam gave a relatively low value for E_{corr} , but test 3, had a much higher value. In test 2 however, it showed two corrosion potentials, one equal to test 1 and another equal to test 3. This may indicate that at 3% concentration, SLF41 causes unstable passivity of the metal as illustrated in Figure 22. From Figure 181 one can see that SLF41 will cause the iron to either be in the immune area, where it will not corrode without applied potential, or in the corroding area. Compared to foam at 100% concentration one can see that at 3% concentration ABR5 shows a slight decrease in j_{corr} and E_{corr} , and that it still holds on to the passive behavior. SLF41 changes the corrosive behavior of the steel at 3%. At 100% concentration it showed no signs of passivating the steel. At 3% however, passivation is present, though it seem to be unstable passivation. SLF47B does not change the corrosion behavior very much at 3% concentration.

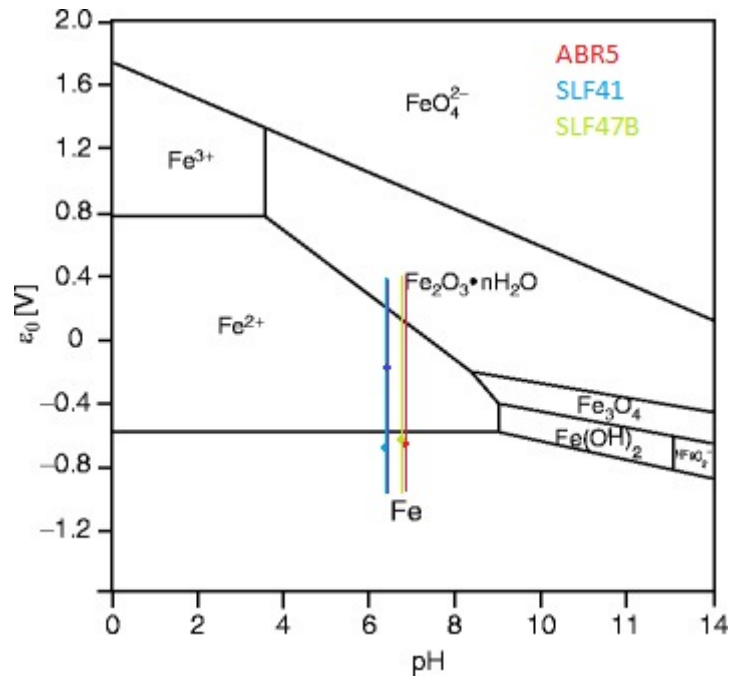


Figure 181 - Pourbaix diagram for iron in water with the results of 3% lubrication.

3% Foam + 1.4% NaCl

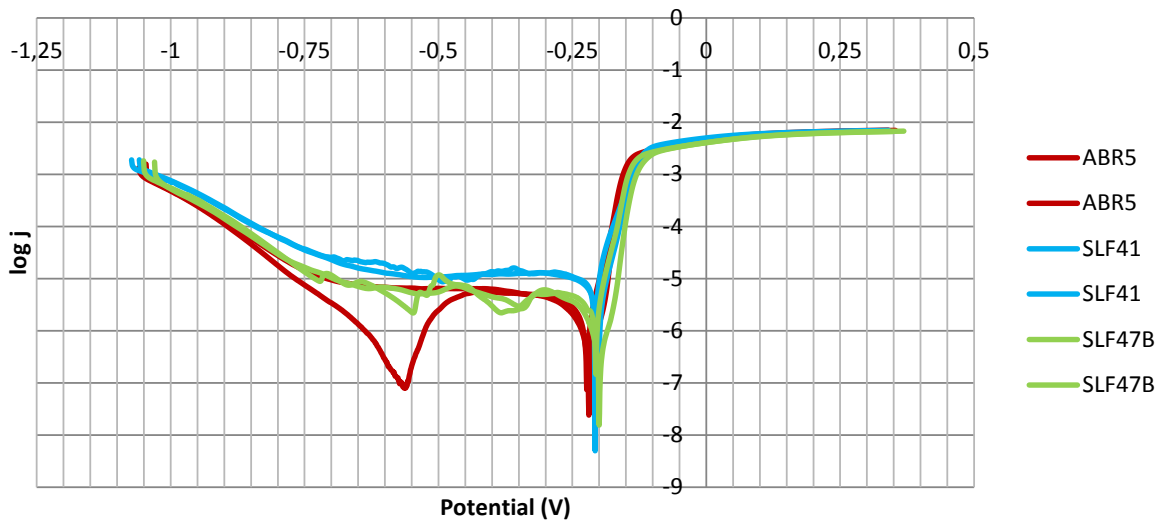


Figure 182 - Polarization curves for all the foams at 3% concentration + 1.4% NaCl.

In Figure 182 all the foams at 3% concentration with 1.4% NaCl is shown. Under these conditions all the foams cause approximately the same values of E_{corr} and j_{corr} , indicating that at under these conditions they all cause equal corrosion of the steel. No passivation occurs either. This shows that with the addition of 1.4% NaCl, the steel no longer passivates. However, ABR5 shows unstable passive behavior with two corrosion potentials in one of its tests. The E_{corr} and j_{corr} caused by SLF41 is similar to some of the values it demonstrated at 3% concentration without NaCl. The presence of NaCl removed its passivating ability causing pure active corrosion to occur. From the pourbaix

diagram in Figure 183, which shows the polarization results for the foams with 1.4% NaCl plotted in a Pourbaix diagram for iron in 3.5% NaCl, one can see that the steel is now in the active region. The loss of passivation is likely caused by the introduction of the aggressive Cl^- anions. It is important to note that the Pourbaix diagram in Figure 183 is for iron in water with 3.5% NaCl and not H13 steel in 3% Foam +1.4% NaCl. Therefore, the findings of plotting the data in this diagram might be inaccurate. The concentration of NaCl is wrong and the alloying elements of the steel and the composition of the foam are not taken into account.

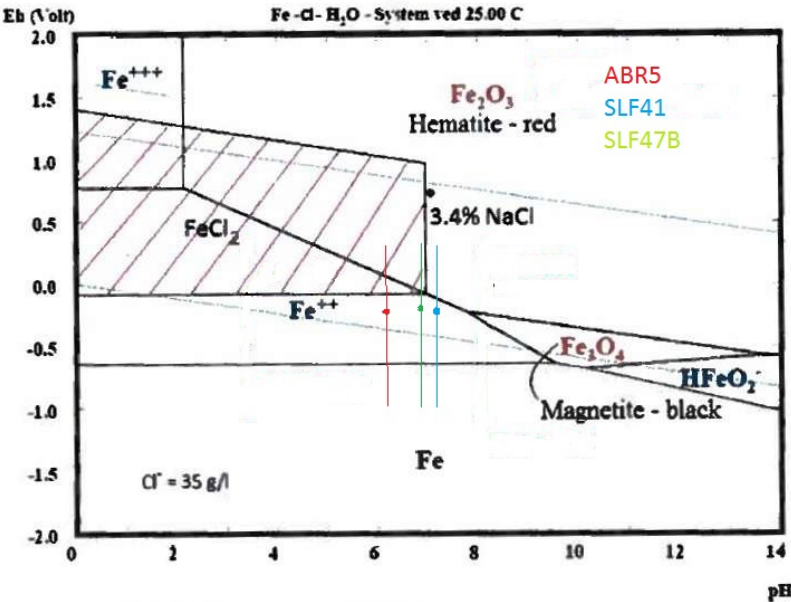


Figure 183 - Purbaix diagram for iron in 3.5% NaCl with the results for foam at 3% concentration with 1.4% NaCl.

3% Foam + 3.4% NaCl

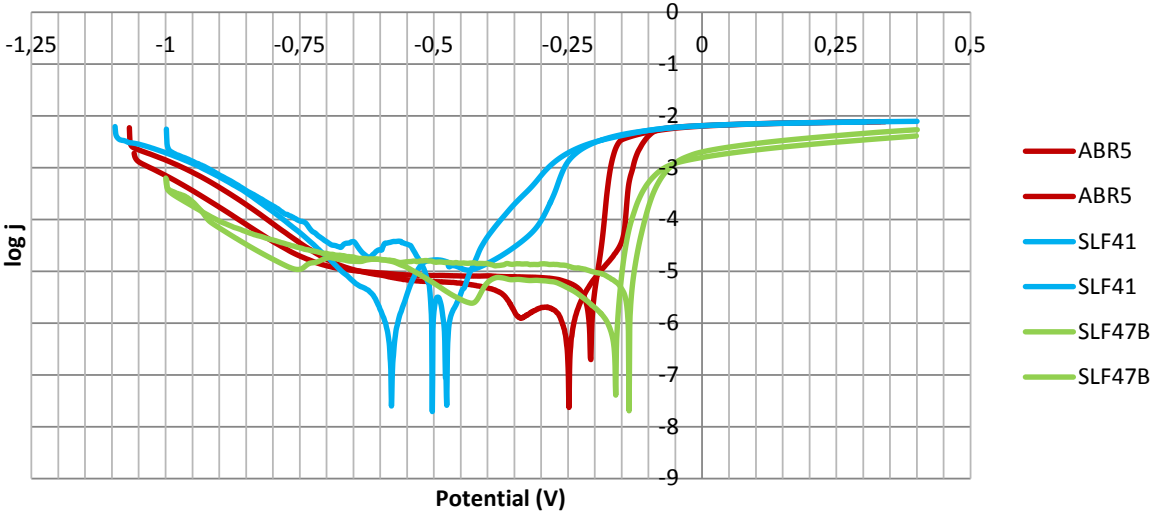


Figure 184 - Polarization curves for all the foams at 3% concentration + 3.4% NaCl.

In Figure 184 the polarization curves for the foams at 3% concentration in 3.4% NaCl is shown. Under these conditions SLF41 shows a much lower E_{corr} than ABR5 and SLF47B. However, the corrosion rate they cause seem to be pretty similar for all the foams, though arguments can be made that SLF47B will cause slightly faster corrosion than the other two foams. One of the SLF41 curves also show slight signs of passivation, but this is very short and the pitting potential comes right after. ABR5 show little change in 3.4% NaCl compared to 1.4% NaCl. SLF47B has a slight increase in E_{corr} , but is relatively unchanged. SLF41 however, shows different corrosional behavior compared to that at 1.4% NaCl concentration. Under these conditions the corrosion potential is much lower and SLF41 even shows signs of passivation, which it did not do before. This unexpected change in behavior could be due to some chemical interaction between the foam and the salt. In the Pourbaix diagram in Figure 185, one can see that all the foams are in the active corrosion area. However, with applied potential, SLF41 could cause passivation of the steel, which ABR5 and SLF47B would not. Again, it is important to consider that the Pourbaix diagram in Figure 185 applies for iron in 3.4% NaCl solution were the alloying elements of the steel and composition of the foams are taken into account. The composition of the foam is unknown. To make more accurate evaluations of the corrosive behavior caused by the foams, a better understanding of the composition of them is needed.

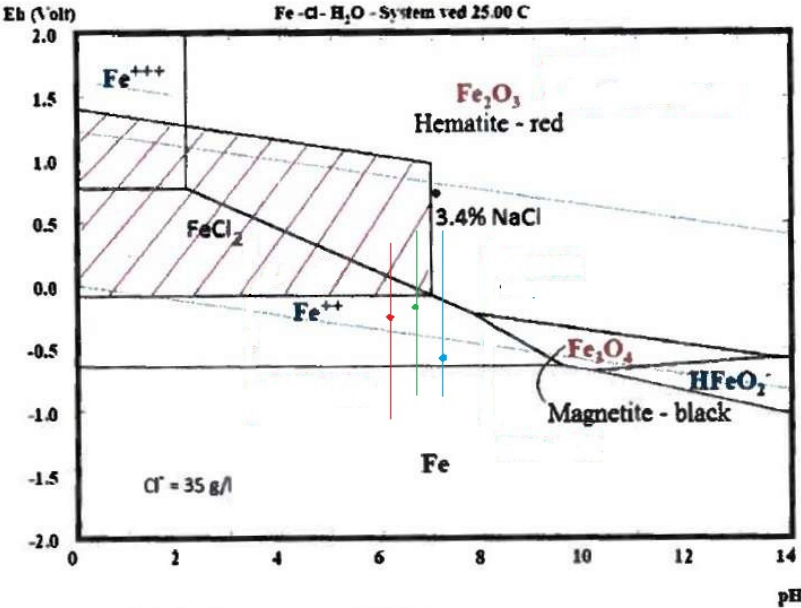


Figure 185 - Pourbaix diagram for iron in 3.5% NaCl with results for foam at 3% concentration with 3.4% NaCl.

5.3 Tribocorrosion

The tests performed under dry conditions had a very high COF (an average of about 1), and from the pictures of the steel balls and the rock, marks with severe wear can be observed. This is as expected considering there is no lubricant and only two rough bodies moving against each other. The wear tracks are wide and deep and a lot of material has been worn away. The wear can be a result of high pressure in the rock/steel ball interface, which has caused the brittle rock to crack and thereby created hard rock debris, which causes abrasion of the steel ball.

The tests that were performed using distilled water showed a bit lower COF than that of the dry conditions, and the average of the recorded COF was at a value of approximately 0.85. However, it was very high, indicating no real formation of a lubricant film. The water minimized the COF only a little but the pictures of the steel ball and the rocks show that the wear has decreased. The wear tracks are smaller, and less debris is present. The measured wear track had an average area of 0.44 mm^2 , compared to that of the dry wear which was at 0.68 mm^2 this is a great reduction in wear. This may be due to the water rinsing worn particles away from the surfaces, which efficiently cleans and prevents particles from attaching to the surfaces making it rougher and more abrasive.

By adding 1.4% NaCl to the solution the COF decreased even more. The average COF was at 0.77. A reduction in the size of the wear track was also seen. The measured wear track was at about 0.44 mm^2 which is also a reduction compared to the wear in distilled water. This decrease may be a result of the formation of corrosion products. In Figure 124 and Figure 125 one can easily spot corrosion products in and around the steel ball. The corrosion products may have acted as a lubricant and thereby lowered the COF, or a third body with a different chemical composition was generated which changed the shear properties of the contact, changing the friction values.

At 3.4% NaCl the COF reduced slightly more, but this reduction to 0.76 (from 0.77 at 1.4% NaCl) is too small to credit the increased concentration of NaCl. However, the wear track of the steel ball increased compared to that of the wear track at 1.4% NaCl concentration. The average wear track area was measured to be 0.38 mm^2 . The reason for this increase may be that at this concentration of NaCl, the corrosion is too aggressive. The increased concentration of NaCl causes faster corrosion, which is easily worn away during the test. In Figure 126 of the steel ball, there is some noticeable corrosion on the ball. Though the test at 1.4% NaCl gave better results, the wear track and COF is still smaller than that of the pure water test.

When the foam was added to the test a severe drop in the COF was recorded. When adding the foam ABR5 the COF dropped to about 0.15. This indicates that the lubricant successfully formed a film and that the obtained lubrication mode was EHL. The wear tracks on the rock and steel samples were much smaller than that of the dry- and wet. By looking at Figure 61, it can be seen that the lubrication failed at times and peaks in the COF occurred, however, lubrication was rapidly restored. The SEM images in Figure 84 to Figure 87 shows that the wear track is barely visible, and no corrosion can be spotted in either them or the images from the confocal microscope in Figure 128 and Figure 129. This corresponds to the findings from the polarization tests, which suggested that the steel showed passive behavior in this solution. The measured size of the wear track averaged at 0.18 mm^2 which is less than half of the wear track size in the distilled water test.

By adding 1.4% NaCl to the ABR5 solution did not affect the COF very much. It was between 0.13 and 0.15. The lubrication was as good as it was without NaCl, suggesting lubrication effect of the foam

was not affected by the salt. The size of the wear track did also slightly decrease, though this decrease is too small to be considered. No corrosion could be spotted in either the SEM or the confocal imaging of the steel balls. The polarizations tests for ABR5 in 1.4% NaCl suggests that the solution might make the steel passivate, as it showed unstable passive behavior. The lack of corrosion may indicate that the steel did indeed passivate and was therefore protected from further corrosion.

Adding 3.4% NaCl to the ABR5 foam test caused an increase in the COF. In fact, their average has doubled. The results of the two performed tests show some variations. However, the lowest achieved COF in the salt containing test is still higher than the highest achieved COF for the test containing only the foam which points to the fact that the salt somehow works against the lubrication ability of the foam. Not enough chemical analysis results have been generated to allow for a proper analysis of how the salt will interact with the foam in this thesis. However, by studying the pictures of the surfaces of the steel ball and the rock samples, some speculations can be made. The picture of the steel surface shows ample amounts of corrosion, and in sample 2, large pits were created. The salt will cause a severe increase in corrosion of the steel, which again causes the steel surface to be rougher. The rougher surface can be the reason for the increase in the COF. Another reason for the increase in wear is that as the steel corrodes the relative movements against the rock, it will cause the corrosion product to be removed. This keeps the steel surface "fresh" which allows for further corrosion to occur. The combination of corrosion and wear as described in the literature (tribocorrosion) severely increases the wear of the steel ball by so-called wear-accelerated corrosion process. The COF for sample 2 was significantly higher than for sample 3. By viewing the pictures of the steel surfaces it can be seen that sample 3 had much more corrosion and pits than sample 2. This shows how the corrosion affects the wear by making the surface rougher. The wear track area has also significantly increased. The average area of the wear track has doubled, from what it was at 1.4% NaCl.

The foam SLF41 also greatly reduced the COF compared to dry wear tests. However, it still has a higher COF than ABR5. SLF41 did not achieve EHL lubrication, instead it provided with boundary lubrication. By looking at the surface pictures one can see that the wear track on the steel balls is bigger than that for ABR5 (almost double), which also indicates a lesser lubrication mode (more contact between the surfaces), and a higher wear rate. The wear area of the steel ball had an average of 0.37 mm^2 . The pictures also show that large pits have formed, which corresponds with the findings from the polarization curves for 3% SLF41, which showed that may display corrosive behavior depending on the state of the metal. The COF graph shows large periodical alterations in the COF. This may be a result of the foam requiring a certain amount of time to fully form a lubricating film.

Adding 1.4% NaCl to the foam solution caused a severe increase in the COF. Under these conditions the COF was at about 0.84, which is significantly higher than without the presence of NaCl. The increase in the COF may be caused by the presence of Cl^- which creates corrosion on the steel surface making it rougher. If one study Figure 186, one can see that compared to SLF41 without the presence of salt, the corrosion behavior is now shifted from unstable passive behavior to, fully corrosive behavior. The area of the wear track for the two tests under these conditions shows some variety. Test 1 showed signs of a lot of corrosion as seen in Figure 100 and Figure 136. Test 3 did not have that much corrosion products present, however, signs of pitting are present, and some roughness

can be spotted at the wear track surface. The reason for test 1 showing so much corrosion may be that it was not properly cleaned after testing, which may have allowed further corrosion to occur after the test was done. However, the steel does corrode under these conditions. The size of the wear track had an average of 0.50 mm² which is the largest for any of the foams under any of the tested conditions. The same is true for the COF, which was the highest recorded COF when any foam, under any condition was used. The increase in COF and wear is likely caused by the corrosive nature of the solution.

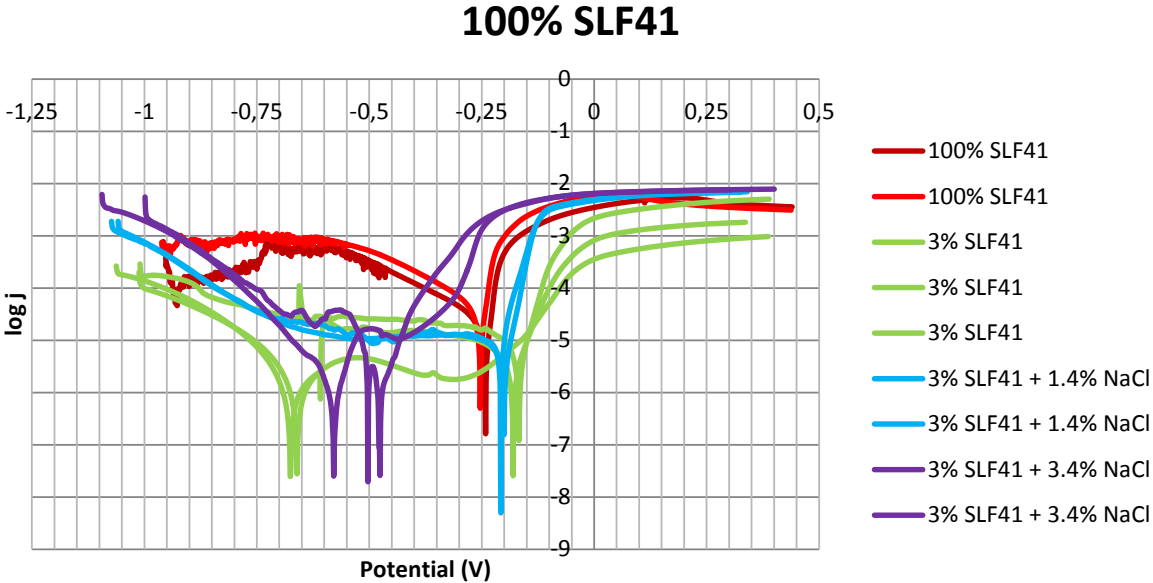


Figure 186 - Polarization curves for SLF41.

Increasing the NaCl concentration to 3.4% causes a decrease in both the COF and the wear track area. However, they are both larger than without the presence of NaCl. The area of the wear track was measured to about 0.40 mm². One could assume that the increase in salt content would increase the corrosion of the steel, but the pictures actually show less corrosion product and pitting than that of the tests where only foam and where 1.4% NaCl and foam was used. In fact, there is no visible corrosion present. If one study the polarization curves in Figure 186, one can see that the corrosion potential of the solution is much lower now. The previously mentioned Pourbaix diagram for iron in 3.5% NaCl in Figure 183 shows that steel in SLF41 is fairly close to the immune area, this may suggest that the since the Pourbaix diagram is not too far off in this situation, the steel may actually be in the immune area, and may therefore not corrode. In 1.4% NaCl the SLF41 foam does not cause the steel to passivate, but offers cathodic protection of the steel. The COF graph shows periodical alterations in the COF. It appears as if the film uses some time to fully form and deliver maximum lubrication as the periodic increase in lubrication occurs at the times where the foam was replaced with “fresh” foam.

The foam SLF47 showed great lubrication performance as it reduced the COF to a value of about 0.19. This low COF indicates that the foam was able to fully achieve an EHL lubrication mode. The COF graph shows some major increases in the COF. These increases are a result of lost lubrication,

which causes contact between the steel ball and the rock. The cause of this may be that the foam “escaped” its position over the test samples or because the foam went back to its liquid state. However, this is quickly fixed and the COF returns to the original value. The wear tracks on the steel balls are the smallest of all the tested conditions, the average wear track was only 10 mm², and minimal corrosion can be spotted. The low wear and absence of corrosion indicates that SLF4B is the best lubricant of all the tested foams.

Adding 1.4% NaCl causes the COF to increase severely. It increases from an average of around 0.19 to 0.41. This increase may be caused by the increase in corrosion behavior. As seen from the polarization curves the addition of NaCl to the solution makes the steel more susceptible to corrosion, which makes the surface of the steel rougher, causing a higher COF between the steel and the rock. The area of the wear track was measured to be about 0.33 mm² which is triple the size of what it was without NaCl. Considering that the polarization curves for SLF47B with 1.4% NaCl and for SLF47B with 3.4% NaCl are fairly similar, and the fact that wear tests show much better results at 3.4% NaCl, it is difficult to explain the results for the 1.4% NaCl situation. The reason for the strange results may be that the foam used in these tests is from a different batch than those in the other tests. However, better results were achieved in another test, but this test was ruined midway and could not be used in this thesis. Another explanation for the unexpected results may be that the testing equipment was acting up and somehow altered the conditions of which the test was run. However, these are speculations and further exploration is required to give a definite answer. The SLF47B +1.4% NaCl test, was done 4 times because of deviations in the results and the results of these tests are presented in Figure 187. In this graph one can see that the first test, gave a very low COF. Its average was at 0.13. The second test also had a low COF at first, but after the first foam change, the COF increased severely (its hidden underneath test 3 and test 4 in the graph). As mentioned, the belief is that something went wrong and that the SLF47B is indeed capable of achieving lower values of COF under these conditions.

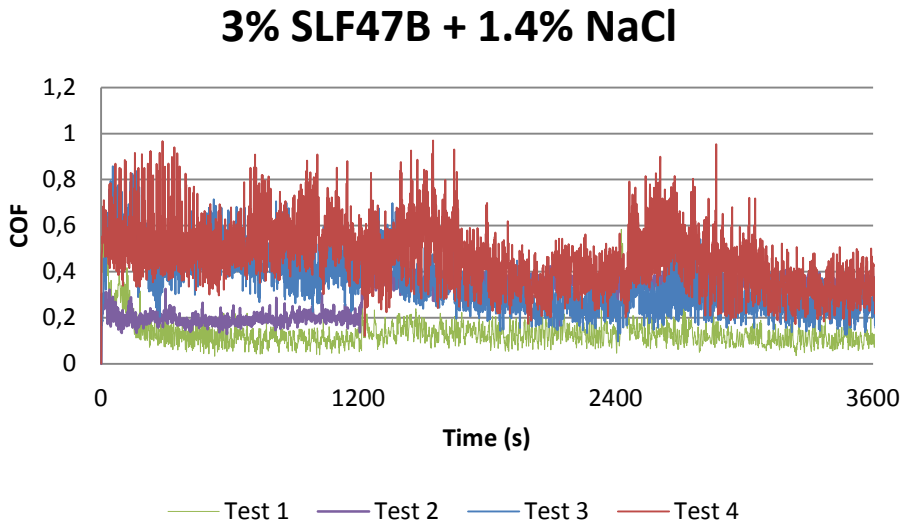


Figure 187 - COF of friction as a function of time for all performed tests of SLF47b + 1.4% NaCl.

When adding 3.4% NaCl to the SLF47B foam the COF decreases compared to that at 1.4% NaCl concentration, and is fairly similar to the COF value without NaCl. The COF stays at an average of about 0.14-0.24. By studying the pictures of the steel surface it can be seen that the wear track is only slightly bigger than that of the steel in the non-salt containing test, the average size of the wear track was only 0.14 mm². No corrosion can be spotted. The previous foams have shown corrosion when the salt has been added. Therefore this may indicate that the foam actually contains some corrosion inhibitors, which can explain the small difference between ABR5 and SLF47B in the polarization curves. It is unlikely that pitting occurred seeing as there are no signs of it. However, though no corrosion is spotted, uniform corrosion may have taken place, but the corrosion product has been removed due to wear. The wear track is larger than what it was without NaCl, and the polarization curves does suggest that corrosion will occur. Considering this, some corrosion may have occurred, but of a less significant nature than for the other foams.

6. Conclusion

Several conclusions can be made from the performed tests. It has been shown that the tests performed without any lubricant cause severe wear to the steel. By adding water, this wear can be reduced, but only slightly, it will also lead to the possibility of corrosion. Water containing salt may reduce wear, but it increases the corrosion rate which, when combined with wear, may cause greater material loss than with clean water. 1.4% NaCl solution gave low wear and a decent COF. At 3.4% NaCl concentration the wear increased, while the COF remained unchanged.

The addition of foam greatly reduces the wear of the steel due to lubrication. However, the foam also increases the risk of corrosion. SLF41 gave the poorest lubrication and the most severe corrosion condition. The wear and corrosion was worst with 1.4% NaCl, however, at 3.4% NaCl concentration, no corrosion was spotted and the wear was less than at 1.4% NaCl concentration. ABR5 gave good lubrication, the addition of 1.4% NaCl should according to the polarization curves have increased corrosion, but the wear remained as without salt, most likely due to unstable passivity. However in a concentration of 3.4% NaCl, large amounts of corrosion were spotted and the wear track area increased. SLF47B had excellent lubrication and showed very little corrosion in the presence of NaCl. At 1.4% NaCl concentration there was an increase in wear and corrosion compared to that in the presence of 3.4% NaCl and no NaCl but this is believed to be a result of failed testing. Therefore, from the present experimental setup it can be concluded that SLF47B gave the best tribocorrosion protection of all the tested foams.

It should be noted that these tests were performed under relatively “clean” conditions. During tunnel boring under real conditions, soil and water with different values of pH and viscosity may be encountered which will affect the performance of the steel and the foams. As seen in the results of this thesis, the environment in which the foam operates has a significant effect on its tribocorrosion properties. It is important to perform proper analyzes of the environment and ground conditions of the boring site before choosing which foam and steel to use.

Finally the addition of a foam lubricant severely decreases the wear and corrosion of the steel. SLF47B showed incredible results in preventing this. The usage and development of new foams will allow for great reductions in the wear and corrosion of cutter steel and thereby reducing the downtime and the costs of tunnel boring.

7. Reference list

1. Askilsrud, O.G., *Development of TBM Technology for Hard Rock Conditions*.
2. Maidl, B., G. Wehrmeyer, and M. Derbort, *Hardrock tunnel boring machines*. 2008: Ernst & Sohn Verlag für Architektur und technische Wissenschaften GmbH und Co.KG.
3. Blindheim, O.T. and A. Bruland, *Boreability Testing*.
4. EFNARC, *Specifications and Guidelines for the use of Specialist Products for Mechanized Tunneling (TBM) in Soft Ground and Hard Rock*. 2005.
5. Girmscheid, G. and C. Schexnayder, *Tunnel Boring Machines*. Practice Periodical on Structural Design and Construction, 2003. **8**(3): p. 150-163.
6. Company, T.R. *TUNNEL BORING MACHINES*. Available from: <http://www.therobbinscompany.com/our-products/tunnel-boring-machines/>.
7. Minnesota, R.o.t.U.o. *Mineral Web Pages*. 2009; Available from: <http://www.geo.umn.edu/courses/1001/minerals/>.
8. Coalition, M.E. *MICA*. 2013; Available from: <http://www.mineralseducationcoalition.org/minerals/mica>.
9. Ralph, J. and I. Chau. *Chlorite Group*. Available from: <http://www.mindat.org/min-1016.html>.
10. Technologies, N. *SOFT GROUND MACHINES*. Available from: <http://www.nfm-technologies.com/-Soft-ground-machines.html>.
11. BESSAC, C., *Full-face TBM CSM Bessac - Earth pressure balance or slurry shield*, CSM BESSAC.
12. Laangmack, L. and J. Ibarra, *Tunneling Lectures 2011 Speciality Chemicals for Tunnel Boring Machines*, 2011: Toronto.
13. Askeland, D.R. and P.P. Phulé, *The Science and Engineering of Materials (International Student Edition)* 2008, Ohio, USA: Cengage Learning.
14. Consultants, M. *Alloying of Steels*. 2012; Available from: <http://www.materialsengineer.com/E-Alloying-Steels.htm>.
15. Kopeliovich, D. *Effect of alloying elements on steel properties*. Available from: http://www.substech.com/dokuwiki/doku.php?id=effect_of_alloying_elements_on_steel_properties.
16. Stavanger, S.S., *Steel Handbook - Materials Reference Book*, S.S.S. AS, Editor 2011.
17. Bardal, E., *Korrosjon og Korrosjonsvern*. 1994, Trondheim: Tapir Akademisk Forlag.

18. Kaesche, H., *Corrosion of metals - Physiochemical Principles and Current Problems*. Engineering Materials and Processes, ed. B. Derby. 2003, New York: Springer-Verlag Berlin Heidelberg New York.
19. MacDougall, B. and M.J. Graham, *Growth and Stability of Passive Films*. 2 ed. Corrosion Mechanisms in Theory and Practice, Second Edition, Revised and Expanded, ed. P. Marcus. Vol. 6. 2002, New York, USA: Eastern Hemisphere Distribution.
20. Siebert, O.W., *Laboratory Electrochemical Test Methods*. Laboratory Corrosion Tests and Standards, 1985: p. 65-90.
21. Landolt, D., *Corrosion and Surface Chemistry of Metals* 2003: CRC Press Taylor & Francis Group. 622.
22. Czichos, H., *TRIBOLOGY a systems approach to the science and technology of friction, lubrication and wear*. Tribology series. Vol. 1. 1978, Amsterdam: Elsevier scientific publishing company.
23. Stachowiak, G. and A.W. Batchelor, *Engineering Tribology (3rd Edition)*. 2005, Burlington, MA, USA: Butterworth-Heinemann.
24. Hardell, J., E. Kassfeldt, and B. Prakash, *Friction and wear behaviour of high strength boron steel at elevated temperatures of up to 800°C*. Wear, 2008. **264**(9-10): p. 788-799.
25. Wang, J., et al., *Tribological behavior of PTFE sliding against steel in sea water*. Wear, 2009: p. 1634-1641.
26. Tomala, A., et al., *Tribological properties of additives for water-based lubricants*. Wear, 2010.
27. LiRan, M., Z. ChenHui, and L. ShuHai, *Progress in experimental study of aqueous lubrication*. 2011.
28. Lee, S., et al., *Boundary lubrication of oxide surfaces by Poly(L-lysine)-gpoly(ethylene glycol) (PLL-g-PEG) in aqueous media*. Tribology Letters, 2003. **15**(3).
29. Klein, J., et al., *Fluidity of water and of hydrated ions confined between solid surfaces to molecularly thin films*. JOURNAL OF PHYSICS:CONDENSED MATTER, 2004: p. 12.
30. Plaza, S., et al., *Tribological performance of some polyoxyethylene dithiophosphate derivatives water solutions*. Wear, 2001. **249**(12): p. 1077-1089.
31. INTELLIGENCE, G.M. *Hardness Conversion Charts*. Available from: <http://www.grantadesign.com/resources/materials/hardnesscharts.htm>.
32. *AISI Type H13 Hot Work Tool Steel*. Available from: http://www.matweb.com/search/datasheet_print.aspx?matguid=e30d1d1038164808a85cf7ba6aa87ef7.